SOLID STATE SPECTROSCOPY

RARE EARTH - HYDRIDE CENTRES IN THE ALKALINE EARTH FLUORIDES

A thesis presented for the degree of
Doctor of Philosophy in Physics
in the University of Canterbury,
Christchurch, New Zealand.

by

I.T. JACOBS

November 1971

The white man drew a small circle in the sand and told the red man, "This is what the Indian knows", and drawing a big circle around the small one, "This is what the white man knows". The Indian took the stick and swept an immense ring around both circles: "This is where the white man and the red man know nothing."

- Carl Sandburg

My thanks are due to Professor McLellan for my acceptance as a research student. In particular I wish to thank Dr G.D. Jones for his enthusiastic supervision as well as Professor Satten and Dr K. Zdansky for their continuing interest and many contributions. Professor B.G. Wybourne's interest in this work has been appreciated together with many helpful discussions with Mr M. Presland.

Thanks are due also to Mr D. Greig for his patience in the cryogenics room and to Mr R. Ritchie for technical assistance.

Financial assistance has been received from the New Zealand University Grants Committee, and from the United States Air Force Office of Scientific Research under AFOSR Grant No. 1275-67. The Grants Committee also provided a Postgraduate Scholarship. Without this assistance this work would not have been possible.

CONTENTS

LIST OF FIGURES

LIST OF TABLES

ABSTRACT

Both the optical and infrared spectra of cerium and praseodymium tri-positive ions in the alkaline earth fluorines have been studied. Various charge compensation mechanisms have been employed including negative hydride, deuteride and tritide ions.

For the hydride centres the degenerate local mode lines are resolved into more than one component. These splittings are attributed to electron-phonon interaction effects between the low lying rare earth 4f electronic states and the hydride ion local mode phonons.

The 4f-5d electronic transitions of the cerium hydride type centres show large isotope shifts up to 50 cm^{-1}. Only the non-degenerate hydride ion vibration appears in the 4f-5d optical spectra and the vibrational interval is increased from absorption to fluorescence by as much as 15%. Both the isotope and vibronic shifts for the tetragonal cerium sites are attributed to electron-phonon interaction effects.

Simple models involving point charges and point dipoles account in a semi-quantitative way for several features of the spectra but fail to account for either the sign or magnitude of the isotope and vibronic shifts.

C H A P T E R I

INTRODUCTION

In recent years considerable progress has been made in the interpretation of the vibrational spectra of light impurity ions in crystals[1,2,3]. The light ions vibrate at frequencies appreciably higher than those propagated by the lattice and so vibrational modes strongly localised about the defect ion are produced. These localised modes are observed, at low temperatures, as sharp absorption lines in the infrared. The number and frequencies of these lines and the appearance of harmonics is determined by the site symmetry of the light ion. The linewidths and relative intensities are determined by the coupling of the local modes to their environment.

Negative hydrogen and deuterium ions incorporated in the alkaline earth halides give rise to good examples of localised modes and have been extensively studied[4].

Similarly the electronic spectra of rare earth ions in many host lattices are now well understood [5,6]. The $4f^n \rightarrow 4f^{n-1}$ 5d transitions are observed in the ultraviolet region of the spectrum as broad intense absorption bands. At low temperatures these are often resolved into pure electronic transitions (zero phonon lines) and their

associated phonon sidebands. In suitable cases these phonon sidebands are resolved into peaks corresponding to peaks in the phonon density of states of the host lattice and to vibrational modes strongly localised in the vicinity of the rare earth ion. A representative example of these transitions is that of trivalent cerium in the alkaline earth fluorides whose spectra have been reported by Kapalanskii[7] among others[8].

The most prominent zero phonon line in the three thousand angstrom region has been identified[9] as a 4f-5d transition of cerium in a crystal field of tetragonal symmetry. In this case charge compensation is effected by an interstitial fluorine ion located in an adjacent empty cube of fluorines in the fluoride lattice (Fig. 2). In this work it is shown that analogous spectra can be produced with hydride ions serving as charge compensators.

These centres have been previously studied by E.S.R. techniques[10,11] and the infrared hydride local mode absorption has been reported by Jones et al.[12].

The effects of replacing the fluoride ion charge compensator by hydride or deuteride ions have been discussed[13] for the gadolinium ion in calcium fluoride. New electronic lines are produced in the optical spectrum of the crystal as a consequence of the changed environment of the gadolinium ion.

The frequencies of these new electronic transitions are slightly different for H^- and D^- charge compensations. This frequency difference constitutes the electronic 'isotope shift'.

Vibronic transitions are observed whose vibrational frequency intervals match the frequencies of the H^- and D^- localised modes. Since the transitions involved in this work were f-f (in this case $^8S_{7/2}$ - $^6P_{7/2}$) these vibronics were very much less intense than their parent electronic transitions.

The above effects were reported previously by Jones and Satten[14] in a study of H^- and D^- ions in the rare earth trifluorides. They interpreted the isotope shifts (defined above) as due to a dynamic coupling between the rare earth and hydride ions. Unfortunately the small size of the effects and uncertainties about the crystal structure and site symmetries made a detailed comparison of theory with experiment impossible.

Imbus et al.[15] report similar small shifts for the R lines of chromium isotopes in ruby and magnesium oxide. Hughs[16] has observed isotope shifts for radiation induced colour centres in ^6LiF and ^7LiF which he attributed to a combination of static and dynamic effects. Again, however, large experimental uncertainties and the approximations required to make the calculations do not allow a detailed evaluation of the models employed.

The coupling between the optically active electrons of a defect ion and the lattice manifests itself in several ways.

(1) Through shifts in the energies of electronic transitions.

(2) By modifications of the lattice or localised vibrations.

(We are not concerned in this work with the destruction of electronic selection rules or with the lifetimes of excited states.)

In many cases these terms are small and/or the interactions so numerous that the various effects, if observable, cannot be unambiguously identified. It is therefore useful to investigate simple experimental situations with well localised vibrational modes where the electron-phonon interaction is not so strong as to preclude the observation of detailed structure and yet strong enough to give rise to effects which may be accurately measured. Rare earth hydride ion pairs in the alkaline earth fluorides largely fulfil these requirements.

The local mode infrared absorption lines are extremely narrow which allows the resolution of fine structure (Ch. IV). The positions of the low lying rare earth energy levels can be determined or estimated from the optical spectra which allows the calculation of second order interaction effects. For interconfigurational (f-d) electronic transitions the isotope shifts are an order of magnitude

greater than the previously observed intraconfigurational isotope shifts. Similarly large vibronic shifts, defined as the difference between the vibrational frequency interval for absorption and fluorescence spectra, are observed for the local mode vibronic progressions. The system is also convenient since the hydride ion may be replaced by the heavier but electronically similar deuteride and in this work tritide ion. The host lattice can also be changed from calcium to strontium fluoride enabling several of the parameters to be varied independently.

C H A P T E R I I

A REVIEW OF THE THEORY

Lattice and Localised Vibrations

If we suppose that the effects of the electrons may be represented as a static internuclear potential we may write the Hamiltonian which describes the atomic vibrations in a perfect crystal as:

$$\mathcal{H} = \sum_{\ell k} \frac{p_\alpha^2(\ell,k)}{2M(\ell,k)} + \tfrac{1}{2} \sum_{\ell k \alpha} \sum_{\ell' k' \alpha'} \mu_\alpha(\ell k) \Phi_{\alpha\beta}(\ell k, \ell' k') \mu_\beta(\ell' k') \qquad (1)$$

where p_α and μ_α are the momentum and displacement of the k^{th} atom in unit cell ℓ, where α defines the cartesian coordinates.

The elements of $\Phi_{\alpha\beta}$ are the so-called force constants and are the second degree coefficients in the Taylor series expansion of the crystal potential energy. Cubic and higher terms in this expansion have been neglected.

The equations of motion are

$$M(\ell k)\ddot{u}_\alpha(\ell k) + \sum_{k' \ell' \beta} \Phi_{\alpha\beta}(\ell' k') \mu_\beta(\ell' k') = 0 \qquad (2)$$

Because of the periodic symmetry of the lattice the atomic force constants depend only on the intercell distance and the displacement amplitude may be written as

$$\mu_\alpha(\ell k) = \frac{e_\alpha(k)}{\sqrt{M_k}} e^{i(\underset{\sim}{k}.\underset{\sim}{r}_i - \omega t)} \qquad (3)$$

The eigenvalue equation determining the relation between ω and $\underset{\sim}{k}$ is found by substituting (3) in (2). The resulting solutions are extensively discussed in the literature[17,18].

For each value of k there are 3τ solutions where τ is the number of atoms per unit cell. The τ branches of the multivalued function $\omega(\underset{\sim}{k})$ for which $\omega(\underset{\sim}{k}) \to 0$ as $\underset{\sim}{k} \to 0$ are labelled acoustic and the remaining $3\tau-3$ branches optical since for an ionic crystal these modes impart a macroscopic fluctuating dipole moment which may interact with an incident electromagnetic wave.

This process is responsible for the restrahlen absorption characteristic of ionic crystals and gives rise to the strong infrared absorption of calcium and strontium fluoride crystals in the 500 cm^{-1} region. If the crystal were perfectly harmonic the absorption spectrum would consist of delta functions. However, since the crystal is not harmonic the delta function peaks are broadened into Lorentzian peaks with sidebands corresponding to multiphonon processes.

If a point defect is introduced into the crystal the translational symmetry is destroyed and the normal modes of vibration are modified.

The possible changes can be illustrated by considering a linear chain of identical atoms with a single mass defect[19,20,21]. If the force constants are unchanged and the impurity mass is heavier as first shown by Rayleigh[22] all the frequencies are lowered but not lower than the next unperturbed frequency. If the impurity is lighter the highest symmetric mode may be greatly displaced above the band and forms the so-called localised mode since it cannot be propagated throughout the lattice and is strongly spatially localized about the defect.

Since the translational symmetry of the lattice is removed by the presence of the defects the selection rules governing infrared absorption are relaxed. Not only may the localised modes be infrared active but also the slightly perturbed band modes give rise to new infrared absorptions which in the case of ionic crystals are superimposed on the dominant restrahlen absorption.

One dimensional models have been discussed by several authors[23,24,25]. To obtain solutions for three dimensional models Greens function techniques are employed. Extensions to the theory have been made by Dawber and Elliot[26]. Recent reviews include those of Maradudin[27] among others[28,29].

More elaborate models have been introduced by several authors since the original development of the rigid ion

model. These include the shell model[30,31] in which the ions are represented as small heavy nuclei coupled by elastic springs to light rigid electron shells.

Provided the impurity ion is significantly lighter than the lattice ions it can be treated as an anharmonic oscillator in an effective static potential well. This approach has been used successfully by Hayes et al.[4,32] for the case of H^- substitutional impurities in the alkaline earth fluorides. In this case the H^- ion is in a tetrahedral environment and one second and two third harmonics are observed. These observations provide sufficient data to determine the anharmonic constants which then allows the calculation of the positions of the forbidden second harmonics. These were later observed by the use of stress[33] in excellent agreement with the predictions.

Maradudin and Peretti[34] have examined the anharmonic oscillator in C_{4v} symmetry and have obtained a solution by treating the cubic terms to second order and the quartic terms in first order perturbation. The first and second excited states of this oscillator are shown in figure (1). The electric dipole operator transforms as $\Gamma_1+\Gamma_5$ in C_{4v} and so there will be two first and three second harmonic transitions allowed.

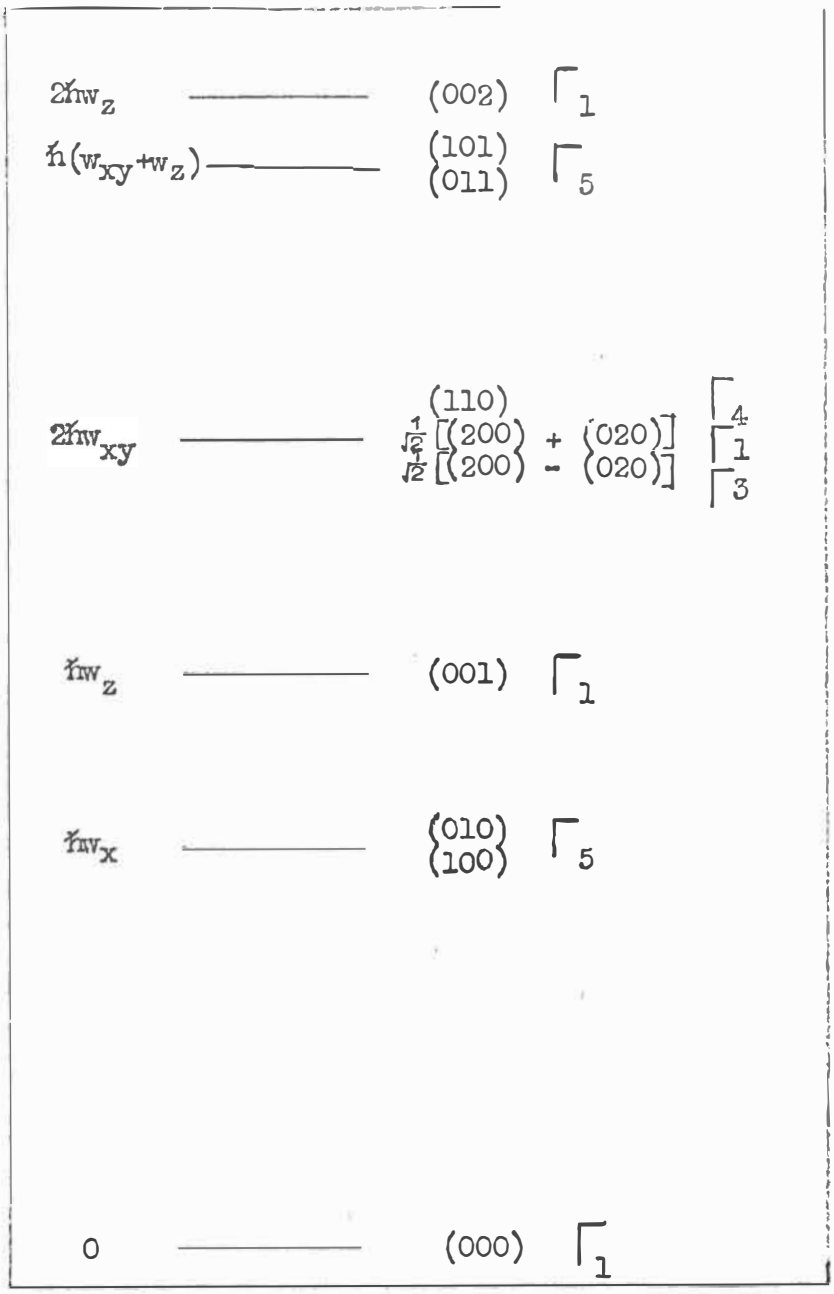

Fig (1). The low lying energy levels of the harmonic oscillator in C_{4v} symmetry. The wavefunctions are labelled with the appropriate irreducible representation. It has been assumed that $w_z > w_{xy}$.

This and several other point symmetries are reviewed by Newman[1]. This static well approximation, together with a large induced hydride ion dipole moment introduced by Zdansky[35] in a study of Gd^{3+}-H^- tetragonal ion pairs in CaF_2 is used in the interpretation of the spectra reported here and will be reviewed in detail.

The hydride ion is situated in an otherwise empty cube of fluorine ions adjacent to the rare earth ion (Fig. (2)). The extra positive charge on the rare earth will result in a non-linear polarization of the hydride ion which is represented by a dipole moment directed in line with the rare earth (Fig. (2b)). This dipole moment is assumed to have a constant magnitude, independent of the hydride ion position. The effective static potential well in which the hydride ion is taken to vibrate can be written as the sum of cubic and tetragonal components:

$$V = a(x^2+y^2) + b(z^2) + c(z^3) + d(z)(x^2+y^2)$$

to third order

$$= V_c + V_{tetg.}$$

The dipole moment p will interact with this field through its gradient. From Fig. (2b)

$$p_x \doteq px/D\ (1 - z/D)$$

$$p_y \doteq py/D\ (1 - z/D)$$

(a)

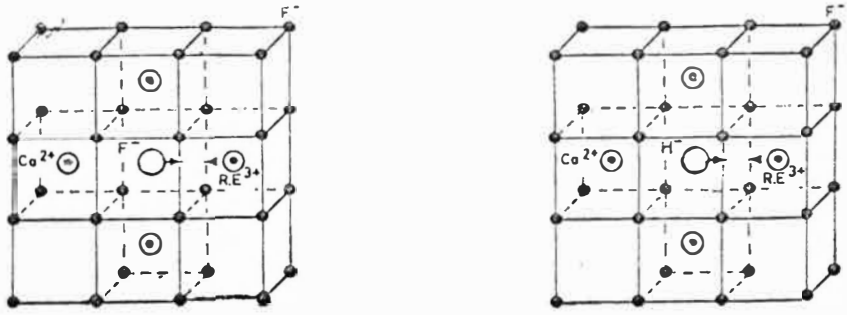

(b)

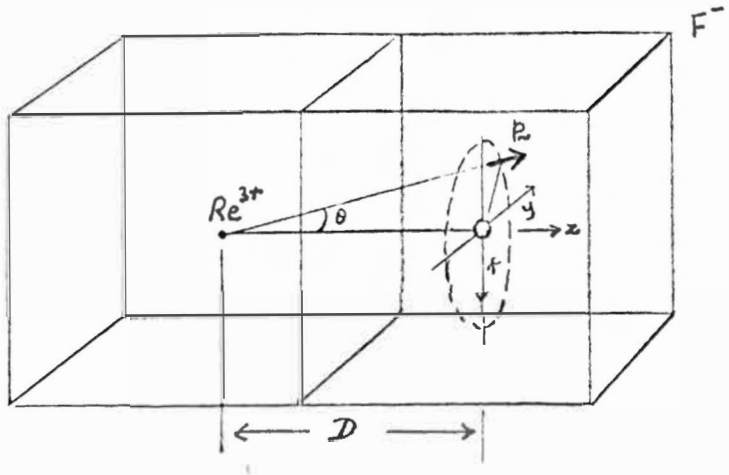

Fig (2).

a . . Schematic representation of the calcium fluoride lattice showing the tetragonal Re^{3+} site with interstitial charge compensators.

b . . Schematic representation of the dipole moment $\underset{\sim}{p}$ of the H^- ion.

2D - The unit cell dimension is 5.45 A^o-CaF_2
5.78 A^o-SrF_2
and 6.19 A^o-BaF_2

$$p_z \doteq p/D \left(1 - \tfrac{1}{2}\left(\frac{x^2+y^2}{D^2}\right) + \frac{z(x^2+y^2)}{D^3}\right.$$

$$V_e = -A/q \quad (x^2+y^2+z^2)$$

$$\therefore \quad \underset{\sim}{p}.\nabla V_e = -\frac{2Ap}{qD}(x^2+y^2) + \frac{3Ap}{qD^2} z(x^2+y^2) - \frac{2Ap}{qD}(z)$$

$$V_{tetg} = \sum_k \frac{\sigma\, v^k}{D^{k+1}} P_k^0(-1)\, Y_k^0(\theta,\varphi) \sqrt{\frac{4\pi}{2k+1}}$$

Expanding in terms of cartesian coordinates etc. gives

$$\underset{\sim}{p}.\nabla V_{tetg} = -\frac{p\sigma}{D^2} + \frac{2p\sigma}{D^3}z - \frac{3p\sigma}{D^4}z^2 + \frac{4p\sigma}{D^5}z^3 \ldots$$

$$+ \frac{p\sigma}{D^4}(x^2+y^2) - \frac{4p\sigma}{D^5}z(x^2+y^2) \text{ to terms in 3rd order.}$$

Which gives, on equating coefficients

$$a = A + \frac{\sigma q}{2D^3} + \frac{p\sigma}{D^4} - \frac{2Ap}{qD}$$

$$b = A - \frac{\sigma q}{D^3} - \frac{3p\sigma}{D^4}$$

$$c = \frac{\sigma q}{D^4} + \frac{4p\sigma}{D^5}$$

$$d = -\frac{3\sigma q}{2D^4} - \frac{4p\sigma}{D^5} + \frac{3Ap}{qD^2}$$

These expressions will be referred to as required.

The Electronic Levels of Ions in Crystals

The crystal field theory dates back to the work of Bethe[36] and Kramars[37] and along with the theory of free ion spectra is well known, at least in general outline.

The free ion Hamiltonian may be written as:

$$H_f = -\frac{\hbar^2}{2m}\sum_i \nabla_i^2 - \sum_i \frac{2e^2}{r_i} + \frac{1}{2}\sum_{i\neq j}\frac{e^2}{r_{ij}} + \sum_i \xi(r)\underset{\sim}{\ell}_i \cdot \underset{\sim}{s}_i$$

where the symbols have their usual meanings.

When the ion is embedded in a crystal lattice the spherical symmetry which characterises the free ion is destroyed. H is no longer invariant under infinitesimal rotations but only under the operations of the point group which describes the site symmetry.

Provided that the electrons are sufficiently localised the effect of the ligands may be represented by a static potential V.

$$H = H_f + V.$$

We may distinguish two cases.

(1) Very weak crystal field having less effect on the energy levels than the spin orbit coupling term. The f electrons of the rare earths are 'shielded' by the 5s and 5p electrons and may be treated in this way.

(2) Weak crystal field where the effect of the ligands is stronger than the spin orbit coupling but weaker than

the Coulomb interaction term. This case is appropriate for treating the excited 5d levels of the rare earths.

The potential V may be conveniently written as a series of spherical harmonics

$$V = \sum_i \sum_{kq} A_k^q \, r_i^k \, p_k{}^q (\cos \theta_i) \, e^{iq\varphi_i}$$

where $k = 0, \infty$, $|q| \leqslant k$ and the summation is carried out over all the 4f electrons. Fortunately only a few of the terms in this infinite expansion give non-zero contributions to the matrix elements between electronic states. The calculation of energy levels will involve integrals of the form

$$\int R_{4f}^2 r^k r^2 dr \iint p_3^{m'} p_3^{m''} p_k^q \, e^{i(m''-m'+q)\varphi} \sin\theta \, d\theta d\varphi$$

The integral over r gives $\langle r^k \rangle$ the average value of r^k. The integral over θ and φ is zero unless $k \leqslant 6$ for f electrons, k is even, and $(m''-m'+q) = 0$.

The A_k^q are often defined in terms of V_k^q (Stevens 1952) see table (Dieke). Alternately they may be expressed in terms of tensor operators $C_q^{(k)}$ or spherical harmonics Y_k^q.

$$V_k^0 = N(C_q^{(k)}) \, C_q^{(k)}$$

$$V_k^{\pm q} = N(C_q^{(k)})[C_q^{(k)} \pm C_{-q}^{(k)}]$$

where the $N(C_q^{(k)})$ are normalisation constants. Since there is no reliable way of accurately determining the radial

integrals the theory has been most successful if the $A_k^q\langle r^k\rangle$ are defined as a single coefficient B_k^q and the B_k^q taken as parameters to be obtained experimentally.

The matrix elements of V with electronic states characterized by the quantum numbers SLJM may be evaluated by making use of the Wigner-Eckart theorem

$$\langle \alpha JM|V_k^q|\alpha' J'M'\rangle = (-1)^{J-M}\begin{pmatrix} J & k & J' \\ -M & q & M' \end{pmatrix}\langle \alpha J||V_k||\alpha' J'\rangle$$

The reduced matrix elements are independent of M and must be calculated for each pair of states. Tables for the evaluation of Rare Earth f level matrix elements in both LS and coupling are given in (5). The lowest lying levels are in general fairly well isolated and the intermediate coupling effects are not large.

Once the interaction matrices have been obtained they must be diagonalised to find the energy levels.

The resulting energy levels for various J values in crystal fields of cubic symmetry have been reviewed by Lea Leosk and Wolf[38]. In fields of lower symmetry the remaining degeneracies are lifted.

The Electron-Phonon Interaction

Following Jones and Satten[14] we write the interaction Hamiltonian as

$$V_{ev} = \sum_i f_i Q_i + \sum_{ij} g_{ij} Q_i Q_j + \cdots$$

where the Q_i and Q_j are normal coordinates of vibration of the lattice and f and g are functions of the electron coordinates.

For the rare earth, hydride ion pair in C_{4v} symmetry this expression becomes

$$V_{ev} = f_x X + f_y Y + f_z Z + \tfrac{1}{2}(g_{xx}+g_{yy})(X^2+Y^2)$$
$$+ \tfrac{1}{2}(g_{xx}-g_{yy})(X^2-Y^2) + g_{xx}X^2 + g_{yy}Y^2 + g_{zz}Z^2$$

where X, Y, Z are the normal coordinates of the hydride ion displacement.

The crystal field potential may be expanded as a Taylor series in the light ion displacements to give

$$V_c = V_{cO} + \sum_i \left(\frac{\partial V_{cO}}{\partial X_i}\right)\Delta X_i + \tfrac{1}{2}\sum_{ij} \frac{\partial^2 V_{cO}}{\partial X_i \partial X_j} \Delta X_i \Delta X_j + \cdots$$

The electronic functions of the electron-phonon interaction can thus be obtained by the differentiation of the crystal field potential with respect to the light ion coordinates. Provided overlap and covalency effects are neglected the crystal field potential of the cerium ions electron in the field of the hydride ion can be expressed in terms of solid harmonics defined as follows:

$$T_{n,x}^{m} = r^{n} p_{n}^{m}(\cos\theta) \cos m\varphi$$

$$T_{n,y}^{m} = r^{n} p_{n}^{m}(\cos\theta) \sin m\varphi$$

where r, θ, φ are the polar coordinates of the electron and $m \leqslant n$ where $p_{n}^{m}(\cos\theta)$ are the legendre polynomials.

The Coulomb potential at r of a point charge at R can now be written down since for $|\underset{\sim}{R}| > |\underset{\sim}{r}|$

$$\frac{1}{|\underset{\sim}{R}-\underset{\sim}{r}|} = \Sigma M_{n}^{m} R^{-(2n+1)} \left[T_{nx}^{m}(\underset{\sim}{R}) T_{n,x}^{m}(\underset{\sim}{r}) + T_{ny}^{m}(\underset{\sim}{R}) T_{n,y}^{m}(\underset{\sim}{r}) \right]$$

where $M_{n}^{m} = 2 \frac{(n-m)!}{(n+m)!}$ for $m \neq 0$

and $M_{n}^{0} = 1$

This relation can also be used to derive the dipole moment potential given by p.grad $\frac{1}{|\underset{\sim}{R}-\underset{\sim}{r}|}$. The resulting expressions are somewhat lengthy and may be obtained from (35). Differentiation is greatly facilitated by the use of recurrence relations also given in (35).

V_{ev} transforms as the totally symmetric representation of $C_{\infty v}$ and the f_{i}, g_{ij} functions will transform as the same irreducible representations as the corresponding functions of light ion displacements. The following relations hold between the solid harmonics and the f_{i} and g_{ij}.

$$f_{z} = a_{0n} T_{n}^{0} \qquad f_{x} = a_{1n} T_{nx}^{1} \qquad f_{y} = a_{1n} T_{ny}^{1}$$

$$g_{zz} = b_{0n}T^0_n \qquad g_{xz} = b_{1n}T^1_{nx} \qquad (g_{xx}-g_{yy}) = b_{2n}T^2_{nx}$$

$$(g_{xx}+g_{yy}) = c_{0n}T^0_n \qquad g_{yz} = b_{1n}T^1_{ny} \qquad g_{xy} = c_{2n}T^2_{ny}$$

The constants a_{0n} etc. will depend on the particular model chosen for the light ion interaction.

The simplest is the point charge model for which the potential of the cerium ion in the point charge field of the hydride ion is a function of the difference in the cartesian coordinates of the electron and hydride ion, so that:

$$\frac{\partial V_c}{\partial X_i} = -\frac{\partial V_c}{\partial x_i}$$

Using this together with the generating function for legendre polynomials,

$$(1 - 2tz + t^2)^{-\frac{1}{2}} = \sum_{k=0} t^k p^0_k(z)$$

gives the following values for the constants.

$$a_{0n} = -(n+1)eq\ D^{-(n+2)}$$

$$b_{0n} = -c_{0n} = \tfrac{1}{2}(n+1)(n+2)eq\ D^{-(n+3)}$$

$$a_{1n} = -eq\ D^{-(n+2)}$$

$$b_{1n} = (n+2)eq\ D^{-(n+3)}$$

$$b_{2n} = c_{2n} = eq\ D^{-(n+3)}$$

where D is the separation, at equilibrium, of the hydride and rare earth ions. Since Laplaces equation is satisfied we have also

$$g_{xx} + g_{yy} + g_{zz} = 0.$$

The corresponding constants for the dipole model are obtained in the same way and their values are given by

$$a_{0n} = -(n+1)(n+2)epD^{-(n+3)}$$

$$a_{1n} = -(n+3)epD^{-(n+3)}$$

$$b_{0n} = \tfrac{1}{2}(n+1)(n+2)(n+3)peD^{-(n+4)}$$

$$c_{0n} = -\tfrac{1}{2}(n+1)[(n+1)(n+2)+2]peD^{-(n+4)}$$

These expressions have been used in the estimation of the magnitudes of the various electron-phonon interaction effects observed in this work. The limitations of the models are best illustrated by a discussion of particular examples and will be dealt with in succeeding sections.

C H A P T E R I I I

EXPERIMENTAL CONSIDERATIONS

Calcium, strontium and barium fluoride have the same crystal structure, space group O_h^5. The lattice may be visualised as the superposition of three face centred cubic lattices or, more usefully for this work as a simple cubic lattice of monovalent fluorine ions every second box of which is occupied by a divalent metal ion (Fig. 2). The crystals are ideal hosts for optical studies being transparent from the middle infrared to the far ultraviolet and non-hygroscopic. The samples used in this work were either cleaved along (111) planes or cut with a diamond saw and polished on a felt lap with tin oxide powder.

Rare earth ions can be incorporated at divalent cation sites when the crystals are grown from a melt containing both metal and rare earth fluorides (Stockbarger method). Since the trivalent rare earths have radii very similar to the ions which they replace no serious disruption of the lattice takes place with rare earth concentrations as high as 5%. Some form of charge compensation is however required. Unless precautions are taken this is achieved by the replacement of F^- by O^{2-} ions. The addition of lead fluoride to the melt removes the oxygen and charge compensation is then effected largely by interstitial fluorine ions (Fig. 2).

The rare earth doped calcium fluoride crystals used were purchased from the Hebrew University of Jerusalem, Israel. Strontium and barium fluoride crystals were obtained from Optovac Inc. Nominal rare earth concentrations of 0.05% were found to be convenient in most cases and have been used except where otherwise stated. At concentrations of 0.2% and above all spectral lines become broadened due to small lattice distortions and in some cases the spectra become confused with many lines due to rare earth ions in a multiplicity of lattice sites.

Hydrogenation

The cut and polished samples were placed in a carbon boat with aluminium metal and heated to 500°C in a high vacuum for several hours in a quartz tube. Hydrogen or deuterium gas introduced to two thirds atmospheric pressure and the temperature raised to 800°C for periods of up to twenty four hours. During this time the molten aluminium must maintain good contact with the crystal and to this end care must be taken to ensure that the hydrogen is both dry and completely free from oxygen. In order to increase the concentration of tetragonal centres relative to other possibilities the crystals were rapidly quenched to room temperature by removal from the furnace. In this way tetragonal rare earth-hydride ion pairs are formed at typically one tenth the density of the analogous interstitial fluorine ion

centres for calcium fluoride and one twentieth for strontium fluoride. It appears[39a] that these centres are not formed for rare earths near the end of the sequence for strontium fluoride.

Tritium was introduced into the crystals in the same way at one tenth atmospheric pressure. A glass capsule containing two cubic centimetres of tritium gas was sealed into the quartz tube and broken with a ball bearing and external magnet. Hydride centres were found to be present in all crystals doped in this way in the approximate ratio ($H^-:T^-$) of 4:1. The tritiated crystals became strongly coloured after several days due to the strong optical absorption of divalent rare earth ions produced by the low energy beta emission from the tritium. Baking at 300°C for several hours largely removed these centres and allowed optical measurements to be repeated. Oxygen was introduced into the as grown crystals by heating to 900°C in an oxygen atmosphere. More complete conversion to oxygen centres is however effected by first hydrogenating the samples as above.

In addition to the two fluorides above barium and cadmium fluoride and strontium chloride have the same crystal structure and were considered as possible host materials. Several attempts to obtain tetragonal hydride centres in barium fluoride were unsuccessful. It has been noted by previous workers[39b] that tetragonal fluorine centres are

also not readily formed in this material. Cadmium fluoride is attacked by molten aluminium and cannot be hydrogenated in the normal way.

Attempts to hydrogenate pure cadmium fluoride by heating to 600°C in an atmosphere of hydrogen and in the presence of cadmium metal were unsuccessful. Strontium chloride cerium doped crystals were grown in this laboratory by R. Ritchie. Since when subjected to the thermal shock required to quench hydrogenated samples these crystals became opaque and since the lattice constant is larger than barium fluoride for which no tetragonal centres could be formed, no effort was made to refine the growth techniques to remove oxygen impurities.

Instrumentation

Measurements were made in the 600-3000 cm^{-1} range with a Beckman IR12 infrared spectrophotometer providing a maximum resolution of 0.3 cm^{-1} at 1000 cm^{-1}.

Optical spectra were recorded photoelectrically using a ¾-meter Czerny Turner spectrometer made by Spex Industries Inc. with a dispersion of eleven angstroms per millimeter in the ultraviolet. This instrument provided sufficient resolution and is more convenient than a larger spectrometer for recording weak fluorescence spectra. Wavelength markers were frequently calibrated with an iron hollow cathode lamp containing a little neon. Wavelength measurements to within 0.2 angstroms can readily be made.

For absorption measurements the dense filament of a one hundred watt quartz-iodine lamp was used as source from 2500-6000 A^{o} being replaced by a deuterium lamp at shorter wavelengths. Various Corning glass filters were used to remove unwanted spectral orders and were placed between the source and the dewar to reduce radiation heating.

Fluorescence spectra were obtained using a Philips 500 watt high pressure mercury lamp for excitation. Interference and glass filters were used to remove the scattered background mercury radiation. This background proved particularly troublesome in the case of cerium fluorescence. Best results were obtained using a Bausch and Lomb monochromator as filter in spite of the considerable loss of fluorescence intensity. In this way selective excitation of sites could be achieved further reducing the background and hence improving greatly the signal to noise ratio.

Low temperature optical spectra were obtained using a variable temperature dewar made by Andonian Associates. Cooling is achieved via thermal contact with a copper block, in contact with the liquid (Helium or Nitrogen).

Low temperature infrared measurements were made with a similar dewar fitted with cesium iodide windows. Thermal contact between the crystal and copper block was improved by the use of indium foil.

Photoelectric rather than photographic recording was used throughout since this provides better reproduction of the structure of absorption bands and of fluorescence spectra with high background radiation levels. The absorption spectra obtained with the Spex are in transmittance scale and must be converted to absorbance scale before comparisons are made.

C H A P T E R I V

EXPERIMENTAL RESULTS. PART ONE

Infrared Spectra

Several rapidly quenched hydrogenated crystals of calcium and strontium fluoride containing cerium and praseodymium were examined in the infrared. Typical absorption spectra obtained at liquid nitrogen temperature are reproduced in figure 3. For each host the predominant tetrahedral substitutional site absorption can be clearly seen at 965 cm^{-1} in calcium fluoride and 893 cm^{-1} in strontium fluoride. The previously reported local mode lines associated with rare earth hydride ion tetragonal pairs in calcium fluoride are reproduced and similar lines appear in the strontium fluoride spectra. New tetragonal hydride ion sites correlated in intensity with these lines in strontium fluoride have recently been observed in this laboratory by ESR[40] which confirms the assignment of these lines to tetragonal sites analogous to those in calcium fluoride. This assignment was initially made on the basis of the similarity of the optical spectra to be discussed in later chapters. The two components are less well separated in strontium fluoride and the separation is subject to more fluctuation with change of rare earth.

On the basis of an approximate 2:1 intensity ratio between the two components in the calcium fluoride rare earth

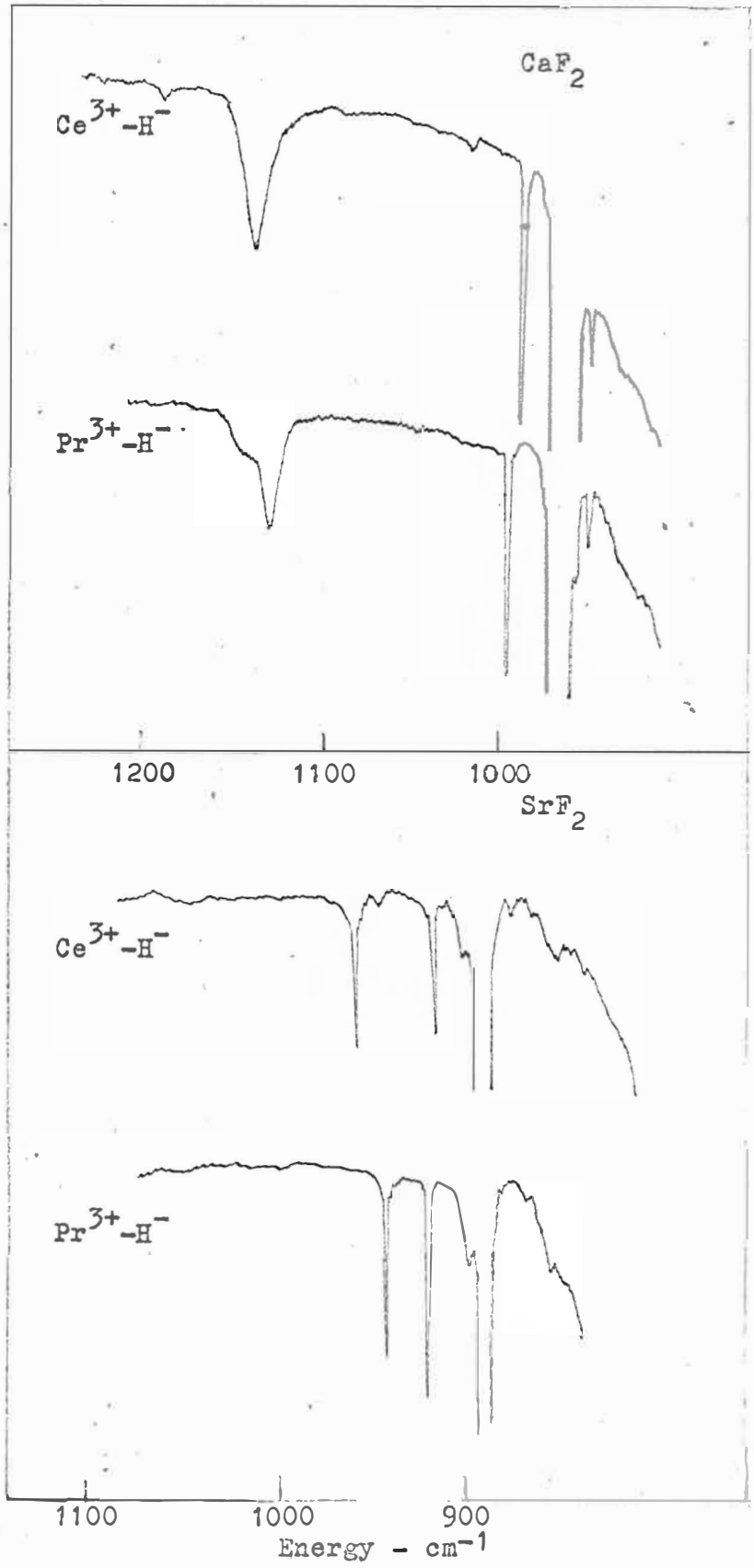

Fig (3). Infrared absorption spectra. (77°K)

series the broad high frequency line was assigned by Jones et al.[12] to the doubly degenerate (xy) vibration and the narrower low frequency line to the (z) vibration. However, as pointed out by Newman[1] and confirmed here, the ratio deviates significantly from 2:1 and for the first two members of the series is closer to 1:1 (see table 1). [The comparison for cerium in calcium fluoride is made more difficult by the superposition of a combination band (lattice phonon plus tetrahedral site local mode) and the high frequency component. The entry in table 1 has been obtained by subtracting this band, the intensity of which was determined by monitoring the intensity of the second harmonic of 965.] The assignment of modes on an intensity basis is seen to be at best tentative and some other means must be sought. Fortunately this is available without resorting to stress or electric fields to raise the degeneracy.

At lower temperatures and at high resolution the low frequency components in both host lattices containing cerium have been themselves resolved into two components. Spectra recorded at 8°K are reproduced in figure 4. The crystal temperature measured with a thermocouple clamped to the outside of the crystal is slightly above that of the liquid helium since a conduction dewar was used and some radiation heating occurred. The resolution of this line into two components explains the anomalous linewidth (viz. 2.2 cm^{-1} at

	Ce^{3+}	Pr^{3+}
CaF_2	1.0	0.9
SrF_2	1.3	1.2

Table (1). The relative intensities of the two infrared local mode absorption lines associated with each rare earth hydride ion tetragonal pair for cerium and praseodymium. The ratio is quoted as:

(low frequency component) / (high frequency component)

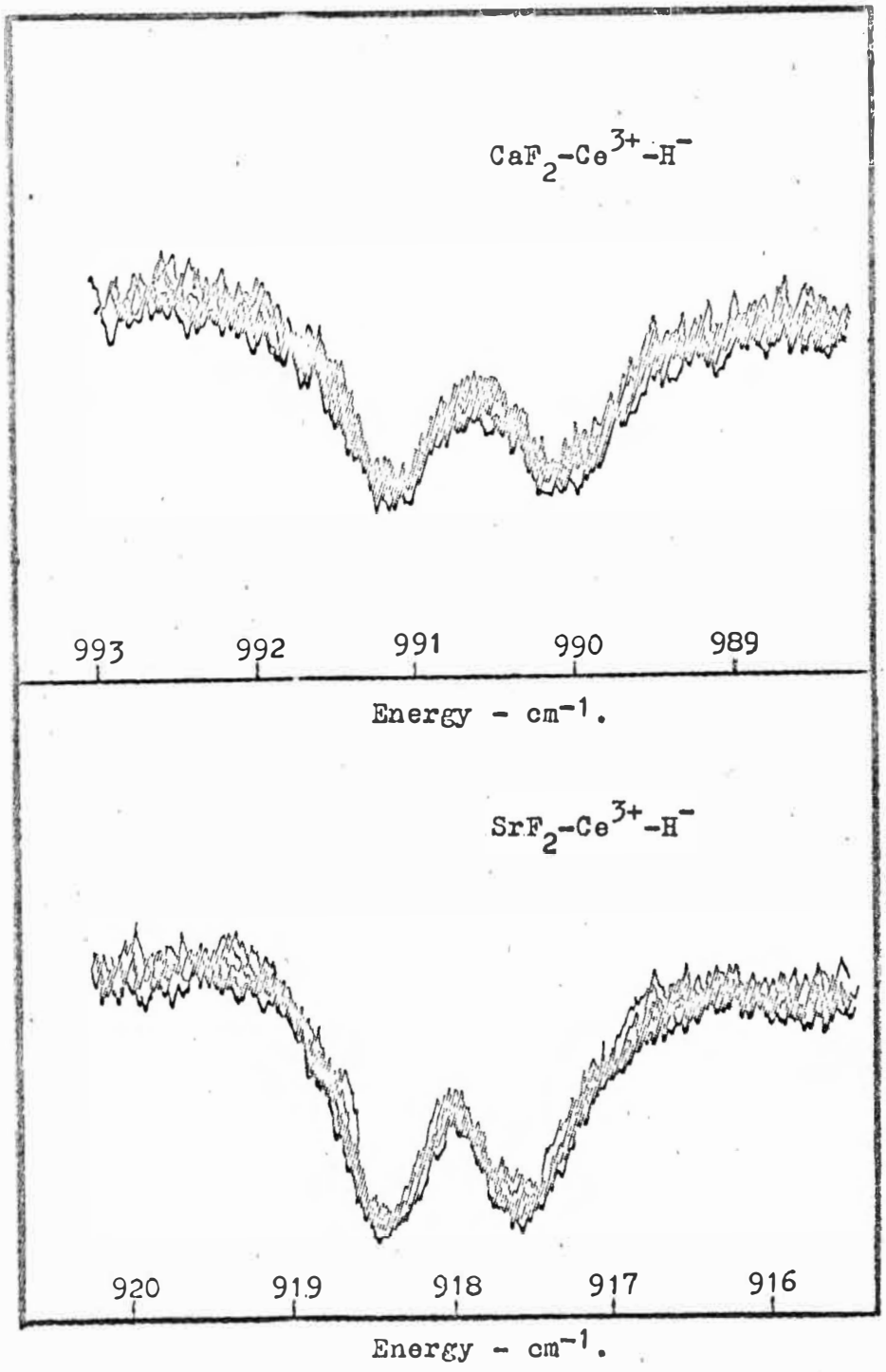

Fig (4). High resolution infra-red absorption spectra showing clearly the (xy) hydride ion local mode vibration split by the order of one wave number. In each case the effects of noise have been minimised by the superposition of several traces. Temperature 8^0K. Resolution 0.3 cm^{-1}.

20°K) listed in (12) without comment. The high energy line remains unsplit (at least with the resolution available) and appears as a single line only a little wider than a wavenumber in strontium fluoride.

Small splittings observed for both components of the analogous erbium and ytterbium centres have been discussed by Newman and Chambers[41]. They have established a mechanism for the splitting which involves a thermally populated rare earth electronic level close to the ground state. Cerium is not expected (Ch. VI) to have an excited level below one hundred wavenumbers and since the two components maintain their relative intensities down to 4°K this mechanism cannot account for the splitting in this case. The above mechanism would also be expected to producea splitting of the high frequency line which is not observed.

The situation is more involved in the case of praseodymium centres. The corresponding low temperature high resolution spectra are reproduced in figure 5. Again the low frequency line is resolved into more than one component and the high frequency line remains unsplit. The overall intensity ratios of the (xy) and (z) components are very similar to the cerium values but the low frequency line does not show the same simple two component structure. The corresponding pattern in strontium fluoride is apparently similar but the overall splitting is reduced by a factor of 3.

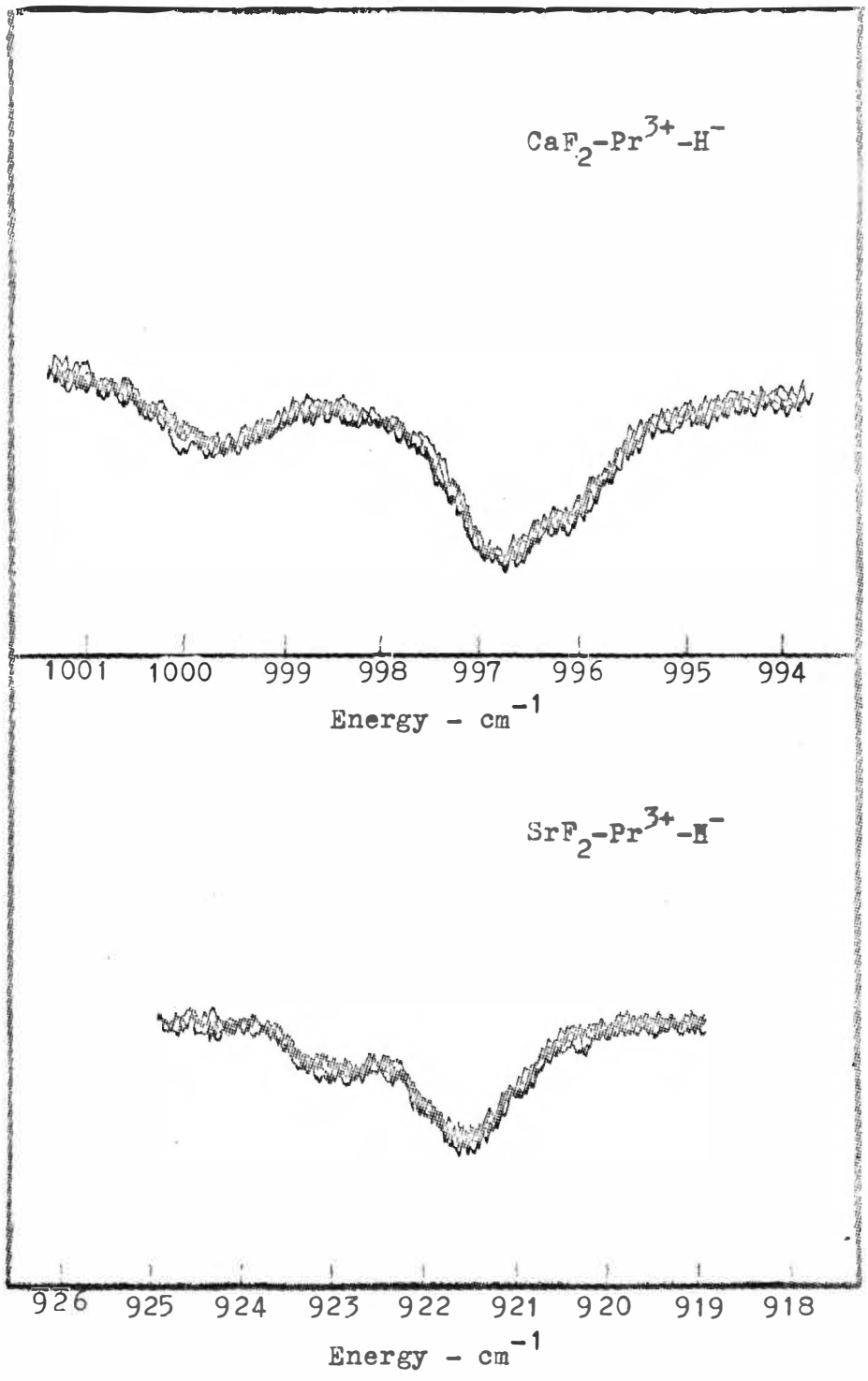

Fig. (5). High resolution infrared absorption spectra showing the splitting of the (xy) four-fold degenerate H^- local mode. Temperature 8^oK
Resolution 0.3 cm^{-1}

Similar splittings have not been observed for the other rare earths. For example, in calcium fluoride, neodymium hydride centres show only a single symmetrical line at similar resolution down to $4^{o}K$. The linewidth, 0.9 cm^{-1}, is similar to that of the individual components above.

It is apparent that the splitting in both magnitude and number of components is closely dependent on the rare earth concerned and that the magnitude of the splitting is in some cases closely dependent on the host lattice. Both these observations suggest that the effects are due to interactions involving the local modes and the low lying energy levels of the rare earths.

Vibronic Levels

Since the hydride ion is much lighter than the lattice ions the static well approximation may be used and since the anharmonic terms are relatively small the nuclear wavefunctions may in first order be written as the product of three one dimensional harmonic oscillator wavefunctions, normal coordinates x, y and z. Since the electron-phonon interaction is small the wavefunctions of the combined system (i.e. vibronic wavefunctions) may be written in the Born-Oppenheimer approximation as products of the form

$$\Psi_{in} = \phi_i \, \phi_n$$

where ϕ_i is an electronic rare earth wavefunction and ϕ_n is a harmonic oscillator wavefunction.

Both the rare earth and hydride ions occupy sites of point group symmetry C_{4v}. The properties of this group are well known[42] and its multiplication table is reproduced in table 2. Both the electronic and nuclear wavefunctions will transform as particular irreducible representations of this group.

Since the cerium ion has a single 4f electron the relevant electronic wavefunctions will have half-integral angular momentum and transform according to either the Γ_6 or Γ_7 representation of the C_{4v} double group. The first excited state of the harmonic oscillator transforms as Γ_5 and thus the combined vibronic wavefunctions will transform as

$$\Gamma_i \times \Gamma_5 = \Gamma_6 + \Gamma_7 \qquad i = 6,7$$

Thus in principle the electron-phonon interactions V_{ev} may split the (xy) vibronic level into two components. The (z) vibronic level will transform as

$$\Gamma_i \times \Gamma_1 = \Gamma_i \qquad i = 6,7$$

and thus cannot be split. Since the splitting occurs for the low frequency components in fig. 3 it is therefore concluded that these must be identified as the (xy) vibronic levels. This reversal of the previous assignment of modes is supported by the optical spectra of Chapter VI.

Γ_1	Γ_2	Γ_3	Γ_4	Γ_5	Γ_6	Γ_7	
Γ_1	Γ_2	Γ_3	Γ_4	Γ_5	Γ_6	Γ_7	Γ_1
	Γ_1	Γ_2	Γ_3	Γ_5	Γ_6	Γ_7	Γ_2
		Γ_1	Γ_2	Γ_5	Γ_7	Γ_6	Γ_3
			Γ_1	Γ_5	Γ_7	Γ_6	Γ_4
				$\Gamma_1+\Gamma_2+\Gamma_3+\Gamma_4$	$\Gamma_6+\Gamma_7$	$\Gamma_6+\Gamma_7$	Γ_5
					$\Gamma_1+\Gamma_2+\Gamma_5$	$\Gamma_3+\Gamma_4+\Gamma_5$	Γ_6
						$\Gamma_1+\Gamma_2+\Gamma_5$	Γ_7

Table (2). Multiplication table of the C_{4v} double group

The remaining odd electron rare earth ions including neodymium will also produce vibronic levels transforming as $\Gamma_6+\Gamma_7$ and in principle V_{ev} may split these levels. The absence of observable splittings for neodymium etc. will be discussed in Chapter V .

In contrast praseodymium has an even number of 4f electrons and so the electronic wavefunctions will transform as Γ_j of C_{4v} where $j = 1 \ldots 5$. If the ground state transforms as Γ_i $i = 1 \ldots 4$ then since $\Gamma_i \times \Gamma_5 = \Gamma_5$ and $\Gamma_i \times \Gamma_1 = \Gamma_i$ both the (xy) and (z) vibronic levels will give rise to single absorption lines. If however the groundstate transforms as Γ_5 then since

$$\Gamma_5 \times \Gamma_5 = \Gamma_1 + \Gamma_2 + \Gamma_3 + \Gamma_4$$

the (xy) vibronic level may in principle be split into four. Since the vibronic is split we conclude that, in agreement with the estimate of Weber and Bierig[57], the Γ_5 electronic level lies lowest in both host lattices. This conclusion is consistent with the optical data discussed in Chapter VIII. The splitting is greatest in calcium fluoride and consequently more structure can be resolved. Figure 6 shows four equal intensity Lorentzian lines fitted to the experimental data. A good fit is obtained with a small variation in linewidth. A similar pattern is apparent for strontium fluoride with an intensity ratio of 3:1 between the two peaks.

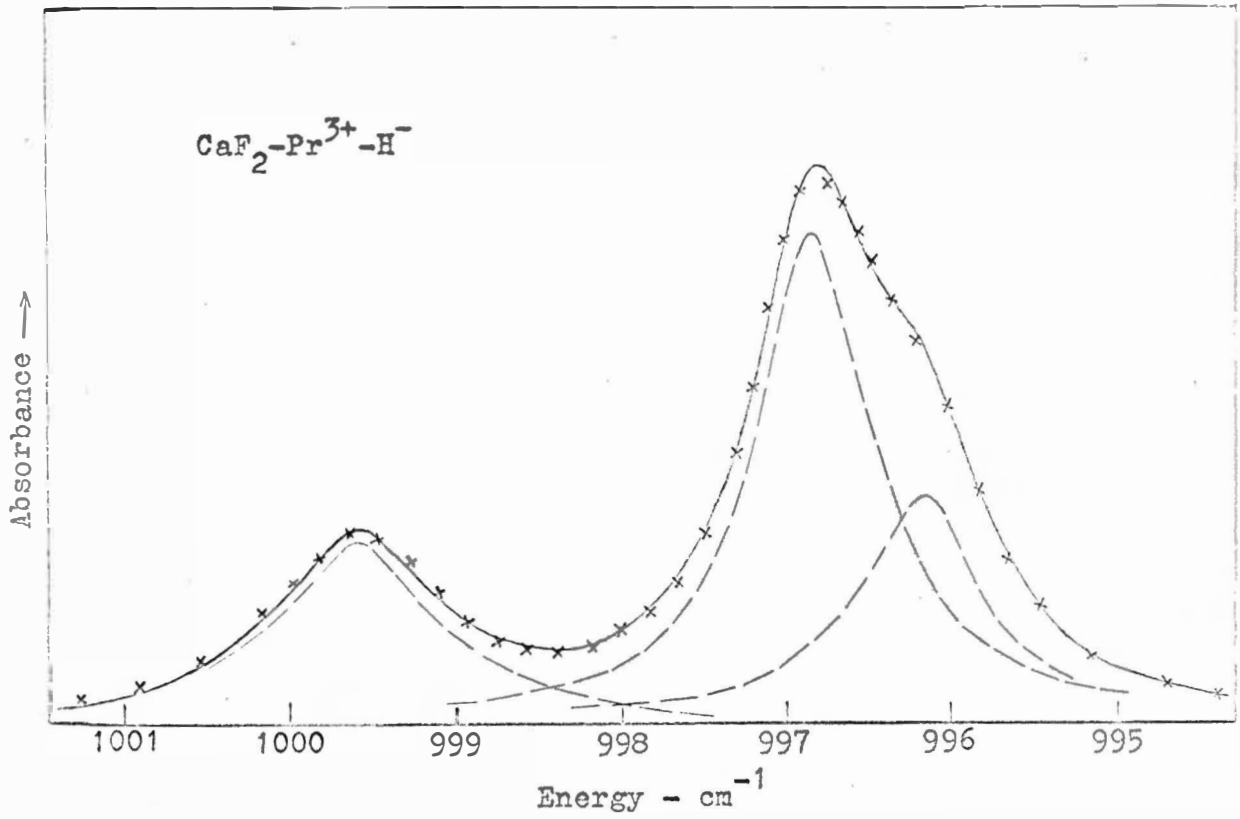

——— Calculated envelope of three lines.

× × × Experimental points.

— — —Individual lines. (See table below.)

Fig (6) above. Computer generated least squares fit of three Lorentzian lines to the infra-red absorption spectrum associated with the low energy H^- local mode vibration. Pr^{3+}-H^- tetragonal centers in CaF_2. Temperature 8^oK. Resolution 0.3 cm^{-1}.

Peak position. cm^{-1}	Width. cm^{-1}	Relative intensity.
999.5(5)	1.2(0)	1.0
996.7(2)	0.9(0)	2.0
996.1(0)	0.9(5)	1.0

The corresponding deuteride and tritide ion charge compensated sites have been observed in the ultraviolet (Chapter VI). Direct observation in the infrared is difficult because of the strong absorption of the host lattices in the appropriate regions. The situation is more favourable in the strontium fluoride case but the strong carbon dioxide absorption at 670 cm^{-1} interferes with the observation of the low frequency deuteride component. Both components were however located by Jones et al. (12) for Gd^{3+}-D^{-} tetragonal centres in CaF_2. Since decay via two phonon processes is possible, they were both 3 cm^{-1} wide even at low temperatures. The observation of fine structure will therefore be more difficult in the deuteride case.

The available data is summarised in Table 3.

Crystal Temp ($8^{o}K$)	Mode	Frequency (cm^{-1})	Linewidth (cm^{-1})	Relative intensity
CaF_2-Ce^{3+}-H^-	w_{xy}	990.0	0.7	1.0
		991.3	0.7	1.0
	w_z	1131.5	6.5	2.0
SrF_2-Ce^{3+}-H^-	w_{xy}	917.5	0.7	1.0
		918.6	0.7	1.0
	w_z	957.7	1.4	1.6
CaF_2-Pr^{3+}-H^-	w_{xy}	996.1	0.9	1.0
		996.7	0.9	2.0
		999.5	1.2	1.0
	w_z	1117.3	7.5	4.8
SrF_2-Pr^{3+}-H^-	w_{xy}	921.5	1.2	3.0
		922.9	1.0	1.0
	w_z	939.7	1.2	3.4
CaF_2-Ce^{3+}-D^-	w_z	817.8	3.7	...
SrF_2-Ce^{3+}-D^-	w_z	696.3	4.3	...

Table (3). Infrared absorption measurements for the tetragonal, rare earth, hydride ion sites.

C H A P T E R V

A DISCUSSION OF THE INFRARED SPECTRA

PART I: Vibronic Splittings

Cerium-Hydride Centres

To estimate the magnitude of the splittings to be expected we must evaluate the first and second order perturbations of the vibronic levels by the electron-phonon interaction. We write:

$$V_{ev} = f_x X + f_y Y + f_z Z + \ldots + \tfrac{1}{2}(g_{xx}-g_{yy})(X^2-Y^2) \ldots$$

First order interactions involving the first degree terms in V_{ev} will be zero since the nuclear parts of matrix elements between the vibronic levels are zero for the harmonic oscillator. First order interactions involving the second degree terms will also not contribute to a splitting since, for example, $(g_{xx}-g_{yy})$ transforms as Γ_4 of C_{4v} and the direct product $\Gamma_7 \times \Gamma_4 \times \Gamma_7$ does not contain Γ_1. The electronic parts of the matrix elements will therefore be zero. The first non-zero contribution will arise from the first degree terms in V_{ev} acting in second order via intermediate vibronic states as follows.

Following Satten (private communication)

$$V_{ev} = \tfrac{1}{2}\left[(f_x+if_y)(X-iY) + (f_x-if_y)(X-iY)\right] + \ldots$$

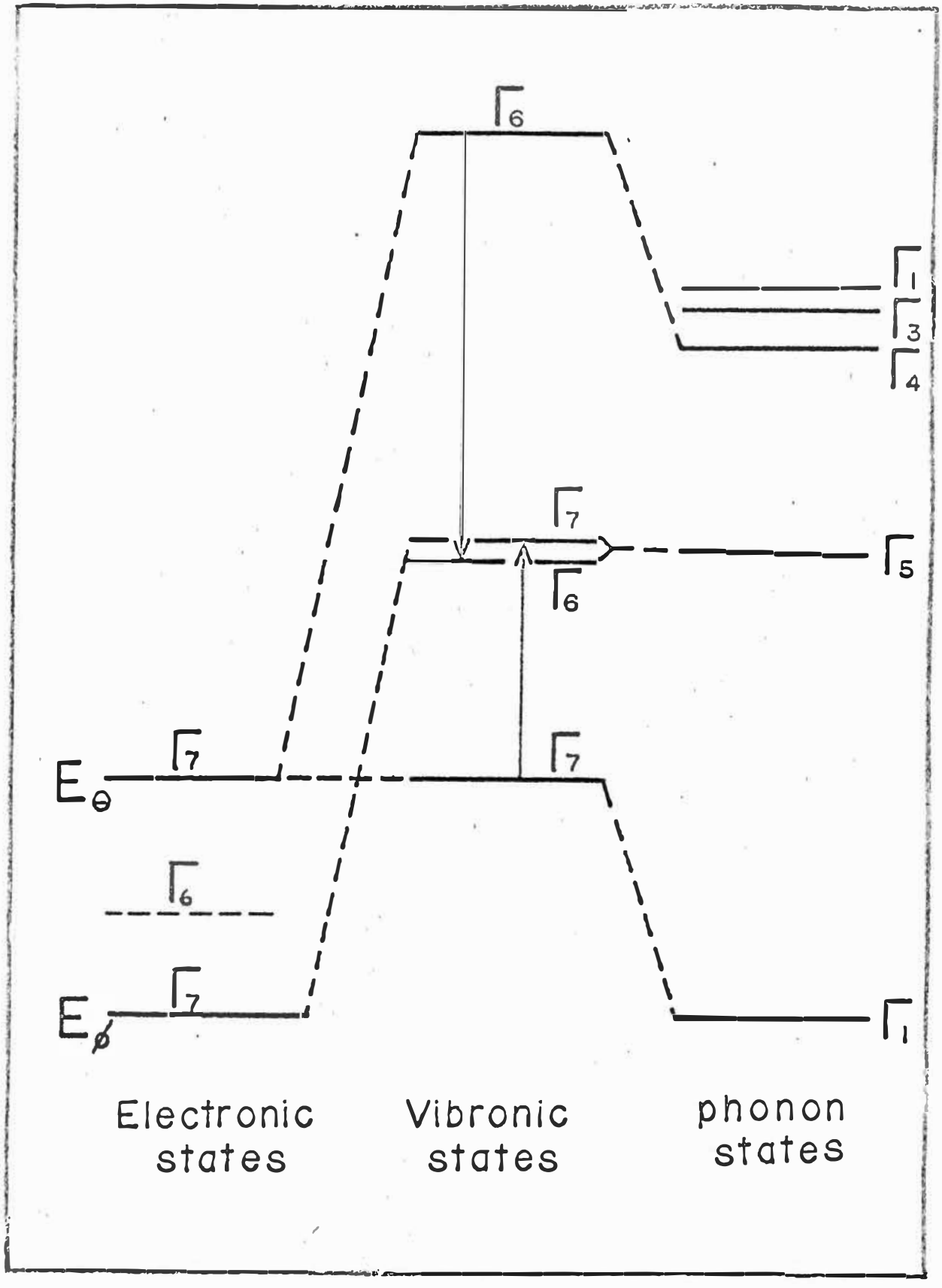

Fig (7). The low lying Cerium electronic states and the (xy) local mode phonon states which give rise to the vibronics shown.

$$= - [f_+ X_- + f_- X_+] + \ldots$$

The f_+ etc. transform as particular rows of Γ_5 and we need now only calculate diagonal matrix elements. If α, β are electronic wavefunctions transforming as Γ_6 and δ, γ as Γ_7 we may list various products which have the same transformation properties (see table 4).

The low lying electronic, vibrational and vibronic states are shown in figure 7. Using standard second order perturbation theory and taking into account all the intermediate vibronic levels of the appropriate symmetry the shift of the Γ_7 level from its unsplit position is:

$$\begin{aligned}
\Delta\varepsilon_{(\Gamma_7)} &= \langle\gamma(100)|V_{ev}|\delta'(110)\rangle\langle\delta'(110)|V_{ev}|\gamma(100)\rangle/(E_{\delta'}-E_0+\hbar\omega) \\
&+ \langle\gamma(100)|V_{ev}|\delta'(000)\rangle\langle\delta'(000)|V_{ev}|\gamma(100)\rangle/(E_{\delta'}-E_0-\hbar\omega) \\
&+ \sum_{+-}\langle\gamma(100)|V_{ev}|\alpha'\ \tfrac{1}{\sqrt{2}}[\pm]\rangle\langle\alpha'\ \tfrac{1}{\sqrt{2}}[\pm]|V_{ev}|\gamma(100)\rangle/(E_{\alpha'}-E_0+\hbar\omega)
\end{aligned}$$

where $[\pm] \equiv [(200) \pm (020)]$ and a similar expression holds for $\Delta\varepsilon_{(\Gamma_6)}$.

Evaluating matrix elements of the form:

$$\langle(100)|X_+|(000)\rangle\langle(000)|X_-|(100)\rangle = -\hbar/2m\omega \quad \text{etc.}$$

we have:

Γ_6		Γ_7	
α	β	δ	γ
γX_-	δX_+	γX_+	δX_-
βX_+	αX_-	βX_-	αX_+
γf_-	δf_+	γf_+	δf_-
βf_+	αf_-	βf_-	αf_+
$\delta[+]$	$\gamma[+]$	$\alpha[+]$	$\beta[+]$
$-\delta[-]$	$\gamma[-]$	$-\alpha[-]$	$\beta[-]$

where $[\pm] = \frac{1}{\sqrt{2}} [(200) \pm (020)]$

Table (4). The transformation properties of the cerium, hydride ion vibronic levels. Each entry in a column transforms in the same way (see page 5.3).

$$\Delta\varepsilon_{(\Gamma_7)} = \frac{\hbar}{2m\omega}\left[\langle\gamma|f_-|\delta'\rangle\langle\delta'|f_+|\gamma\rangle/(E_{\delta'}-E_0+\hbar\omega) + \langle\gamma|f_-|\delta'\rangle\langle\delta'|f_+|\gamma\rangle/(E_{\delta'}-E_0-\hbar\omega)\right] + \frac{\hbar}{m\omega}\left[\langle\gamma|f_+|\alpha'\rangle\langle\alpha'|f_-|\gamma\rangle/(E_{\alpha'}-E_0+\hbar\omega)\right]$$

and

$$\Delta\varepsilon_{(\Gamma_6)} = \frac{\hbar}{2m\omega}\left[\langle\gamma|f_+|\alpha'\rangle\langle\alpha'|f_-|\gamma\rangle/(E_{\alpha'}-E_0+\hbar\omega) + \langle\gamma|f_+|\alpha'\rangle\langle\alpha'|f_-|\gamma\rangle/(E_{\alpha'}-E_0-\hbar\omega)\right] + \frac{\hbar}{m\omega}\left[\langle\gamma|f_-|\delta'\rangle\langle\delta'|f_+|\gamma\rangle/(E_{\delta'}-E_0+\hbar\omega)\right]$$

The difference in these two values gives the desired splitting.

$$\Delta\varepsilon = \frac{\hbar}{2m\omega}\Big[2i\langle\gamma|f_x|\delta'\rangle\langle\delta'|f_y|\gamma\rangle(1/(E_{\delta'}-E_0-\hbar\omega) - 1/(E_{\delta'}-E_0+\hbar\omega)) - 2i\langle\gamma|f_x|\alpha'\rangle\langle\alpha'|f_y|\gamma\rangle(1/(E_{\alpha'}-E_0-\hbar\omega) - 1/(E_{\alpha'}-E_0+\hbar\omega))\Big]$$

where the matrix elements are written in terms of f_x and f_y.

The greatest contribution will come from those intermediate vibronic states which lie closest to that of the local mode phonon. For the cerium case these energy levels have been shown in figure 7 and their energies are discussed in Chapter VI. The two states are, in terms of $|M_L\ M_S\rangle$,

$$|^2F_{5/2},\Gamma_7\rangle = -\sqrt{\frac{1}{42}}\,|\mp2,\mp\tfrac{1}{2}\rangle + \sqrt{\frac{6}{42}}\,|\mp2,\pm\tfrac{1}{2}\rangle + \sqrt{\frac{10}{42}}\,|\pm1,\pm\tfrac{1}{2}\rangle - \sqrt{\frac{25}{42}}\,|\pm2,\mp\tfrac{1}{2}\rangle$$

and

$$|^2F_{5/2},\Gamma_6\rangle = \sqrt{3/7}\ |0\mp\tfrac{1}{2}\rangle - \sqrt{4/7}\ |\mp 1,\pm\tfrac{1}{2}\rangle$$

similarly the ground state wave function is the $|^2F_{5/2},\Gamma_7\rangle$ Kramers doublet given by:

$$|^2F_{5/2},\Gamma_7\rangle = \sqrt{\frac{5}{42}}\ |\mp 2,\mp\tfrac{1}{2}\rangle - \sqrt{\frac{30}{42}}\ |\mp 3,\pm\tfrac{1}{2}\rangle$$
$$+ \sqrt{\frac{2}{42}}\ |\pm 1,\pm\tfrac{1}{2}\rangle - \sqrt{\frac{5}{42}}\ |\pm 2,\mp\tfrac{1}{2}\rangle \text{ (see ref. 43)}$$

We may obtain an estimate of the order of magnitude of the splitting by using these wavefunctions and the point charge model outlined in Chapter II. The matrix elements given in the expression for $\Delta\varepsilon$ above are non zero only for a_{12} and a_{14} in the point charge expressions for f_x and f_y given in Chapter II. These matrix elements are:

$$\left[\frac{6}{35}\sqrt{10}\langle r^2\rangle a_{12}\right]^2 + \left[\frac{2}{21}\sqrt{10}\langle r^4\rangle a_{14}\right]^2$$

and

$$\left[\frac{2}{35}\sqrt{6}\ \langle r^2\rangle a_{12}\right]^2 + \left[\frac{5}{63}\sqrt{6}\ \langle r^4\rangle a_{14}\right]^2$$

Using the point charge values of a_{12}, a_{14}; the values of $\langle r^2\rangle$ and $\langle r^4\rangle$ given by Bron[44] and the energy level separations given in Chapter VI (Fig. 7) gives the contributions to the xy splitting as 5.2 and -0.2 cm^{-1} for the Γ_7 and Γ_6 derived states respectively. The net splitting of 5 cm^{-1} is in reasonable agreement with the observed value considering the limitations of the point charge model and shows that V_{ev} can account for the splitting.

The corresponding intermediate levels for strontium fluoride have not been found but a comparison with other rare earth ions in the two lattices indicates that the excited (Γ_7) level probably lies about 450 cm^{-1} above the ground state.

This reduction in separation is largely compensated for by the reduction in local mode frequency. This coupled with the relative insensitivity of the splitting to the exact energy difference leads to a predicted reduction in splitting of only ~5%. Including a small increase in the value of D (fig. 1) the point charge model leads to an expected value of the splitting in strontium fluoride of about 90% of that in calcium fluoride in good agreement with experiment (Table 3).

Other contributions to the splitting will arise due to second order interactions via the remaining 4f levels. These are the $^2F_{7/2}$ levels (Chapter VI) which lie about 2000 cm^{-1} above the ground state. Using the wave functions given in (43) their total calculated contribution is of the order of 0.1 cm^{-1} and they may thus be neglected. Similarly second and higher degree terms in V_{ev} acting via intermediate vibronic states involving (z) as well as (xy) phonon states in all cases give contributions too small to account for the observed splittings.

The dipole model, outlined in Chapter II, gives a further contribution of 6 cm^{-1} taking $a_{12} = 5ep/D^5$ and $a_{14} = 7ep/D^7$ with p ~ 1.1 Br (page 2.15).

Praseodymium Hydride Centres

The calculation of the local mode splitting in this case proceeds in the same way. There are however many more contributions since the $^3H_4$ ground state splits into seven levels in a tetragonal field (figure 8). The second degree terms of V_{ev} can also contribute in first order since $\Gamma_5 \times \Gamma_i \times \Gamma_5$ where $i = 1 \ldots 4$ contains Γ_1 and so the electronic parts of the matrix elements need not be zero as above.

To determine the expected splitting pattern we shall first evaluate the dominant second order contributions as above, followed by the first order effects due to the second degree terms in V_{ev}.

The wavefunctions of the doubly degenerate Γ_5, $^3H_4$ groundstate of the praseodymium ion in terms of $|J\ M_j\rangle$ states are:

$$\psi^+ = \sqrt{\tfrac{7}{8}}\ |+3\rangle - \sqrt{\tfrac{1}{8}}\ |-1\rangle$$

$$\psi^- = \sqrt{\tfrac{7}{8}}\ |-3\rangle - \sqrt{\tfrac{1}{8}}\ |+1\rangle \qquad (45)$$

Forming vibronic wavefunctions as products of these states with the (100) and (010) vibrational wavefunctions gives the following states which transform according to particular single valued representations of C_{4v}.

$$\psi_1 = \frac{1}{\sqrt{2}} [\psi_\alpha(010) + i\psi_\beta(100)] \ldots \Gamma_1$$

$$\psi_2 = \frac{1}{\sqrt{2}} [\psi_\alpha(100) - i\psi_\beta(010)] \ldots \Gamma_2$$

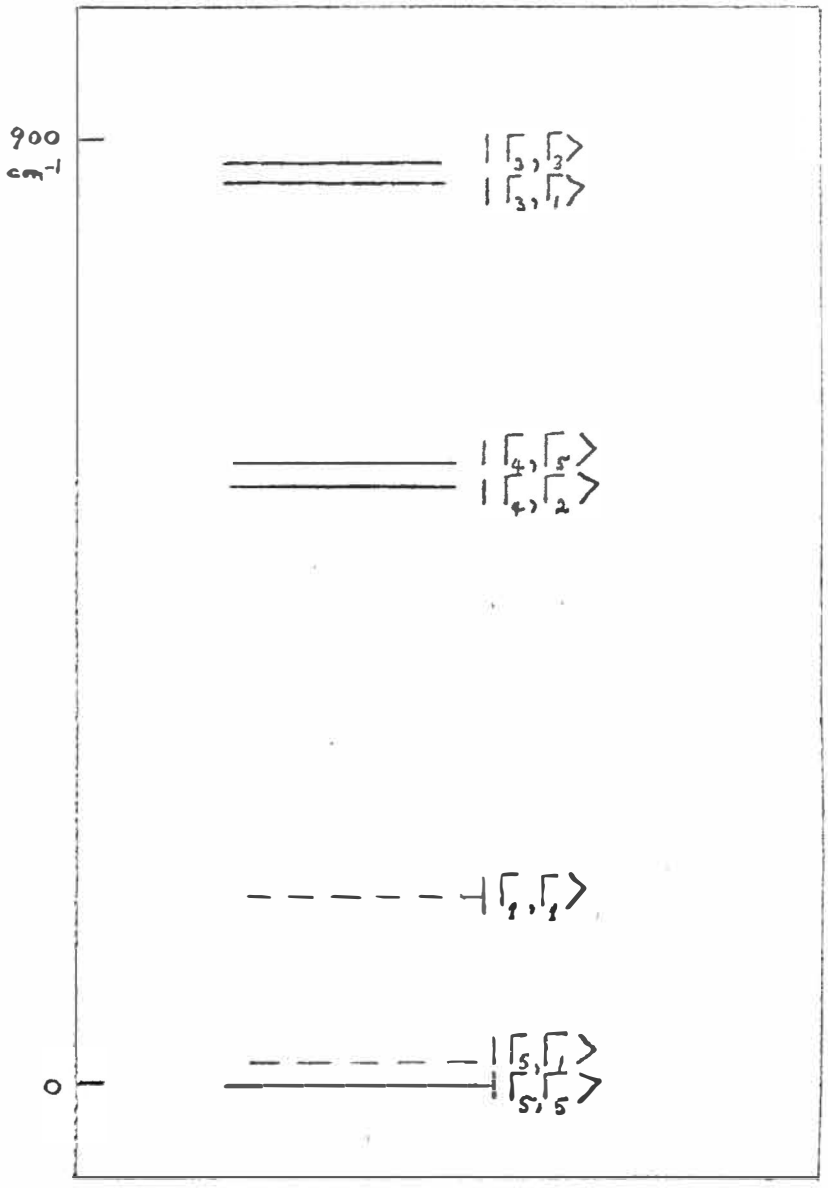

Fig (8).

Approximate energy level diagram for the Pr^{3+} ion (Pr^{3+}-H^- tetg. centres) based on the availible F^- and O^{2-} site data. (Chapter VIII).

$$\psi_3 = \frac{1}{\sqrt{2}}[\psi_\alpha(010) - i\psi_\beta(100)] \ldots \Gamma_3$$

$$\psi_4 = \frac{1}{\sqrt{2}}[\psi_\alpha(100) + i\psi_\beta(010)] \ldots \Gamma_4$$

$$\text{where } \psi_\alpha = \frac{1}{\sqrt{2}}(\phi^+ + \phi^-)$$

$$\psi_\beta = \frac{1}{\sqrt{2}}(\phi^+ - \phi^-)$$

The wave functions of the excited levels of the $^3H_4$ ground state are given by: (45)

$$|\Gamma_3,\Gamma_3\rangle = \frac{1}{\sqrt{2}}|2\rangle + \frac{1}{\sqrt{2}}|-2\rangle$$

$$|\Gamma_3,\Gamma_1\rangle = \sqrt{\frac{7}{24}}|4\rangle - \sqrt{\frac{5}{12}}|0\rangle + \sqrt{\frac{7}{24}}|-4\rangle$$

$$|\Gamma_4,\Gamma_2\rangle = \frac{1}{\sqrt{2}}|4\rangle - \sqrt{\tfrac{1}{2}}|-4\rangle$$

$$|\Gamma_4,\Gamma_5\rangle = \frac{1}{\sqrt{8}}|\pm 3\rangle + \sqrt{\tfrac{7}{8}}|\mp 1\rangle$$

$$|\Gamma_1,\Gamma_1\rangle = \sqrt{\frac{5}{24}}|4\rangle + \sqrt{\frac{7}{12}}|0\rangle + \sqrt{\frac{5}{24}}|-4\rangle$$

$$|\Gamma_5,\Gamma_4\rangle = \frac{1}{\sqrt{2}}|2\rangle - \frac{1}{\sqrt{2}}|-2\rangle$$

where the first Γ signifies the cubic state from which they are derived.

We may draw up a table of all the relevant intermediate vibronic states which transform according to particular single valued representations of C_{4v} (table 5). Each vibronic wave function ψ_i will be shifted by second order interactions, (via the first degree terms in V_{ev}) with each state in column i of table 5.

Γ_1	Γ_2	Γ_3	Γ_4
$\|\Gamma_3\Gamma_1\rangle(000)$ $\|\Gamma_1\Gamma_1\rangle(000)$	$\|\Gamma_4\Gamma_2\rangle(000)$	$\|\Gamma_3\Gamma_3\rangle(000)$	$\|\Gamma_5\Gamma_4\rangle(000)$
$\|\Gamma_3\Gamma_2\rangle[+]$ $\|\Gamma_1\Gamma_1\rangle[+]$	$\|\Gamma_4\Gamma_2\rangle[+]$	$\|\Gamma_3\Gamma_3\rangle[+]$	$\|\Gamma_5\Gamma_4\rangle[+]$
$\|\Gamma_5\Gamma_4\rangle(110)$	$\|\Gamma_3\Gamma_3\rangle(110)$	$\|\Gamma_4\Gamma_2\rangle(110)$	$\|\Gamma_3\Gamma_1\rangle(110)$ $\|\Gamma_1\Gamma_1\rangle(110)$
$\|\Gamma_3\Gamma_3\rangle[-]$	$\|\Gamma_5\Gamma_4\rangle[-]$	$\|\Gamma_3\Gamma_1\rangle[-]$ $\|\Gamma_1\Gamma_1\rangle[-]$	$\|\Gamma_4\Gamma_2\rangle[-]$

where $[\pm] = \frac{1}{\sqrt{2}}[(200) \pm (020)]$

Table (5). The transformation properties of the low lying vibronic levels of the tetragonal praseodymium, hydride ion pair.

An initial approximation may be obtained by considering only those states lying close to the ψ_i. These are, according to Chapter VIII, the two states $|\Gamma_3, \Gamma_3\rangle(000)$ and $|\Gamma_3, \Gamma_1\rangle(000)$. Considering only these two levels and using the expressions for f_x and f_y in terms of $C^{(k)}_q$ gives

$$\Delta E_1 = \frac{\hbar}{2m\omega_x}\sqrt{\frac{(n+1)!}{(n-1)!}}\, r^n a_{1n} |\langle\psi^+ |C^n_{-1}||\Gamma_3, \Gamma_1\rangle\rangle|^2 \times$$

$$\left[\frac{1}{\hbar\omega_x - E(\Gamma_3, \Gamma_1)} - \frac{1}{\hbar\omega_x + E(\Gamma_3, \Gamma_1)}\right]$$

and

$$\Delta E_3 = \frac{-\hbar}{2m\omega_x}\sqrt{\frac{(n+1)!}{(n-1)!}}\, r^n a_{1n} |\langle\psi^+ |C^n_{+1}||\Gamma_3, \gamma_3\rangle\rangle|^2 \times$$

$$\left[\frac{1}{\hbar\omega_x - E(\Gamma_3, \Gamma_3)} - \frac{1}{\hbar\omega_x + E(\Gamma_3, \Gamma_3)}\right]$$

where for convenience we have used the tensor operators defined by

$$C^n_{\pm m} = r^{-n}\sqrt{\frac{(n-m)!}{(n+m)!}}\,(T^m_{nx} \pm iT^m_{ny})$$

Using the wavefunctions listed above the relevant matrix elements are given by:

$$\langle\psi^+ |C^2_{-1}||\Gamma_3, \Gamma_1\rangle\rangle = \frac{-13}{11.15^2} \cdot 22$$

$$\langle\psi^+ |C^2_{+1}||\Gamma_3, \Gamma_3\rangle\rangle = \frac{-13}{11.15^2} \cdot 22\sqrt{3}$$

Using these values together with the point charge expressions for a_{12} and $\langle r^2\rangle$ and the estimated energy levels from

fig. 8 give the energy shifts as:

$$\Delta\varepsilon_1 \sim 15\ \text{cm}^{-1}$$

$$\Delta\varepsilon_2 \sim 4\ \text{cm}^{-1}, \text{ for calcium fluoride.}$$

The remaining contributions from the other intermediate levels to these and the remaining energy levels are small $\sim 1\ \text{cm}^{-1}$ and the energy levels alone are not known with sufficient accuracy to warrant their inclusion.

We need however to estimate the contributions to the energy shifts from the second degree terms of V_{ev} acting in first order perturbation. We need only calculate diagonal matrix elements of V_{ev} and remembering that for the point charge model $g_{zz} = -(g_{xx}+g_{yy})$ gives the energy shifts as:

$$E_n = \frac{\hbar}{2m\omega}\sqrt{\frac{4!}{0!}}\,\langle r^2\rangle\Big[\pm b_{22}\langle\phi^+|C^{(2)}_2+C^{(2)}_{-2}|\phi^-\rangle \pm c_{22}\langle\phi^+|C^{(2)}_{-2}-C^{(2)}_2|\phi^-\rangle\Big]$$

which includes contributions from g_{xy} and $(g_{xx}-g_{yy})$. The shifts of the individual components are given by taking the appropriate signs in the above, viz. (-,-); (+,+); (+,-); and (-,+) for E_1, E_2, E_3 and E_4 respectively.

The matrix elements $\langle\phi^+|C^{(2)}_2|\phi^-\rangle$ and $\langle\phi^+|C^{(2)}_{-2}|\phi^-\rangle$ are given by $7.13/52.11\sqrt{6}$ and $-13/11.15\sqrt{6}$ respectively. Taking these values together with the point charge values of $b_{22} = c_{22} = eq/D^5$ gives:

$$E_n = \frac{eq\langle r^2\rangle}{D^5} \frac{\hbar}{2m\omega_x} \left(\frac{13}{11.5.15}\right) \varepsilon_n$$

where $\varepsilon_1 = -\varepsilon_2 = -42$

and $\varepsilon_3 = -\varepsilon_4 = 10.$

For calcium fluoride e = q = 0.85e, $\langle r^2\rangle_{4f}$ = 1.0 Au and ω_x = 995 cm^{-1} which gives $E_n = 0.06\varepsilon_n$ and the splitting pattern shown below:

The pattern obtained previously by considering only second order interactions will be perturbed only slightly to give a final expected pattern which is shown in figure 9. This corresponds closely with the observed line structure for calcium fluoride except for a scale factor of about 5 as found previously for cerium. (The apparent agreement with experiment for the three lower levels may well be fortuitous since the calculation involves the sum of two terms and depends on imperfectly known energy levels.)

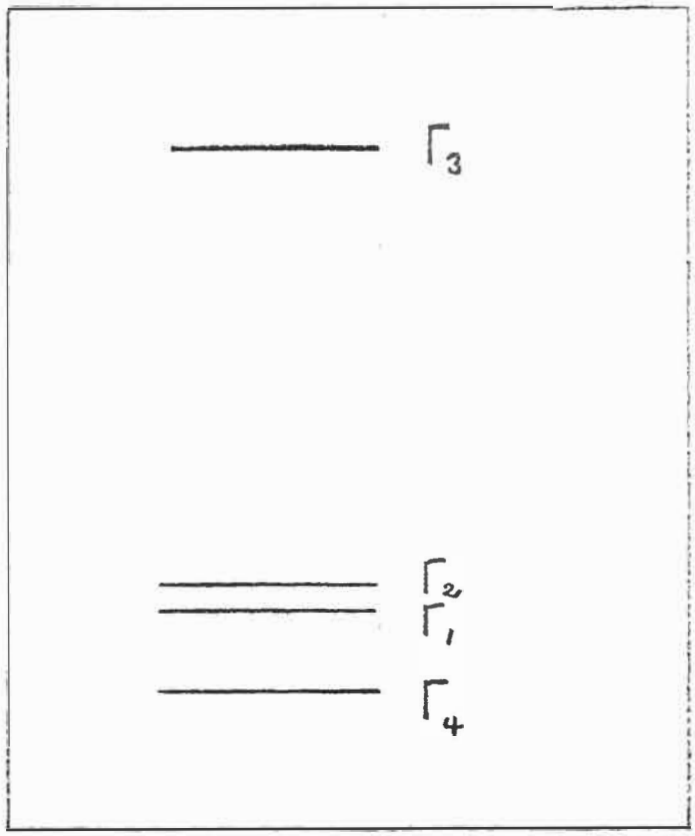

Fig (9).

Estimated splitting pattern for the four-fold degenerate (Pr^{3+}-H^{-}) local mode.

A similar estimation of energy levels may be made from the optical data for strontium fluoride as host lattice (Chapter VIII). This puts the separation between the upper electronic states and the (xy) vibronic levels as about 200 cm^{-1} which gives a corresponding reduction in splitting by a factor of about 3 in good agreement with experiment.

The above calculations account well for the splittings except for a scale factor of about five. Calculations of the magnitude of crystal field parameters on the basis of point charge models give values which are also too large. Several attempts have been made[46,47] to account for this discrepancy by supposing that the 4f electrons are shielded by the outer 5s and 5p shells. A similar effect may well account for large values obtained above.

Neodymium and the Other Rare Earths

Neodymium has an odd number of 4f electrons and hence the first excited vibronic level will transform as $\Gamma_6+\Gamma_7$ of C_{4v} and may in principle be split. The available optical data[48] puts the upper component of the lowest multiplet no more than 200 cm^{-1} above the ground state. The second order interactions will therefore be small. The xy component local mode linewidth of 0.9 cm^{-1} is a little greater than the width of the individual cerium components and may well reflect a small unresolved splitting.

For the remaining rare earths splittings will only occur if the electronic groundstates are degenerate and there are excited electronic levels close to the local mode phonons. Using Weber and Bierig[57] leaves five possibilities; samarium, dysprosium, gadolinium, erbium and ytterbium of which only ytterbium is expected to have excited levels in the 1000 cm^{-1} region. Ytterbium-hydride tetragonal centres are not formed in the usual way but have been obtained by Newman et al.[49]. It would be of interest to examine these spectra under high resolution at $4^{o}K$.

PART II: The Hydride Ion Dipole Moment

It was shown in (12) that if the separation between the two components of the hydride ion vibrations was taken on an electrostatic model as being due to the perturbing effect of the extra positive charge of the rare earth ion on the triply degenerate first excited level of an isolated interstitial hydride ion then the (z) vibration lies lowest. In view of the reversed assignment of these modes this model is seen to be inadequate.

The odd electric field acting on the hydride ion will produce a non-linear polarisation of this ion. The ground state will not be a pure $1s^2$ state but will have admixtures of higher configurations, e.g. 1s2p, present. This polarisation has been discussed in Chapter II and expressions have been given there for the coefficients in the expansion of the hydride ion potential energy including terms up to third order only.

Taking the value of the isolated interstitial vibration from (12) and approximating the observed frequencies as their harmonic values gives:

$$\omega_c = (2A/m)^{\frac{1}{2}}$$

$$\omega_{xy} = (2a/m)^{\frac{1}{2}}$$

$$\omega_z = (2b/m)^{\frac{1}{2}}$$

We can now solve the four expressions for a, b, c and d for c, d and p the dipole moment provided we know σ and q, the effective charges on the rare earth and hydride ions. For $|q| = |\sigma| = |e|$ the equations are not consistent. However, taking $|q| = |\sigma| = 0.85|e|$ and the gadolinium values for A, a, and b since the local distortions for this site are expected to be a minimum, gives p = 1.1 Bohr radii. If it were assumed that the measured value of p at low fields[50] could be extrapolated to high fields an estimate of p = 7.7 Br is obtained. Due to the non-linearity of the dependence of p on E the actual value for high fields will be much less than this: The estimated value of 1.1 Br while large is not unreasonably so.

The situation in strontium fluoride is expected to be similar. To date attempts to observe a cubic hydride site analogous to that reported in calcium fluoride (12) have been unsuccessful.

It has been noted that the ratio of intensities of the hydride local mode components I(xy)/I(z) is significantly different from 2:1. This can be qualitatively accounted for by considering the above induced dipole moment p. The intensity of a given line is proportional to the square of the electric dipole operator between the ground and excited states. Thus I(z) is proportional to $q^2\hbar/2m\omega_z$. Since for the (xy) vibration the dipole rotates with respect to the z axis, q is replaced by (q - p/D). I(xy) is proportional to $2(q - p/D)^2\hbar/2m\omega_x$ and $I(xy)/I(z) \sim 2(1 - p/D)^2\omega_z/\omega_x$. With the estimated values of q and p this gives I(xy)/I(z) ~ 1.3 for calcium fluoride and 1.2 for strontium fluoride in better agreement with experiment than the 2:1 ratio initially assumed (table 1).

Linewidths

A detailed study of the infrared linewidths has not been made but we may make the following comments.

It is generally agreed that lifetime broadening is responsible for the linewidths of hydride ions in these lattices[51] rather than static strains or lattice distortions. The observations that the tetrahedral line is not broadened by the introduction of 0.05% rare earth ions and the line shapes being in general Lorentzian or nearly so supports this contention.

The low temperature data of table (2) is consistent with the assumption that spontaneous decay into two or more lattice or local-mode phonons is responsible for the lifetimes.

In each case the low frequency hydride local modes are very narrow indicative of their stability against decay into two lattice phonons. The higher energy (z) modes are considerably broadened when their separation from the (xy) mode lies in a region of high lattice phonon density of states $\sim 140\ cm^{-1}$ and much narrower when it does not, i.e. $\sim 30\ cm^{-1}$. This is indicative of two phonon decay via the low energy local mode and one lattice mode. The (z) deuteride vibration lines show much less variation for the two lattices since decay may proceed via two lattice phonons in each case.

CHAPTER SIX

THE ULTRAVIOLET SPECTRA OF CERIUM CENTRES IN THE ALKALINE EARTH FLUORIDES

PART I: Experimental Results

Trivalent cerium ions have a relatively simple energy level scheme shown in figure (10). Electric dipole transitions may take place between the ^2F and ^2D levels, the lowest of which occurs in the ultraviolet around 3000 A^o.

Kapalanskii et al's measurements[7] of the low temperature absorption and fluorescence spectra of cerium, interstitial fluoride ion, tetragonal pairs were repeated for all three alkaline earth fluorides. In each case the absorption spectra in the 3000 A^o region are characterised by a single intense zero phonon line accompanied by a broad intense phonon sideband with well developed structure. A representative example is shown in figure (11). A single well developed vibronic progression is superimposed on the lattice vibration spectrum in each case. The separation interval lies just a little above the highest longitudinal optical lattice frequencies (see table 6).

In fluorescence the phonon sidebands are mirrored in the zero phonon line and appear on the low energy side (see figures 12, 13). Again a single vibrational series is

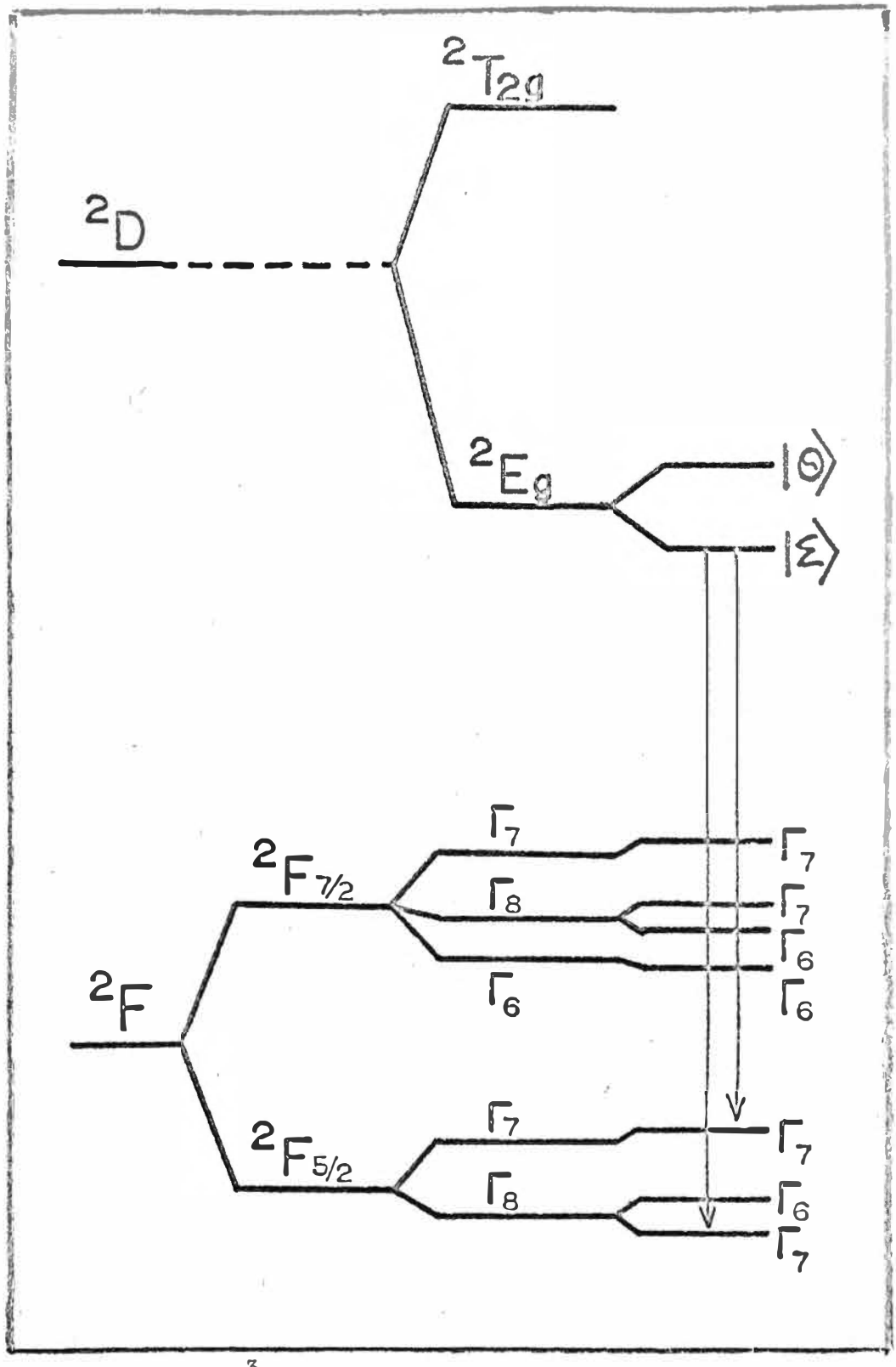

Fig (10). Ce^{3+} electronic energy levels showing in a schematic way, spinorbit coupling, followed by a cubic and then tetragonal crystal field.

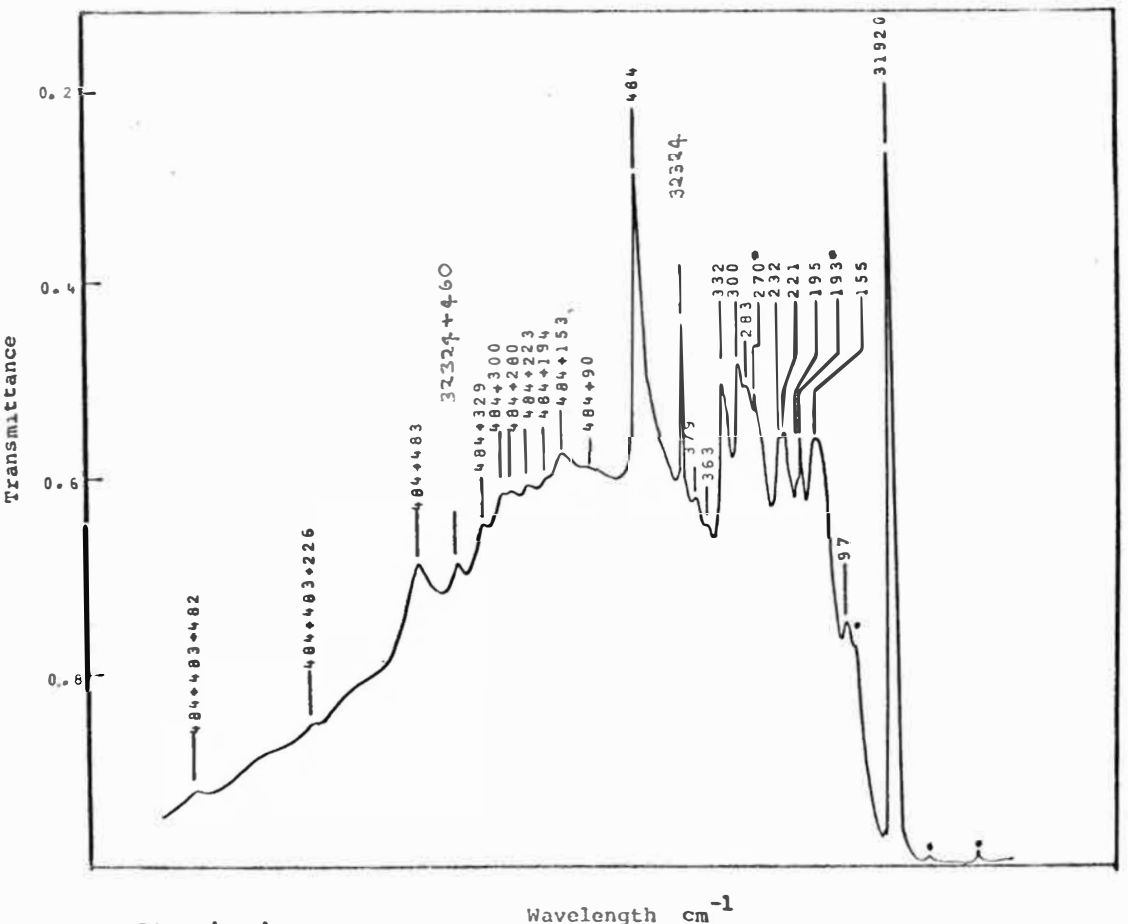

Ultraviolet absorption spectrum of crystals of calcium fluoride containing 0.05% cerium recorded at 12°K. The separations of the peaks in the vibronic spectrum from the no-phonon electronic transition at 3131.9 Å are shown in cm^{-1}; the lines marked with asterisks are electronic transitions.

Fig (11).

	Absorption cm^{-1}	Fluorescence cm^{-1}	LO_1 (k=0) cm^{-1}
CaF_2	484	478	463
SrF_2	438	425	374
BaF_2	403	398	326

Table (6). Vibronic progression intervals observed for Ce^{3+}-F^- tetragonal sites in the alkaline earth fluorides compared with the highest longitudinal optical branch lattice frequencies at k = 0.

evident with a reduced separation in each case (table 6). The anomalous reversal of this trend reported by Kapalanskii et al[7] was found to be in error. The assignments of these vibrational progressions will be discussed following the treatment of the analogous hydride centres.

Many additional sharp zero phonon lines close to 3100 A° were observed in as grown crystals containing 0.01% cerium. In all but one case these were at least a factor of one hundred weaker than the main line and did not maintain a constant intensity ratio to it from crystal to crystal.

They are therefore assigned to the same f-d transition originating from cerium ions in a multiplicity of lattice sites associated with different charge compensating mechanisms and/or cerium clusters. The one remaining line at 3092.2 A° in calcium fluoride occurs in these crystals at typically greater intensity (figure 11). It also occurs strongly in crystals double doped with cerium and sodium or lithium where the tetragonal interstitial fluorine charge compensated site is totally absent[56]. The assignment of this line will be discussed in Part II.

In fluorescence, transitions to the ground state are strongly self absorbed (figures 12,13). In addition to the phonon sidebands now appearing on the low energy side of the resonance line several other electronic lines were observed. These are associated with transitions to the upper components of the ^2F levels and their assignments will be discussed in Part II.

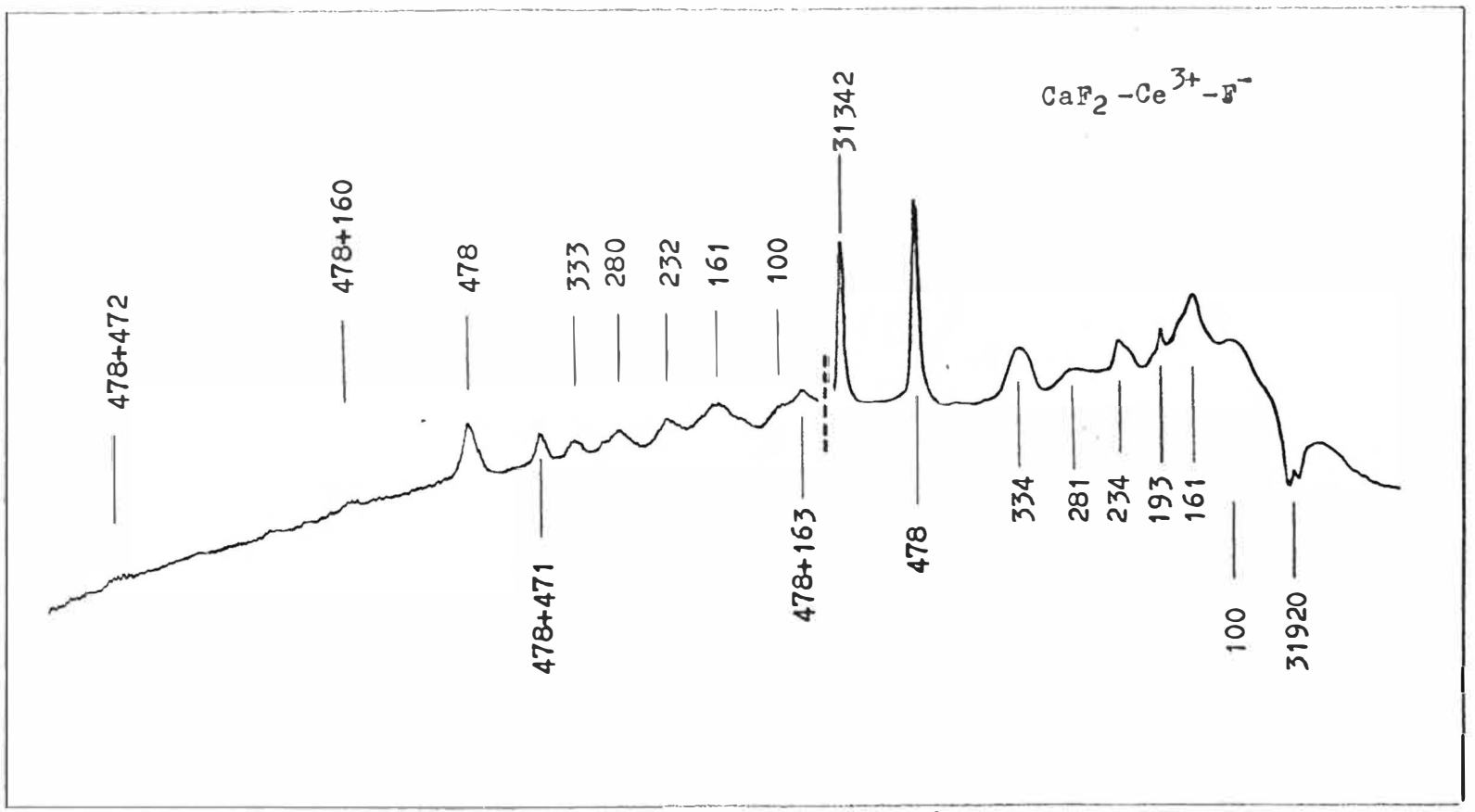

Fig (12). Fluorescence spectrum at $8^{o}K$ showing the two observed electronic transitions to $^{2}F_{5/2}$ levels and their associated vibronics.

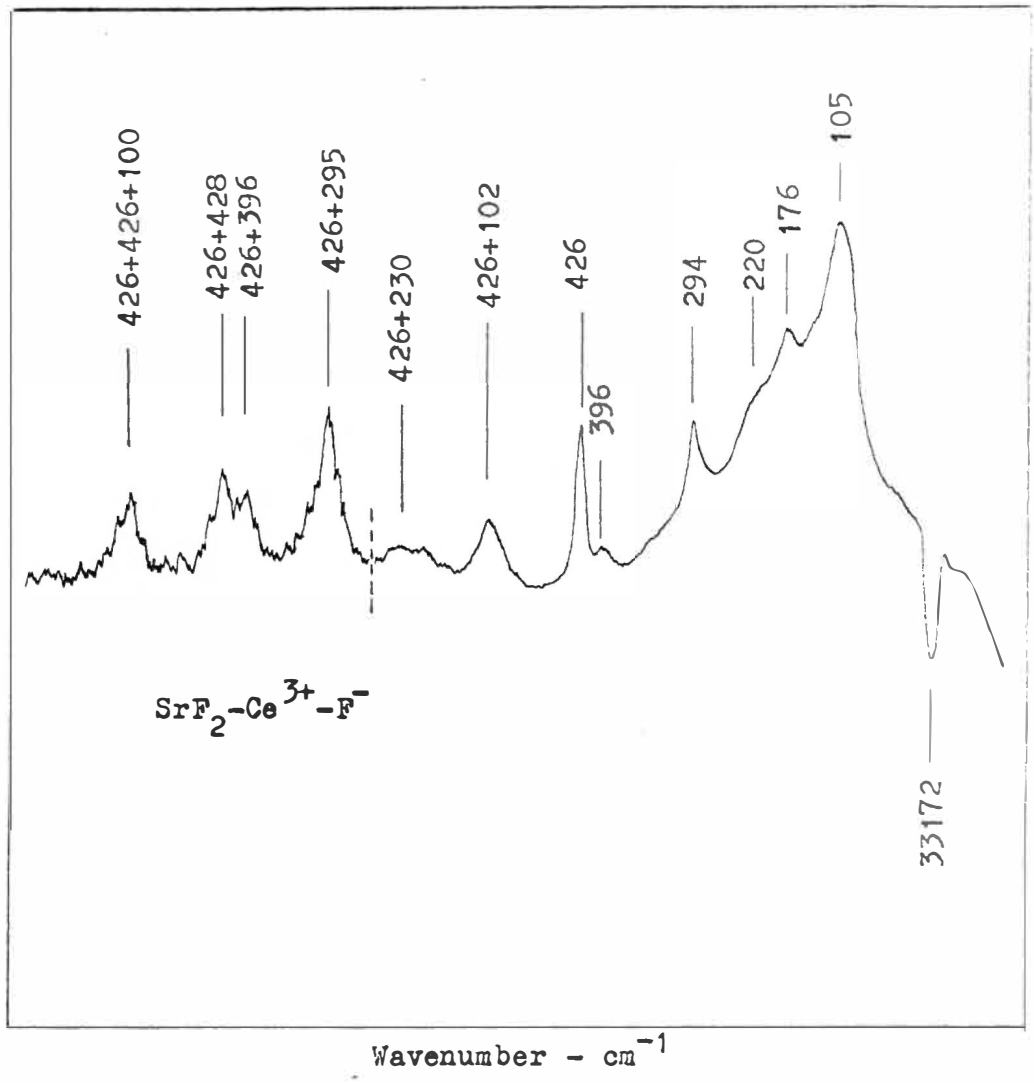

Fig (13). Fluorescence spectrum at $8^{o}K$ showing the electronic transition to the ground state (self absorbed) and its associated vibronics. Note the vertical scale reduction (by a factor of 10) to the right of the devision. All the vibronic intervals shown are observed elsewhere (table 11) for the SrF_2 lattice.

In particular the relativly sharp line at 294 cm^{-1} corresponds to a similar feature in the vibronic side-band associated with fluoresence to the $^2F_{7/2}$ levels. The possible assignment of this line as an electronic transition is therefore rejected.

	CaF_2 A^o	SrF_2 A^o	BaF_2 A^o
$^2F_{5/2}$	3131.9*	3013.7*	2966.0*
	-	-	-
	3189.6	-	-
$^2F_{7/2}$	-	-	-
	3362.5	3229.0	3170.0
	3375.5	3235.3	3174.0
	-	-	-

Table (7a). Electronic fluorescence transitions associated with Ce^{3+}-F^- tetragonal sites in the three alkaline earth fluorides at 8^oK.

*Resonant in absorption.

CaF_2 Ce^{3+}-F^- Δcm^{-1}	SrF_2 Ce^{3+}-F^- Δcm^{-1}	BaF_2 Ce^{3+}-F^- Δcm^{-1}
100*		
100	105	75
234	178	124
281	230	170
333	292	265
~460**	396	325

Table (7b). Summary of the lattice modes observed on each electronic transition in table (7a) at 8°K.

* Assigned to the Ce^{3+} pseudolocalised mode.

** Shoulder which appears on the main vibronic progression Table 6.

Cerium Hydrogenic Centres

After hydrogenation, at room temperature, a new absorption band appears on the long wavelength side of the Ce^{3+}-F^- tetragonal site band. A low resolution spectrum recorded on a Cary 14 spectrometer is shown in figure 14.

Similar structure to that noted for the Ce^{3+}-F^- sites was resolved on these new bands below 150°K for calcium fluoride and 80°K for strontium fluoride. No structure down to 2°K was visible on a similar but weaker absorption band in barium fluoride.

At low temperatures the most prominent zero phonon line, at 3417.7 A° for Ce^{3+}-H^- centres in calcium fluoride, is at least a factor of 40 stronger than other hydrogenic lines and occurs at typically one tenth the intensity of the F^- site line at 3131.9 A°.

The broad band accompanying the new line (3417.7 A°) is centred at a greater distance from its parent than the corresponding F^- site band. The well developed vibronic progression noted for the F^- sites is replaced by another progression with greatly increased interval. The replacement of the hydride, by deuteride or tritide ions, results in a shift of the zero phonon line by several angstroms and the reduction of the progression interval by a factor of about $\sqrt{2}$ and $\sqrt{3}$ respectively. The broad bands and main progression lines are shown in figure 15. Tritium spectra have not been

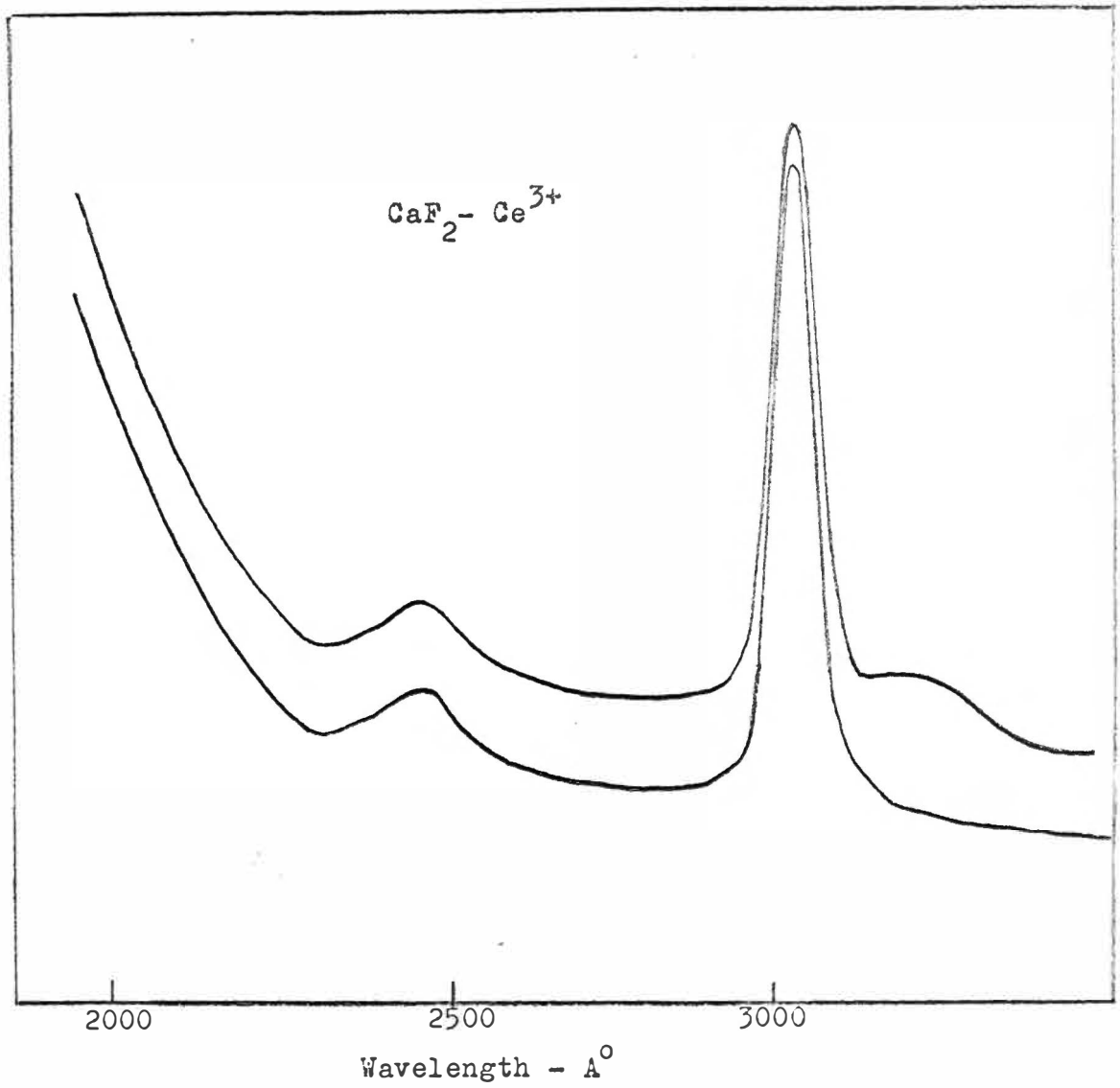

Fig (14). Room temperature absorption spectra showing the new band (upper curve) which appears after hydrogenation and the strong cerium tetragonal site absorption at 3100 A°. The weaker band at 2450 A° appears more strongly in higher concentration crystals and has been assigned to cerium in sites of unknown symmetry by Low.
Only the lower energy bands show detailed structure at lower temperatures.

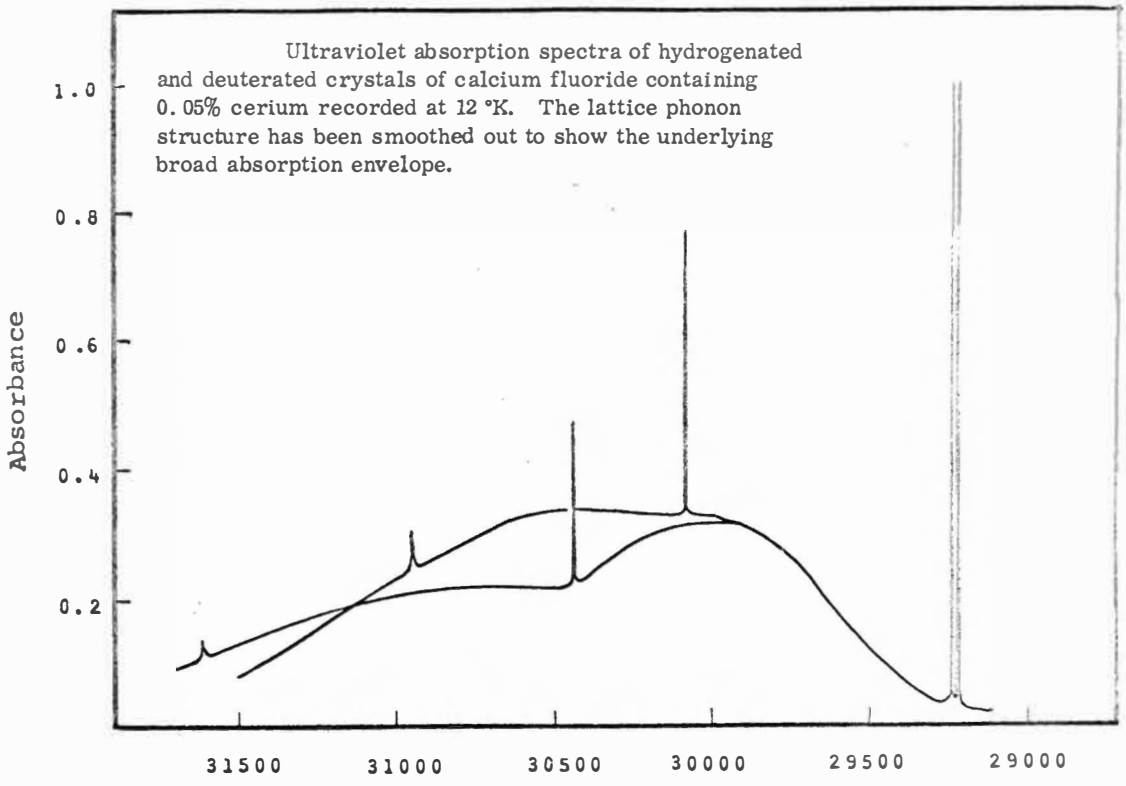
Ultraviolet absorption spectra of hydrogenated and deuterated crystals of calcium fluoride containing 0. 05% cerium recorded at 12 °K. The lattice phonon structure has been smoothed out to show the underlying broad absorption envelope.
Absorbance
1.0
0.8
0.6
0.4
0.2
31500
31000
30500
30000
29500
29000

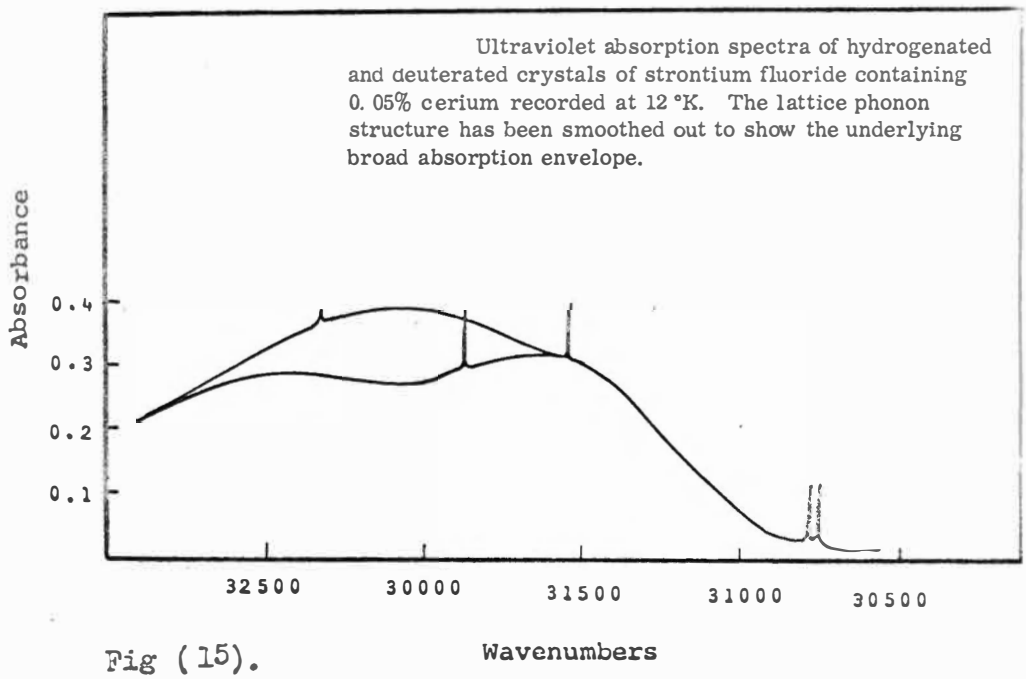
Ultraviolet absorption spectra of hydrogenated and deuterated crystals of strontium fluoride containing 0. 05% cerium recorded at 12 °K. The lattice phonon structure has been smoothed out to show the underlying broad absorption envelope.
Absorbance
0.4
0.3
0.2
0.1
32500
30000
31500
31000
30500
Wavenumbers

Fig (15).

included in this figure since the available spectra were heavily contaminated with hydrogen.

Fluorescence from the hydrogenic sites is relatively weak but with care sufficiently noise-free spectra were obtained (figure 16) to enable many features to be identified.

Transitions to the ground state are self-absorbed and successive absorption, re-emission cycles within the crystal[52] are responsible for considerably enhancing the intensity of their vibronic sidebands. Transitions to upper ^2F levels are not so affected and the intensity ratios of electronic and vibronic lines may be measured, (figure 16). The relative intensities of vibronics were found to be less by a factor of about 3 in fluorescence. In figure 16 transitions are identified as electronic (zero phonon) and are associated with the main resonance line if they have the same isotope shift, do not appear in absorption, always bear a constant intensity ratio among themselves and do not correspond to phonons coupled to electronic lines. Three such transitions have been definitely identified for hydride centers in Part II.

Associated with each of these zero phonon lines single well defined vibronics (figure 16a,b) are seen whose separation from their respective parents matches closely the infrared (z) local mode frequencies of the hydride type ions in tetragonal centres. These spectra are therefore associated with the Ce^{3+}-H^- type centres observed in the

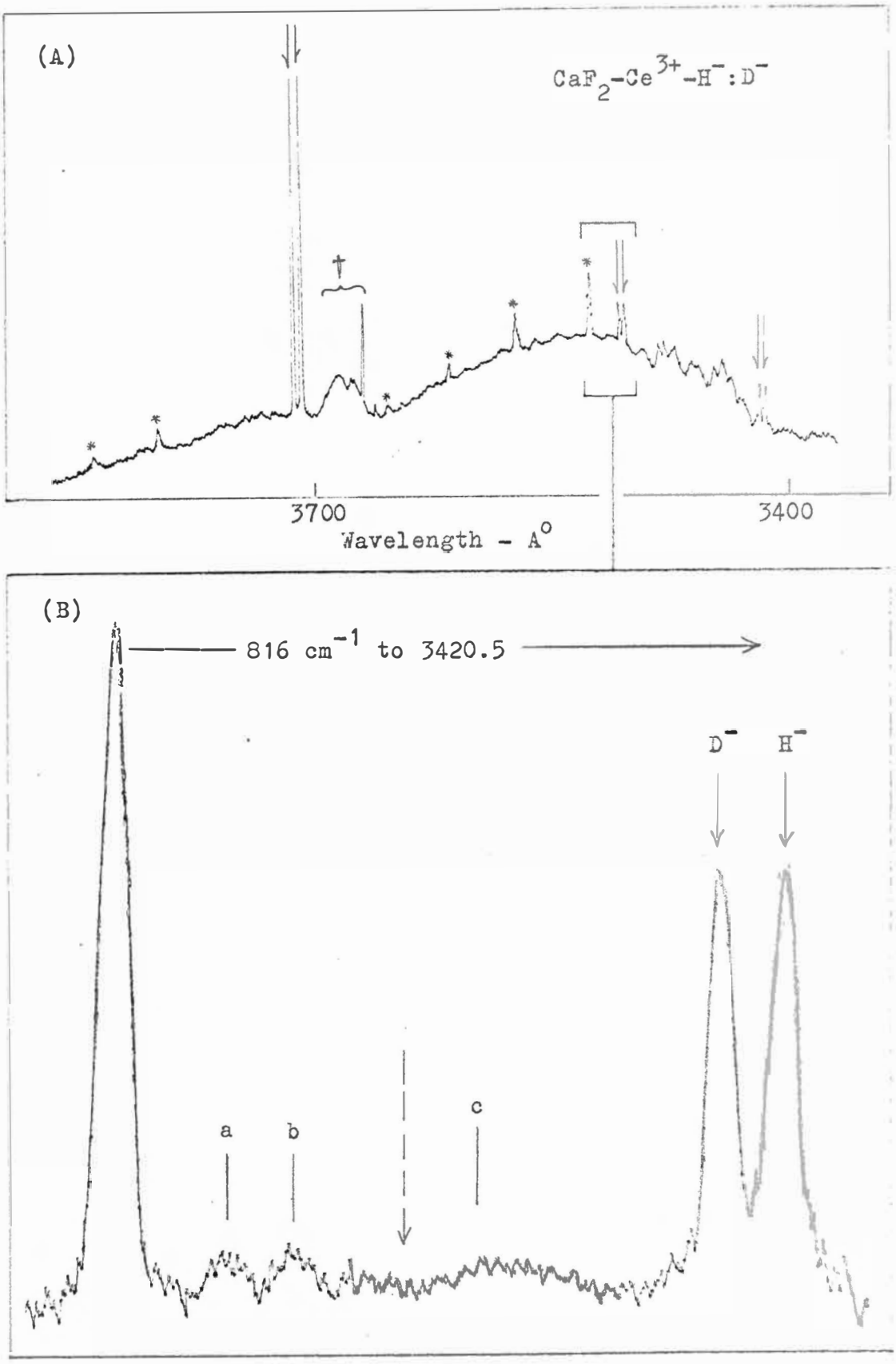

Fig. (16) A. Fluorescence of H^-:D^- tetragonal sites at 8°K. (⇓) Electronic lines. (*) H^-:D^- vibronics. (†) Hg lamp.

B. Detail showing the electronic isotope shift and single w_z D^- vibronic. (a) (b) and (c) are lattice modes on the electronic lines shown.

infrared and discussed previously. The corresponding vibronics in absorption (figure 15) are assigned to the same (z) local mode coupled to the upper d electronic state. The occurrence of one vibronic in each case (figure 16b) contrasts sharply with the results of Jones et al.[12] for the corresponding Gd^{3+}-H^- centres in calcium fluoride for which they report both ω_z and ω_{xy}. In the course of this work the gadolinium spectra were recorded photoelectrically and the previous results confirmed. Both vibronics occur in the intensity ratio (xy):(z) of 2:1. The gadolinium results are typical of rare earth (f-f) spectra[53] and this work (Chapter VIII) where in general both vibronics are found.

The second members of the (z) vibronic progressions are weak and efforts to observe them made more difficult by confusion with a weak electronic line not associated with the tetragonal site for the Ce^{3+}-D^- line on $^2F_{5/2}$ and the lattice modes associated with $^2F_{7/2}$ for the Ce^{3+}-H^- line on the $^2F_{5/2}$ ground state. Corresponding results are obtained for the calcium fluoride Ce^{3+}-T^- crystals and for the strontium fluoride crystals. These are listed with the above in table 8. The fluorescence of the strontium fluoride crystals is less intense and consequently less information is available from these spectra.

Crystal	(Å)	Assignment	Separation from parent line (cm^{-1})	Relative intensity	Linewidth (cm^{-1})
$CaF_2:Ce^{3+},H^-$	3417.7	Parent electronic line	...	1	5.1
	3279.3	First H^- local-mode vibronic	1235	0.54	10.2
	3155.1	Second H^- local-mode vibronic	2435	0.07	12.9
$CaF_2:Ce^{3+},D^-$	3420.5	Parent electronic line	...	1	5.2
	3319.1	First D^- local-mode vibronic	893	0.61	7.5
	3225.4	Second D^- local-mode vibronic	1768	0.13	11.5
$CaF_2:Ce^{3+},T^-$	3421.9	Parent electronic line	...	1	5.8
	3337.4	First T^- local-mode vibronic	739	0.70	9.4
$SrF_2:Ce^{3+},H^-$	3244.8	Parent electronic line	...	1	6.4
	3132.7	First H^- local-mode vibronic	1103	1.05	7.9
$SrF_2:Ce^{3+},D^-$	3248.3	Parent electronic line	...	1	6.2
	3165.8	First D^- local-mode vibronic	802	1.10	7.0
	3089.6	Second D^- local-mode vibronic	1581	0.39	9.9
$SrF_2:Ce^{3+},T^-$	3249.9	Parent electronic line	...	1	6.2
	3180.8	First T^- local-mode vibronic	669	0.6	9

Table (8a). Electronic and local-mode vibronic lines of hydrogen, deuterium, and tritium sites in calcium and strontium fluoride crystals containing 0.05% cerium. Crystal temperature 12°K.

Crystal	Terminating state of the transition	Wavelength of electronic line (Å)	Wavelength of the vibronic line (Å)	Separation (cm^{-1})	Infrared-mode frequency (cm^{-1})
$CaF_2:Ce^{3+},H^-$	$^2F_{5/2}\|\Gamma_8,\gamma_7\rangle$ ground state	3417.7	3554.7	1131±4	
$CaF_2:Ce^{3+},H^-$	$^2F_{5/2}\|\Gamma_7,\gamma_7\rangle$	3486.6	3628.1	1120	1131
$CaF_2:Ce^{3+},H^-$	$^2F_{7/2}$	3691.8	3853.4	1135	
$CaF_2:Ce^{3+},D^-$	$^2F_{5/2}\|\Gamma_8,\gamma_7\rangle$	3420.5	3517.7	816±4	
$CaF_2:Ce^{3+},D^-$	$^2F_{5/2}\|\Gamma_7,\gamma_7\rangle$	3489.4	3590.7	806	817
$CaF_2:Ce^{3+},D^-$	$^2F_{7/2}$	3695.1	3810.3	818	
$CaF_2:Ce^{3+},T^-$	$^2F_{5/2}\|\Gamma_8,\gamma_7\rangle$	3421.9	3503.5	672	
$CaF_2:Ce^{3+},T^-$	$^2F_{5/2}\|\Gamma_7,\gamma_7\rangle$	3490.8		...	
$CaF_2:Ce^{3+},T^-$	$^2F_{7/2}$	3696.5			
$SrF_2:Ce^{3+},H^-$	$^2F_{5/2}\|\Gamma_8,\gamma_7\rangle$	3244.8	...	...	
$SrF_2:Ce^{3+},D^-$	$^2F_{5/2}\|\Gamma_8,\gamma_7\rangle$	3248.3	3323.5	696	
$SrF_2:Ce^{3+},T^-$	$^2F_{5/2}\|\Gamma_8,\gamma_7\rangle$	3250.0	...	...	

Table (8b). Fluorescence spectra data for hydrogenated, deuterated and tritiated crystals of calcium and strontium fluorides containing 0.05% cerium showing the correlation of the local-mode vibronics observed in fluorescence with the local-mode frequencies observed directly in the infrared. Crystal temperature 12°K.

Other Hydrogenic Sites

In the absorption spectra of hydrogenated calcium fluoride cerium crystals other weak hydrogenic lines are present. Different quenching rates alter the intensity ratios of these lines to the tetragonal site line and among themselves so that they must be associated with other hydrogenic sites.

In suitable crystals the doublet at 3355.6 and 3357.2 A^{o} (for H^{-}) occurs at sufficient intensity for a single vibronic of comparable intensity to be observed on each component. These vibronics are separated from their respective parents by 1235 cm^{-1} for H^{-} and 890 cm^{-1} for D^{-}. It is thus possible since these intervals correspond to those observed for the tetragonal centre that these lines arise from the tetragonal centre perturbed either by another defect at one of two 'equivalent' lattice sites or by another paramagnetic ion. However, since the electronic lines are shifted some 500 cm^{-1} from the tetragonal lines such a perturbation would be expected to alter the hydride frequencies somewhat and the correspondence in vibronic interval may well be accidental and arise from an H^{-} ion in another lattice position. These sites should prove interesting for future work if they can be obtained at sufficient intensity to be observed by ESR and site symmetries obtained.

Irradiation of the calcium fluoride Ce^{3+}-H^{-} crystals with the unfiltered output ($<$ 2000 A^{o}) of a high pressure

mercury lamp converts the tetragonal sites to another optically similar hydrogenic site. Virtually complete conversion is achieved by irradiation for periods of from one to two hours provided the crystal temperature is maintained at 77°K throughout by immersion in liquid nitrogen. Conversion does not occur at 4°K which indicates that some rearrangement of site ions is involved. On warming to room temperature the new site quickly reverts to the tetragonal site without loss of intensity. Absorption spectra are reproduced in figures 17 and 18.

The zero-phonon lines of these new sites (uv sites) are shifted even further from the F^- tetragonal site lines ($\sim 4000\ cm^{-1}$) and show reversed isotope shifts. The phonon sidebands are more intense and the superimposed structure less well defined than for the tetragonal sites. Only one light ion vibronic appears with increased separation. This increased frequency is reflected in the ratios of $\omega H/\omega D$ and $\omega H/\omega T$ which are closer to $\sqrt{2}$ and $\sqrt{3}$ respectively, (table 9). In addition the phonon sideband shows a peak at 472 cm^{-1} which suggests that the site involves an interstitial F^- ion.

The local mode vibronics are relatively less intense than for the tetragonal site and a steeply sloping background hinders their observation in fluorescence. In the D^- crystals a weak vibronic $\sim 1/30$th the intensity of the parent line has been identified at 3986.7 A°, a separation of

Fig (17a). Absorption spectra ($77^{\circ}K$) showing progressive conversion of the tetragonal site to the new UV site.

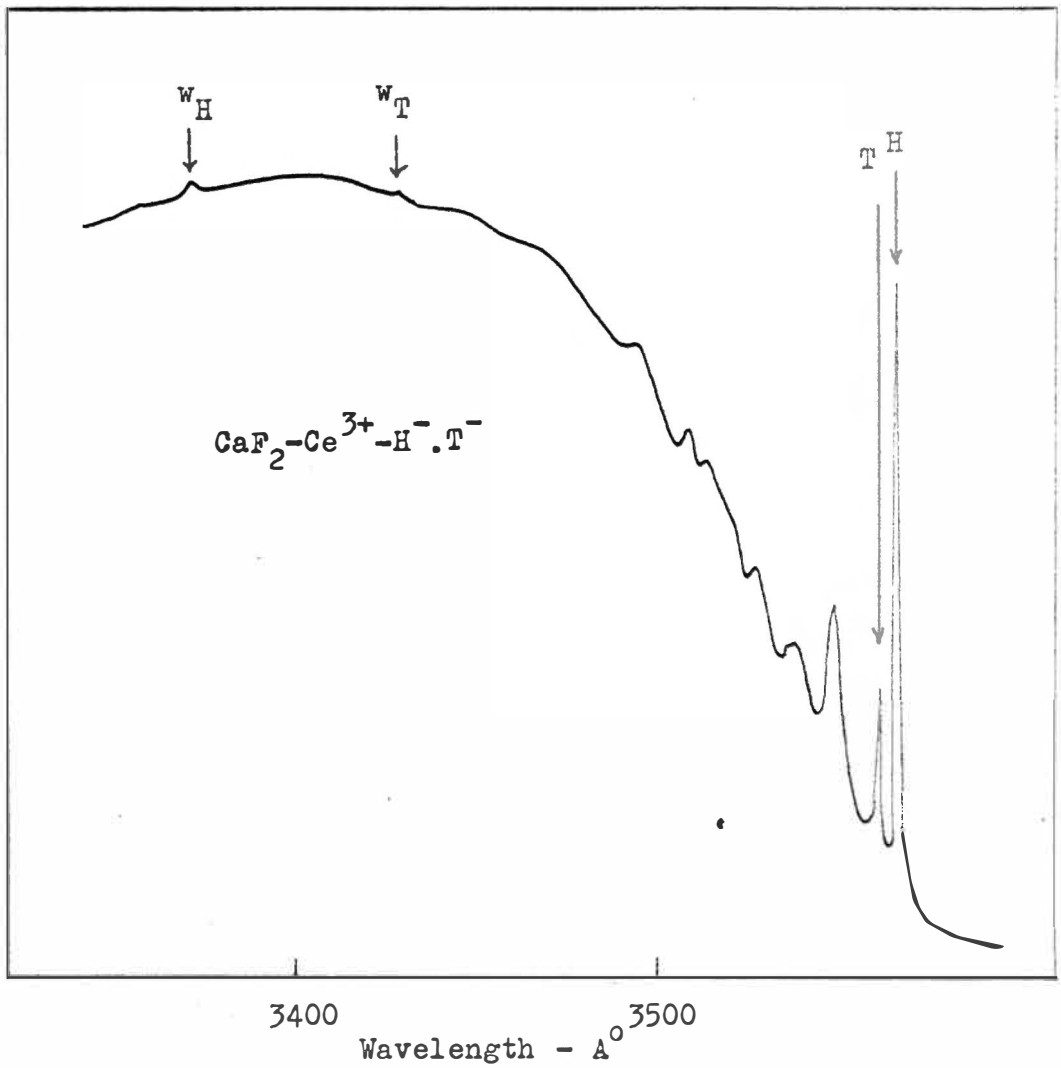

Fig (17b). Helium temperature absorption spectrum after several hours of ultraviolet irradiation at 77°K.

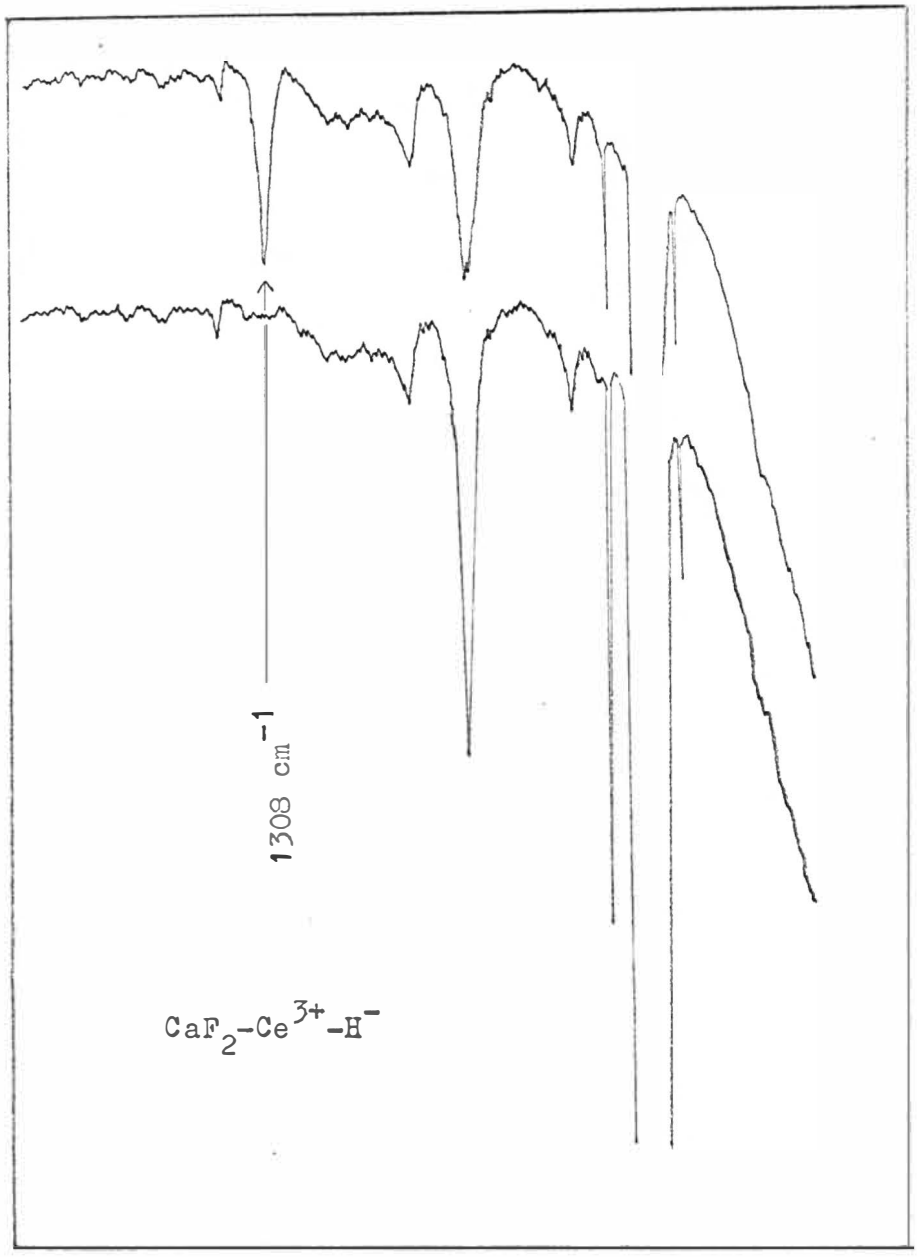

Fig (18). Infrared absorption spectra (77°K). Following irradiation the tetragonal site lines are seen to be reduced in intensity and a new line appears. (upper curve)
On warming to room temperature the spectrum reverts to its initial appearence. (lower curve)

Host Crystal and site	(H) A°	(D) A°	(T) A°	Isotope Shifts	
				$\delta_{H,D}$ cm^{-1}	$\delta_{H,T}$ cm^{-1}
CaF_2:Ce (doublet)	3355.6 3357.2	3355.1 3356.6	... ...	- 4.8 - 4.8	... ...
CaF_2:Ce (?)	3369.6	3371.6	3372.4	+17	+25
CaF_2:Ce(UV)	3548.9	3547.1	3546.3	-14.2	-20.6
CaF_2:Ce (UV doublet)	3458.5 3459.7	3457.3 3458.5	... ...	-10 -10	... ...
SrF_2:Ce (UV)	3391.0	3389.5	3388.4	-13.4	-20.0

Host crystal and site	H(vibronic) A°	D(vibronic) A°	T(vibronic) A°
CaF_2:Ce (UV)	3367.1 Δ=1421 cm^{-1}	3424.5 Δ=1009 cm^{-1}	3345.5 Δ= 825 cm^{-1}

Table 9. Wavelengths of electronic lines of associated with several cerium 'hydride' centres. Temp. 12°K.

934 cm^{-1}. The corresponding H^- vibronic at ~1300 cm^{-1} has not been identified and must be at least a factor of three weaker. In the infrared the irradiated crystals show single new absorption lines at 77°K at 1308 cm^{-1} for H^- and 935 cm^{-1} for D^- which are correlated in intensity with the uv optical site.

Similar but less complete conversion is observed for the corresponding strontium fluoride crystals under the same conditions. The phonon sidebands are less well defined. The isotope shifts are similar and are listed in table 9 along with the calcium fluoride data.

The above observations are consistent with the tentative interpretation of the uv site as involving the interchange of the interstitial hydride ion with a cerium nearest neighbour fluorine ion to form a triclinic site. In this configuration the large hydride ion is extremely close to the cerium and overlap effects are likely to be of importance. The explanation of the large shift in zero phonon lines, increase of hydride ion frequency from that of the normal substitutional site (at 965 cm^{-1} in CaF_2) and the observation of only one infrared absorption must lie in these effects.

The alternative interpretation, that the site involves the diffusion of the H^- ion into a more distant empty fluorine box can account for the higher local mode frequency (i.e. ~ cubic interstitial site) but not for the large

vibronic shifts and the large perturbation of the electronic lines from the cubic site (Ch. VI, part II).

Facilities are being developed in this laboratory to irradiate the crystals at 77°K and to obtain the ESR spectra at 4°K to determine the site symmetry. Until this information is available the above interpretation remains tentative and further speculation is unprofitable.

The low lying electronic levels

In principle the upper components of the ^2F levels may be observed via absorption transitions in the infrared or at elevated temperatures as 'hot' lines in the electronic absorption spectra.

In the infrared the $^2F_{5/2}$ levels lie in an inaccessible region and attempts to observe the $^2F_{7/2}$ levels in the 2000 cm^{-1} region have been unsuccessful. Several lines attributed to cerium appear in this region but none which may be identified with the tetragonal levels observed optically. At temperatures much above liquid air the electronic spectra become too broadened to observe detailed structure. At 77°K all sites show broad weak hot lines which correspond to the phonons at 100 cm^{-1} and 150 cm^{-1} only.

PART II: Analysis of the Cerium Electronic Spectra

The principle electronic transition is from the lowest level of the 4f configuration to the lower level of the 5d configuration and is electric dipole allowed.

The effect of a tetragonal crystal field on the ^2D levels is described by Storosten[54]. The ^2D free ion multiplet is split by the dominant cubic component of the crystal field into an orbital triplet $^2T_{2g}$ and a doublet ^2E_g with the latter lowest. These are further split by the tetragonal component. Kapalanskii et al. have assigned bands in the 2000 A^o region to the $^2T_{2g}$ levels. Loh[55] has postulated a large tetragonal splitting of the E_g levels placing one at 2020 A^o just below the $^2T_{2g}$ levels and the other at 3131 A^o in CaF_2.

However, the line at 3092.2 A^o (figure 11) which appears in many cerium doped calcium fluoride crystals has been attributed to cerium ions in sites of cubic symmetry[56]. This would place the other E_g component in the 3000 A^o region. A careful search in this region for the zero phonon transition has been unsuccessful.

The cubic field wavefunctions $|\varepsilon\rangle$ and $|\varphi\rangle$ appropriate for the two E_g levels are, in terms of $|M_L, M_S\rangle$ states:

$$|\varepsilon\rangle = \frac{1}{\sqrt{2}} |\pm 2, \mp\tfrac{1}{2}\rangle + \frac{1}{\sqrt{2}} |\mp 2, \pm\tfrac{1}{2}\rangle$$

$$|\varphi\rangle = |0, \pm\tfrac{1}{2}\rangle$$

The wavefunctions for the ^2F levels have been given (pp 5.5, 5.6). The relative transition probabilities are given by the ratio of the square of the matrix elements of the electric dipole operator between the ground and excited states. This ratio for incident unpolarised light is 3/49 so that transitions to $|\varphi\rangle$ are expected to be considerably weaker. Since also, in general, transitions to upper crystal field levels are usually broadened this result is consistent with the non-observation of the upper component.

The most obvious effect of the substitution of H^- for F^- charge compensators is the large shift of the electronic lines ($\sim 3000\ cm^{-1}$). Such large shifts cannot be accounted for solely on the basis of a change in crystal field splitting the ^2D multiplet. It would appear that the ^2D multiplet is centred at lower energies for the hydrogenic sites. This is either a consequence of a reduced central field acting on the cerium ion through covalency and overlap effects or is due to configurational interactions of the crystal field depressing the ^2D levels to lower energies for the hydrogenic sites. These effects cannot be measured without the location of the other ^2E level, and the T_{2g} levels for the hydrogenic sites.

There are three and four tetragonal crystal field levels arising from the $^2F_{5/2}$ and $^2F_{7/2}$ multiplets respectively. In fluorescence, transitions to four of these levels have been identified (table 7).

The electric dipole transition probabilities from the upper $|\varepsilon\rangle$ level to the components of the $^2F_{5/2}$ levels are given by ~(15:1:15) to the Γ_7', Γ_6 and Γ_7 levels respectively (figure 10). Since also the Γ_6 level has been estimated to be about 150 cm^{-1} above the ground state[57] the two observed transitions are assigned to the Γ_7 and Γ_7' levels. The corresponding transition to the upper (Γ_7') level in strontium fluoride has not been observed (figure 13).

The tetragonal Ce^{3+}-H^- type centres also show two transitions to $^2F_{5/2}$ levels and these are assigned to the same electronic states. The very similar energy separation ($\lesssim$ 580 cm^{-1}) of these two levels for the H^- and F^- tetragonal centres is probably accidental since in general[58,59] the tetragonal crystal field splittings are found to be considerably increased for H^- centers. One would thus expect the Γ_6 level to be located about 200 cm^{-1} above the ground state for the H^-centres and maintenance of the centre of gravity of the $^2F_{5/2}$ multiplet would seem to require some small reduction of the cubic crystal field component for these centres (figure 10).

Two $^2F_{7/2}$ levels are observed for the F^- centres. The separation is markedly reduced for strontium fluoride and barium fluoride (table 7) which suggests that they belong to the cubic Γ_8 level split into two components (Γ_6+Γ_7) by the tetragonal field. The weaker, upper line, cannot be easily

identified for the H^- sites since it is confused with the lattice bands on the stronger line. A peak separated from the main line by ~208 cm^{-1} and not observed elsewhere as a lattice phonon may correspond to this transition.

The location of the $^2F_{5/2}$ (Γ_7') level in strontium fluoride is of importance for the calculation of vibronic splitting (Chapter V). It is found in other systems[60,61] that the splitting of levels whose degeneracy is raised by the tetragonal crystal field component is reduced by about 50% on changing the host lattice from CaF_2 to SrF_2 whereas the splitting of cubic field levels is reduced by some 15%. These reductions place the upper level 450 ± 50 cm^{-1}, above the groundstate in strontium fluoride H^- centres.

Vibronic Transitions

A characteristic feature of all the cerium spectra is the appearance of one intense local mode vibronic progression in either absorption or fluorescence spectra whereas two local mode lines are observed in infrared absorption. Vibronic transitions arise from the coupling of the cerium ions' electronic states to the lattice and local mode phonons.

As in Chapter V we write the wavefunction of the coupled system as the product of the individual electronic and nuclear wavefunctions:

$$\Psi_{in}(rQ) = \Psi_i(r,Q)\Psi_{in}(Q)$$

where r represents the electron, and Q the nuclear coordinates. Following Bron[62] the probability of an electric dipole transition between these states is:

$$\langle \Psi_{in}(r,Q) | P | \Psi_{jn'}(r,Q) \rangle \qquad (1)$$

$$= \langle \phi_i(r,Q) | P | \phi(r,Q) \rangle \Pi_k \langle \psi_{in}(Q^{(k)} - \alpha_{o_i}^{(k)}) | \psi_{jn'}(Q^{(k)} - \alpha_{o_j}^{(k)}) \rangle$$

where $\alpha_{o_j}^{(k)}$ is the shift in equilibrium position for the j^{th} electronic state and is given by Wagner[63] as:

$$\alpha_{o_j}^{(k)} = \frac{1}{m\omega_k^2} \langle \psi_j | f_k | \psi_j \rangle$$

where ω_k is the frequency of the k^{th} normal mode. The appearance of vibronics is governed by the non-vanishing of the displacement parameter $a_o^{(k)} = a_{o_i}^{(k)} - a_{o_j}^{(k)}$.

The first non-zero matrix element of f_k using the point charge expression given on page (2.13) involves the constant term T_o^o in f_2. Since this gives the same contribution for both levels no net shift results. The next non-zero elements involve the quadratic terms in the f_k and for these, since $\langle r^n \rangle$ is widely different for f and d levels, $a_o^{(k)}$ is non-zero. In order to obtain an estimate of $a_o^{(k)}$ the values of $\langle r^n \rangle$ given by Bron[44] are used together with the value of $\langle r^4 \rangle_{5d} \sim 70$ au extrapolated from the data of Rajnak[64] giving a contribution from the point charge model of 0.07 A^o and a further 0.07 A^o from the dipole model to the value of $a_o^{(z)}$.

More significantly the matrix elements of the quadratic terms in f_x and f_y are zero for the particular upper electronic state so in first order the shifts $a_o^{(x)}$, $a_o^{(y)}$ are zero and the (xy) vibronics are not expected to appear.

Following Wagner[63] the intensities of the (z) vibronics with respect to the zero phonon line will be given by

$$p^n = \frac{1}{n!}\left[\frac{m\omega_k(\alpha_o^{(k)})^2}{\hbar} \cdot \frac{2\beta_k^2}{(1+\beta^2 K)}\right]^n$$

where p^n is the transition probability of transitions involving n local mode phonons and β_k^2 is the ratio of frequencies (ω'_k/ω_k) of the k^{th} local mode in the excited and ground states.

The relative intensities of the local mode vibronic lines are given in Table (8). From this data the displacements are found to be: 0.18, 0.16, 0.15 A^o for H^-, D^- and T^- in CaF_2 respectively and 0.27, 0.20 and 0.16 A^o for the corresponding SrF_2 values. These are the same order of magnitude as the estimate above. The corresponding vibronics have been observed in fluorescence and reported[65] to be typically one tenth the intensity of their parent transitions. Since that time improved relative intensity measurements have been made and the intensities of these lines relative to their respective parents are listed in table (8). Their reduced relative intensities along with the apparent reduced intensities of the lattice phonon bonds are indicative of a

weaker coupling to the lattice in fluorescence and cannot be accounted for on the above model.

The Isotope and Vibronic Shifts

The electron phonon interaction V_{ev} will cause a shift in each electronic level to which all the lattice modes will contribute. It is assumed that the coupling of lattice modes is unaffected by whether H^- or D^- charge compensators are present since the local mode frequencies lie well above the lattice frequencies. This assumption is supported by the observation of identical lattice phonon sideband structure associated with hydrogen or deuterium site electronic lines. The contribution of the lattice modes to the isotope shift is therefore taken as negligible.

We again write the total wavefunction as the product of electronic and nuclear parts where the local mode wavefunction is taken as that of an anharmonic oscillator in a static potential well. The Hamiltonian H is given by

$$H = T_{kn} + \tfrac{1}{2}m\omega_z{}^2Z^2 + \tfrac{1}{2}m\omega_x{}^2(X^2+Y^2) + cZ^3 + dZ(X^2+Y^2)$$

$$+ \langle\phi_i|f_z|\phi_i\rangle Z + \langle\phi_i|g_{zz}|\phi_i\rangle Z^2 + \langle\phi_i|g_{xx}+g_{yy}|\phi_i\rangle \tfrac{1}{2}(X^2+Y^2)$$

where the T_{kn} are the kinetic energy terms.

The electron phonon interaction will shift the potential minima of the oscillator. The equilibrium condition $\frac{\partial V}{\partial z} = 0$ gives the displacement as $\langle\phi_i|f_z|\phi_i\rangle/m\omega_z{}^2$ to terms in first

order and the corresponding potential energy minimum as

$$V_0 \simeq 3|\langle\psi_i|f_z|\psi_i\rangle^2|/2m\omega_2^2$$

The energy of the combined system to terms in second order is:

$$E_{i\ n_x n_y n_z} = E_i + (n_x+n_y+1)\hbar\omega_x + (n_z+\tfrac{1}{2})\hbar\omega_z + \frac{|\langle\psi_i|f_z|\psi_i\rangle|^2}{2m\omega_z^2}$$

$$+ (n_2+\tfrac{1}{2})\frac{\hbar}{m\omega_z}\langle\psi_i|g_{zz}|\psi_i\rangle$$

$$+ (n_x+n_y+1)\frac{\hbar}{2m\omega_x}\langle\psi_i|g_{xx}+g_{yy}|\psi_i\rangle$$

$$- 3(n_z+\tfrac{1}{2})\frac{\hbar c}{m^2\omega_z 3}\langle\psi_i|f_z|\psi_i\rangle - (n_x+n_y+1)\frac{\hbar d}{m^2\omega_x\omega_z 2}\langle\psi_i|f_z|\psi_i\rangle$$

The energies $E_{i\ 000}$ of the zero phonon levels will differ for different light ion charge compensations, for those terms which depend on $\frac{\hbar}{m\omega_k}$ only, since $\frac{\hbar}{m\omega_k^2}$ is very nearly constant. The terms involving the anharmonic constants c and d will also contribute.

A second order contribution may also occur due to interactions with close electronic levels. In this case the calculation proceeds in a similar way to that of Chapter V and gives a contribution for each electronic level of:

$$\frac{\hbar}{2m\omega_x}\frac{|\langle\psi_i|f_x|\psi_j\rangle|^2}{\Delta E_{ij}+\hbar\omega_x} + \frac{\hbar}{2m\omega_z}\frac{|\langle\psi_i|f_z|\psi_j\rangle|^2}{\Delta\varepsilon_{ij}+\hbar\omega_x}$$

Neglecting, for the present, this possibility the expression

for the isotope shift can be written as

$$\delta = \frac{\hbar}{2m\omega_z}\,[\varepsilon|z|\varepsilon] + \frac{\hbar}{2m\omega_x}\,[\varepsilon|x|\varepsilon]$$

where $$[\varepsilon|z|\varepsilon] = \left(\langle\varepsilon|g_{zz}|\varepsilon\rangle - \frac{3c\langle\varepsilon|f_z|\varepsilon\rangle}{m\omega_z^2}\right)$$

and $$[\varepsilon|x|\varepsilon] = \left(\langle\varepsilon|g_{xx}+g_{yy}|\varepsilon\rangle - \frac{2d\langle\varepsilon|f_z|\varepsilon\rangle}{m\omega_z^2}\right)$$

The local mode shifts can be calculated in the same way. The observed local mode shift is the difference in the shift of the excited state relative to the ground state and the contributions from the quadratic terms are given by:

$$\frac{n\hbar}{m\omega_k}\,\langle\psi_i|g_{kk}|\psi_j\rangle$$

The anharmonic terms give contributions of

$$\frac{-\hbar}{m\omega_z}\left(\frac{3c\langle\psi_i|f_z|\psi_i\rangle}{m\omega_z^2}\right) \quad \text{and} \quad \frac{-\hbar}{m\omega_x}\left(\frac{2d\langle\psi_i|f_z|\psi_i\rangle}{m\omega_z^2}\right)$$

If the possibility of interactions with close electronic levels is included there is a further contribution of:

$$\frac{\hbar|\langle\psi_i|f_k|\psi_j\rangle|^2}{2m\omega_k}\left[\frac{1}{\Delta E_{ij}-\hbar\omega} + \frac{1}{\Delta\varepsilon_{ij}+\hbar\omega}\right]$$

Including only the quadratic and anharmonic terms the net vibronic shifts may be written as

$$\delta_{nz} = \frac{h\hbar}{m\omega_z}\,[\varepsilon|z|\varepsilon]$$

and $$\delta_{nx} = \frac{n\hbar}{m\omega_x} [\varepsilon|x|\varepsilon]$$

We have in the above, neglected the possible contribution from interactions with close electronic levels.

For the particular upper d electronic wave functions here these interactions are small. The matrix elements of the other E_g level, $|\varphi\rangle$, with $|\varepsilon\rangle$ are zero. The T_{2g} levels lie ~20,000 cm^{-1} above the E_g levels and consequently interactions via these levels will be small. On the point charge model these contributions to the (z) vibronic shift are estimated to be ~1 cm^{-1}.

One other observed vibronic shift occurs for the (z) vibronics on the $^2F_{5/2}$ (Γ_7') level. The second order interactions of the first degree terms in V_{ev} have been shown (Chapter V) to give small contributions to the splitting of the $n_x = 1$ levels coupled to the ground state. The second order contributions to the vibronic shifts, are, on the point charge model, similarly small and tend to cancel. In particular if these interactions are responsible for the vibronic shifts, because of the placement of the electronic levels, the vibronic shift for D^- should be ~3 times that for H^-. This is not observed, the shifts being ~-11 cm^{-1} for H^- and -8 cm^{-1} for D^-. It is therefore concluded that we may again neglect these contributions.

The tritium results are in good agreement with the above model for the isotope shifts. If the contribution from the

(xy) levels is relatively small the isotope shifts should cancel in the following ratio:

$$\delta_{H,T}/\delta_{H,D} = \frac{1 - m_H\omega_H/m_D\omega_D}{1 - m_H\omega_H/m_T\omega_T} = 1.44$$

using the experimental values of ω_H, ω_D and ω_T. The ratios of isotope shifts for the five cases observed are tabulated below. The agreement is seen to be good irrespective of the sign of the isotope shift.

The vibronic shifts should, on the above model, cancel in the ratios $\delta_H/\delta_D = m_D\omega_D/m_H\omega_H = 1.44$ and $\delta_H/\delta_T = m_T\omega_T/m_H\omega_H = 1.78$. The experimental values are in reasonable agreement with this, being 1.37 and 1.55 respectively for the tetragonal site. From the vibronic shifts the value of $[\varepsilon|z|\varepsilon]$ for calcium fluoride is 7×10^3 erg/cm^2.

The tetragonal site isotope and vibronic shifts are uniformly 40% greater in strontium fluoride. This increase is only partially accounted for by the reduction in the local mode frequencies and requires the slightly larger value of 8.3×10^3 erg/cm^2 for $[\varepsilon|z|\varepsilon]$.

For the tetragonal sites the internal consistency of the expressions for isotope and vibronic shifts requires that the (xy) vibronic shifts be 30 and 42 cm^{-1} for calcium and strontium fluoride respectively. It is unfortunate that the (xy) vibronics are too weak to be observed in the optical spectra.

Host Crystal and Site	Sign of Isotope Shift	Ratio of Isotope Shifts $\delta_{H,T}/\delta_{H,D}$
CaF_2-(Tetg.)	+	1.47 ± 0.02
SrF_2-(Tetg.)	+	1.47 ± 0.02
CaF_2-(?)	+	1.5 ± 0.1
CaF_2-(UV)	-	1.45 ± 0.02
SrF_2-(UV)	-	1.49 ± 0.05

Table (10). The sign and ratio of the electronic isotope shifts observed for cerium hydride centres.

It would appear that while the indications are that the above model can account for the shifts in the tetragonal sites the same cannot be said for the u.v. site. It is apparent that in this case the (z) vibronic shifts are +ve while the isotope shift is -ve. More information is required about this site before any positive statements can be made.

Lattice Vibrations and the Fluorine Site Vibronic Progressions

The separations of resolved peaks in the lattice vibrational spectra from their respective parent lines are listed in tables 7, 11 and 12 for several sites in the three alkaline earth fluorides. A number of characteristic separations are evident for each lattice but there is no evidence for the low frequency (160 cm^{-1}) vibronic progression suggested by Loh[55] on the basis of liquid air spectra. The phonon structure is best resolved for calcium fluoride and the various peaks have been assigned (table 12) to modes of the lattice using the data of Kaiser[66] and Fray et al.[67]. The longitudinal optical modes at 460 cm^{-1} in calcium fluoride appear in the hydrogenic and cubic site spectra and strongly in the vibronic progression of figure 11 as evidenced by the skewing of the 484 cm^{-1} line to lower separations.

The weak broad vibronic peak at 100 cm^{-1} which occurs for all the calcium fluoride cerium spectra and is clearly shown in figure 19, corresponds to a resonance mode of the

3417.7Å	3279.3Å	3420.5Å	3319.1Å	3225.4Å
107 ± 8	100	100	100	...
170*	169	168	170	...
182	181	182	183	185
192	191	193	193	
238	237	237	237	235
284	280	283	279	280
319	320	318	319	320
330	333	332	330	...
368	367	368	367	...
435	433	433	435	430
475	472	474	476	...
512	510	513	511	...
564	554	563	553	...
612	614	615	610	...
650	...	655	650	...
700	...	701	700	...
746	748	750	743	

Table (11a). Vibrational sidebands associated with the (i) 3417.7-Å electronic line observed in hydrogenated crystals, (ii) the first local-mode vibronic line observed in hydrogenated crystals, (iii) the 3420.5-Å electronic line observed in deuterated crystals, (iv) the first local-mode vibronic line of deuterium observed in deuterated crystals, and (v) the second local-mode vibronic line of deuterium observed in deuterated crystals. All values are in cm^{-1} and are accurate to ±3 cm^{-1}. The crystals were calcium fluoride containing 0.05% cerium and the spectra were recorded at 12°K. The parent line for the vibronics is at the head of each column.

3244.8Å	3132.7Å	3248.3Å	3165.8Å
121	120	120	119
171	171	170	168
180	...	180	...
196	197	197	195
240	241	244	243
272	270	272	270
291	289	292	289
320	322	321	319
400	394	399	396
...	520[a]	...	...
535	540	540	535
...	560[a]	...	...
674	669	674	671
800	790	...	...

[a]Just resolved lines

Table (11b). Vibrational sidebands associated with the (i) 3244.8-Å electronic line observed in hydrogenated crystals, (ii) the first local-mode vibronic line observed in hydrogenated crystals, (iii) the 3248.3-Å electronic line observed in deuterated crystals, and (iv) the first local-mode vibronic line observed in deuterated crystals. All values are in cm^{-1} and are accurate to ± 3 cm^{-1}. The crystals were strontium fluoride containing 0.05% cerium and the spectra were recorded at 12°K. The parent line for the vibronics is at the head of each column.

Assignment	Frequency	Observed line frequency (average of values of Table IV)
	...	100
	...	169
	...	182
	...	192
	...	237
LO_2	286[a]	282
k=0 Raman[a]	321	319
TO_2	325[a]	332
LO_1	368[a]	367
LO_2 + TA	431	434
TO_2+TA, LO_1 at k=0[a]	463[a]	474
LO_1 + TA	516	512
LO_2 + LO_2	564	558
LO_2 + TO_2	614	612
LO_2 + LO_1	649	652
LO_1 + TO_2	700	700
LO_1 + LO_1	734	747

[a]Data of Fray et al.

Table (12). Assignment of the lattice frequency vibronics observed in hydrogenated and deuterated crystals of calcium fluoride containing 0.05% cerium. Crystal temperature 12°K.

heavy cerium ion in the lattice which has been observed in the far infrared by Wood[68] for several rare earths. A similar peak in the spectrum of divalent thulium in calcium fluoride has been attributed to the same mode by Kiss[69]. Neither the hydrogenic nor cubic site spectra show evidence of the fluorine site progressions. These progressions were postulated by Kopalanskii to be localized vibration modes but the nature of these was not elucidated. By comparison with the hydrogenic spectra we can now assign these to the (z) vibrational mode of the interstitial fluorine charge compensator. The vibronic shifts from absorption to fluorescence are of the same sign as the hydrogenic ones and much smaller. Extrapolation from the hydrogen values will be likely to give values which are too high since the fluorine vibration is not localised to nearly such a good approximation. The extrapolated values are 13 cm^{-1} for calcium fluoride and 17 cm^{-1} for strontium fluoride. These may be compared with the experimental values of 6 cm^{-1} and 13 cm^{-1} respectively. The agreement is better for strontium fluoride which is to be expected since this mode is better separated from the lattice frequencies (see table 6). The barium fluoride vibronic shift of 5 cm^{-1} is smaller but of the same sign indicating similar coupling for this lattice also.

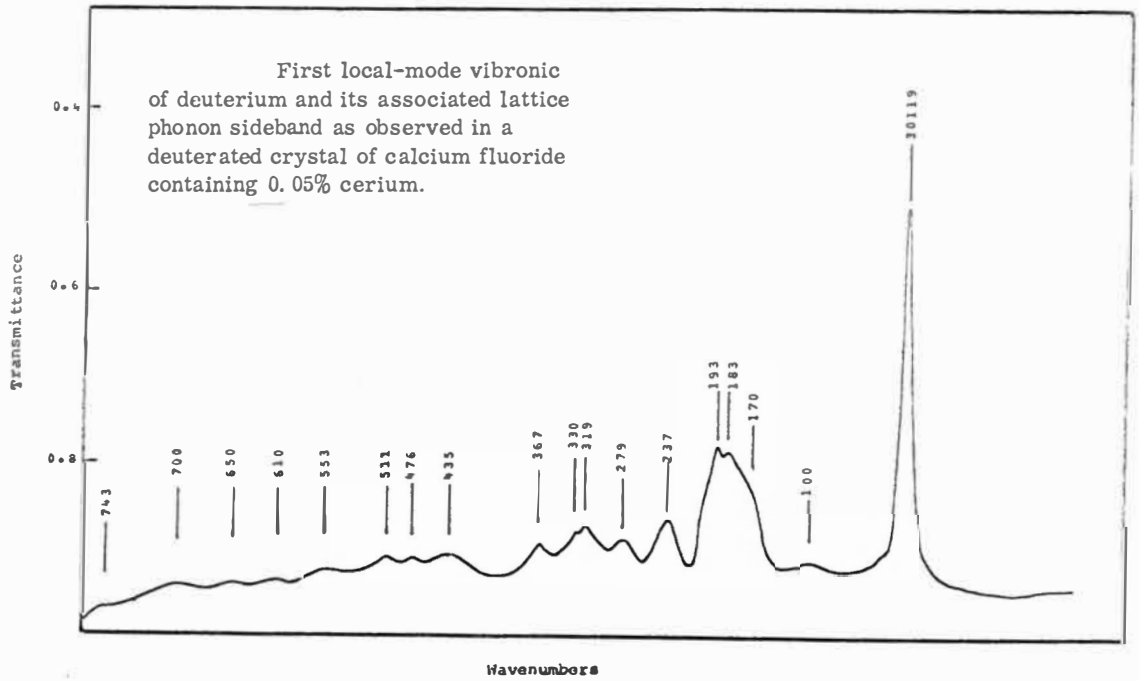
First local-mode vibronic
of deuterium and its associated lattice
phonon sideband as observed in a
deuterated crystal of calcium fluoride
containing 0. 05% cerium.
Transmittance
0.4
0.6
0.8
743
700
650
610
553
531
476
435
367
330
319
279
237
193
183
170
100
30119
Wavenumbers

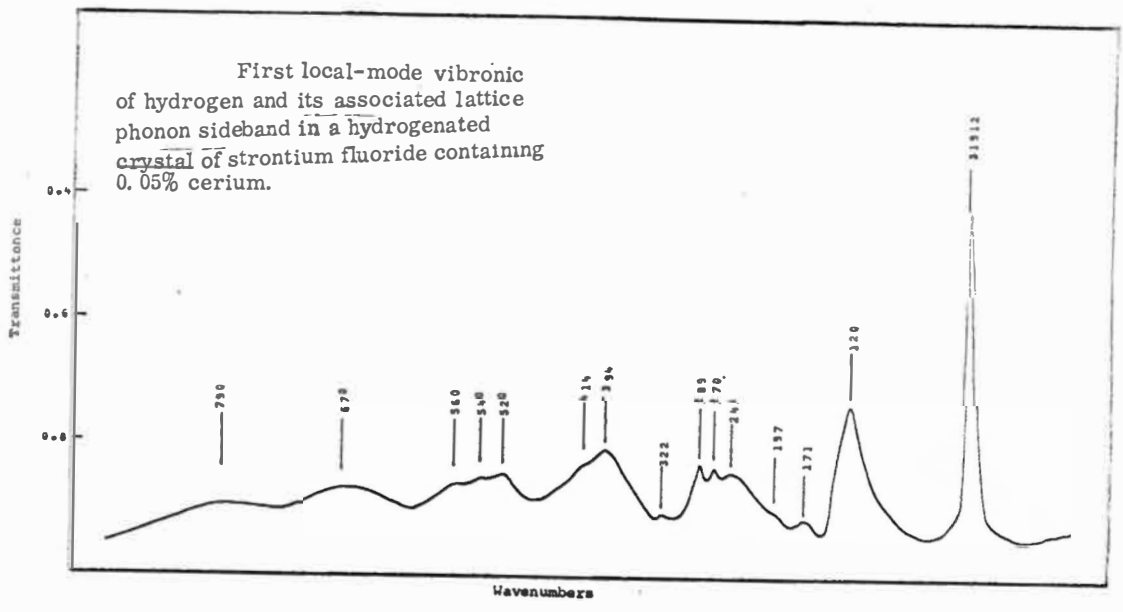
First local-mode vibronic
of hydrogen and its associated lattice
phonon sideband in a hydrogenated
crystal of strontium fluoride containing
0. 05% cerium.
Transmittance
0.4
0.6
0.8
790
678
560
548
528
414
394
322
193
170
241
197
171
120
31912
Wavenumbers

Fig (19)

CHAPTER VII

POINT-CHARGE MODEL FOR ELECTRONIC ISOTOPE SHIFTS AND LOCAL-MODE VIBRONIC SHIFTS

The experimentally observed electronic line isotope shift is the difference in isotope shift for the two electronic states involved in the transition. For the several cerium-ion interconfigurational transitions investigated in fluorescence the one common emitting state is the lowest crystal field level of the 5d configuration, and the terminating states comprise crystal field components of the $^2F_{5/2}$ and $^2F_{7/2}$ multiplets of the $4f^1$ configuration. The electronic isotope shifts of all these transitions are the same to within 1 cm^{-1} so the principal part of the observed isotope shift is attributed to electron-phonon interaction effects in the 5d electronic state.

The experimentally observed local-mode vibronic shift is the difference in vibronic shift between the excited and ground electronic states. The shifts are nearly all the same for the various electronic states of the $4f^1$ configuration and are small so, as in the case of the electronic line isotope shifts, the observed vibronic shifts must be attributed primarily to electron-phonon interactions in the 5d electronic state.

The lowest 5d electronic state φ of cerium in a tetragonal C_{4v} symmetry crystal field is the cubic-field $|\varepsilon\rangle$ wave function (page 6.24).

It is required to evaluate the matrix elements of the g_{zz}, $g_{xx} + g_{yy}$ and f_z electronic functions for this cerium-ion electronic state, and to determine the cubic anharmonic constants c and d.

Two simple models for the electron-local-mode-phonon interaction are the point-charge and dipole models introduced in Chapter II. The nonvanishing matrix elements of the electronic functions g_{zz} and $g_{xx} + g_{yy}$ for the cerium $|\varepsilon\rangle$ wave function are

$$\langle\varepsilon|g_{zz}|\varepsilon\rangle = -\langle\varepsilon|g_{xx}+g_{yy}|\varepsilon\rangle = \frac{-12eq\langle r^2\rangle}{7D^5} + \frac{5eq\langle r^4\rangle}{7D^7}$$

for the point charge, and

$$\langle\varepsilon|g_{zz}|\varepsilon\rangle = \frac{-60ep\langle r^2\rangle}{7D^6} + \frac{5ep\langle r^4\rangle}{D^8}$$

$$\langle\varepsilon|g_{xx}+g_{yy}|\varepsilon\rangle = \frac{6ep\langle r^2\rangle}{D^6} - \frac{80ep\langle r^4\rangle}{21D^8}$$

for the dipole model, where $\langle r^n\rangle$ is the average value of r^n for the cerium 5d orbital and is taken as 7.00 a.u. and 70.66 a.u. for $\langle r^2\rangle$ and $\langle r^4\rangle$, respectively, in the following numerical calculations.

The nonvanishing matrix element of the f_z electronic coordinate function for the cerium ε wave function is

$$\langle\varepsilon|f_z|\varepsilon\rangle = \frac{6eq\langle r^2\rangle}{7D^4} - \frac{5eq\langle r^4\rangle}{21D^6}$$

for the point-charge model, and

$$\langle\varepsilon|f_z|\varepsilon\rangle = \frac{24ep\langle r^2\rangle}{7D^5} - \frac{10ep\langle r^4\rangle}{7D^7}$$

for the dipole model.

The cubic anharmonic constants c and d may be estimated from the infrared local-mode spectra. The anharmonic terms of the potential well cause shifts in the frequencies of the local modes of the light ions and also allow the observation of harmonics. Because these terms are relatively small, their effect may be estimated by perturbation theory and this has been done by Maradudin and Peretti[34] to first order in the quartic terms and to second order in the cubic terms since both are comparable contributions; having the same ratio of displacement to interionic distance. The frequency shift of the second-harmonic lines from twice the fundamental frequencies yields three equations in the six anharmonic constants c, d, f, g, h, and k:

$$E(002) - 2E(001) = 12\beta^4 g - \frac{60c^2\beta^6}{\hbar w_z},$$

$$E(101) - [E(100)+E(001)] = 4h\alpha^2\beta^2 - \frac{12cd\beta^4\alpha^2}{\hbar w_z} - \frac{16d^2\alpha^4\beta^2}{\hbar w_x[4-(w_z/w_x)^2]},$$

$$E(200) - 2E(100) = 2\alpha^4(k+6f) + \frac{16d^2\beta^4\alpha^2[2-(w_z/w_x)^2]}{\hbar w_x[4-(w_z/w_x)^2]},$$

where $\alpha = (\hbar/2mw_x)^{\frac{1}{2}}$, $\beta = (\hbar/2mw_z)^{\frac{1}{2}}$ and E(nmp) is the energy of the (nmp) state.

Three second-harmonic transitions are expected and have been observed[13] for calcium fluoride crystals containing gadolinium, thulium, and yttrium. The observation of the corresponding transitions in the crystals containing cerium is confused by the presence of overlying absorption due to the $^2F_{5/2} \rightarrow {}^2F_{7/2}$ electronic transitions of cerium in the 2000-cm^{-1} region. The frequencies of these second-harmonic transitions can, however, be estimated to within 10 cm^{-1} by extrapolation from the gadolinium, thulium, and yttrium values to be 1975, 2110 and 2240 cm^{-1}. The frequency shifts of the second-harmonic lines from twice the fundamental frequencies are all negative which requires the quartic anharmonic constants g, h and k+6f to be negative. As an upper limit, the contribution of the cubic terms is set to equal the observed anharmonic shifts, which yields

$$|c| \leqslant 2 \times 10^{12} \text{ erg/cm}^3, \quad |d| \leqslant 3.5 \times 10^{12} \text{ erg/cm}^3.$$

An alternative estimate of the value of these anharmonic constants c and d can be made from the point-charge and dipole-model expressions

For $q = \sigma = 0.85e$ and $p/e = 1.1$ Bohr radii,

$$c = 6 \times 10^{11} \text{ erg/cm}^3, \quad d = 6.5 \times 10^{11} \text{ erg/cm}^3.$$

These are taken as the values for the following numerical calculations.

The shift in equilibrium position of the hydrogen, deuterium, and tritium ions from the center of the harmonic potential due to these cubic anharmonic terms is

$$\langle 000' | z | 000' \rangle = \frac{6c\beta^4}{\hbar^2 w_z} + \frac{4d\alpha^2\beta^2}{\hbar^2 w_x},$$

which is 0.006, 0.004 and 0.003 Å for hydrogen, deuterium and tritium respectively.

The shift in the first z vibronic line is,

$$\delta_{z1} = \frac{\hbar}{m w_z} [\varepsilon | z | \varepsilon].$$

For $w_z = 1130$ cm^{-1} and $e = q = 0.85$ of the electronic charge, the point-charge-model value of δ_{z1} is -60 cm^{-1}, and the dipole-model value is -66 cm^{-1}.

The shift δ in the zero-phonon electronic line is

$$\delta = \frac{\hbar}{2m w_z} [\varepsilon | z | \varepsilon] + \frac{\hbar}{2m w_x} [\varepsilon | x | \varepsilon].$$

The isotope shift consists of the difference in this shift in going from hydrogen to deuterium, and for $w_x = 990$ cm^{-1}

and w_z = 1130 cm^{-1} for hydrogen the point-charge value of $(\delta_H - \delta_D)$ is -3.1 cm^{-1} and the dipole-model value is -5.7 cm^{-1}. In both cases, both models give values that are of opposite sign to those observed.

The first-degree terms f_x, f_y and f_z can contribute in second-order perturbation via the other 5d electronic states of the cerium ion. Of these, the second E_g level which has the cubic field wave function $|\theta\rangle$ has zero matrix elements with $|\varepsilon\rangle$ while the three levels of the $5d,T_{2g}$ state are 8000 cm^{-1} away and their total contribution to the Z vibronic frequency shift is ~ 2 cm^{-1} which is negligible compared to the contribution from the second-degree g_{zz} terms.

Both the point-charge and the dipole model are thus incapable of explaining the sign of either the observed Z vibronic frequency shift or the observed zero-phonon electronic line isotope shift, and it is necessary to consider other mechanisms to explain these effects.

Satten and Zdansky have investigated possible effects of the four fluorine ions between the cerium ion and the hydride ion. Their results are reported below.

(a) The motion of the hydride and deuterium ions can induce motion of the four fluorine ions at their local-mode frequencies. The deuterium ion will drive the four fluorine

ions with larger amplitude since its local-mode frequency is closer to the lattice frequencies. Calculations on a model of four point-charge fluorine ions being driven by a vibrating hydride ion show that to account for the observed magnitude of the isotope shifts the hydride ion must drive the four fluorine ions from $\frac{1}{10}$ to $\frac{1}{4}$ of the mean-square amplitude typical of a normal vibrational mode of a four fluorine-ion complex. However, the value of 1.38 for the ratio of the hydrogen-to-deuterium local-mode frequencies sets the upper limit for the amplitude of the neighbouring fluorine ions as $\frac{1}{50}$, so this mechanism is not capable of explaining the magnitude of the observed electron-phonon effects.

(b) The motion of the hydride ion induces a dipole moment on the four fluorine ions through the short-range repulsive forces between these ions. This so-called distortion dipole moment can follow the rapid hydrogen or deuterium ion motion because it is a purely electronic effect and does not require the fluorine nuclei to vibrate at the local-mode frequencies. A point-charge model for this interaction yields values for the f_z, g_{zz}, and $g_{xx}+g_{yy}$ electronic coordinate functions which are given in the Appendix. For the case of the hydride and fluorine ions located in the lattice positions of the undistorted calcium fluoride lattice,

$$\langle\varepsilon|g_{zz}|\varepsilon\rangle = \frac{-2^{11} \times 0.7\alpha eq}{3^6 D^8} T_2^0,$$

$$\langle\varepsilon|f_z|\varepsilon\rangle = \frac{2^{10}\alpha eq}{3^5 D^7} T_2^0,$$

$$\langle\varepsilon|g_{xx}+g_{yy}|\varepsilon\rangle = \frac{-2^9 \times 0.25\alpha eq}{3^6 D^8} T_2^0,$$

where α is the polarizability of the fluorine ions and T_2^0 is defined in the Appendix. For $\alpha = 0.99$Å,[50] these values become

$$\langle\varepsilon|g_{zz}|\varepsilon\rangle = -0.96 \frac{eq}{D^5} T_2^0,$$

$$\langle\varepsilon|f_z|\varepsilon\rangle = +0.21 \frac{eq}{D^4} T_2^0,$$

$$\langle\varepsilon|g_{xx}+g_{yy}|\varepsilon\rangle = -1.7 \frac{eq}{D^5} T_2^0.$$

$\langle\varepsilon|g_{zz}|\varepsilon\rangle$ is about $\frac{1}{6}$ and of opposite sign to the direct-interaction point-charge value. Similarly, $\langle\varepsilon|f_z|\varepsilon\rangle$ is about $\frac{1}{15}$ and of opposite sign to the point-charge direct-interaction value. The net shift δ_{z1} in the first Z vibronic line is thus +9.7 cm^{-1}. $\langle\varepsilon|g_{xx}+g_{yy}|\varepsilon\rangle$ is of the same sign as the point-charge direct-interaction value, and the electronic line isotope shift δ is +6.1 cm^{-1}.

A refinement to the model is to include the effect of the change in the environment of the cerium and hydride ions caused by the change in the position of the surrounding

fluorine ions, as postulated by Kiro and Low[70] on the basis of ENDOR measurements. If the four fluorine ions between the cerium and hydride ion are displaced 0.15 Å outwards along the hydride-fluorine ion directions, then

$$\langle\varepsilon|g_{zz}|\varepsilon\rangle = -0.91\,\frac{eq}{D^5}\,T_2^0,$$

$$\langle\varepsilon|f_z|\varepsilon\rangle = +0.26\,\frac{eq}{D^4}\,T_2^0,$$

$$\langle\varepsilon|g_{xx}+g_{yy}|\varepsilon\rangle = -1.0\,\frac{eq}{D^5}\,T_2^0,$$

while if the equilibrium position of the hydride ion is also moved 0.1 Å towards the cerium ion, then

$$\langle\varepsilon|g_{zz}|\varepsilon\rangle = -1.0\,\frac{eq}{D^5}\,T_2^0,$$

$$\langle\varepsilon|f_z|\varepsilon\rangle = +0.29\,\frac{eq}{D^4}\,T_2^0,$$

$$\langle\varepsilon|g_{xx}+g_{yy}|\varepsilon\rangle = -1.2\,\frac{eq}{D^5}\,T_2^0.$$

These changes indicate that distortions of the calcium fluoride lattice of the magnitude postulated by Kiro and Low are not very significant in influencing the calculated values of the electron-phonon interaction effects.

The participation of the four fluorine ions in the cerium-hydride ion interaction thus gives a contribution whose sign is in agreement with observation, but whose

magnitude is smaller than required.

The several contributions to the electronic line isotope shift and to the z vibronic isotope shift comprise (a) the point-charge interaction between the cerium ion and the hydride ion, (b) the dipole moment interaction between the cerium ion and the hydride ion, and (c) the interaction via the polarization of the four fluorine ions between the cerium and hydride ion. The net electronic line isotope shift is $-4.7\ cm^{-1}$ and the net z vibronic line shift is $-115\ cm^{-1}$, which are comparable to the observed values, but of the wrong sign.

It can be concluded that purely electrostatic models for the electron-phonon interaction are unable to quantitatively explain the sign of the observed shifts. Nevertheless, these models are of some value in that they indicate the relative importance of the several contributions to these shifts. It is not feasible with the present data on the cerium system to attempt to develop covalency models for the cerium-ion system. Instead, more experimental investigations would be desirable to determine the effect of change in site symmetry and possibly charge state of the hydride ion on the sign and magnitude of the electron-phonon interaction effects. The importance of these changes is shown by the preliminary data for the cerium UV site. This has a reversed electronic line isotope shift but the same z

vibronic frequency shift as the principal C_{4v} symmetry site.

The cerium-ion system is a convenient system for these studies because of the large magnitude of electron-phonon interaction effects in transitions to and from 5d electronic states.

C H A P T E R V I I I

PRASEODYMIUM OPTICAL SPECTRA

The infrared local mode absorption spectra associated with Pr^{3+}-H^- tetragonal pairs in both calcium and strontium fluoride have been discussed in Chapter IV. In order to determine the expected splitting of the four-fold degenerate (xy) local mode vibronic line observed in the infrared it is necessary to know the positions of the low lying $^3H_4$ praseodymium electronic energy levels. Attempts were therefore made to detect the f-d transitions and so to locate the ground state energy levels from the allowed fluorescence transitions.

The f-d tetragonal fluorine ion charge compensated site absorption lies in the 2000 Å region[71]. The lowest energy zero-phonon transition was located with the 'Spex' using a deuterium lamp as source. In contrast to the cerium case however, no hydride centre absorption spectra were detected in the 2000-3000 Å range down to 4^oK. The non-appearance of any sharp hydride centre lines suggests that either the coupling to the lattice is considerably stronger than the cerium case or that these lines are shifted to an inaccessible spectral region below 2000 Å.

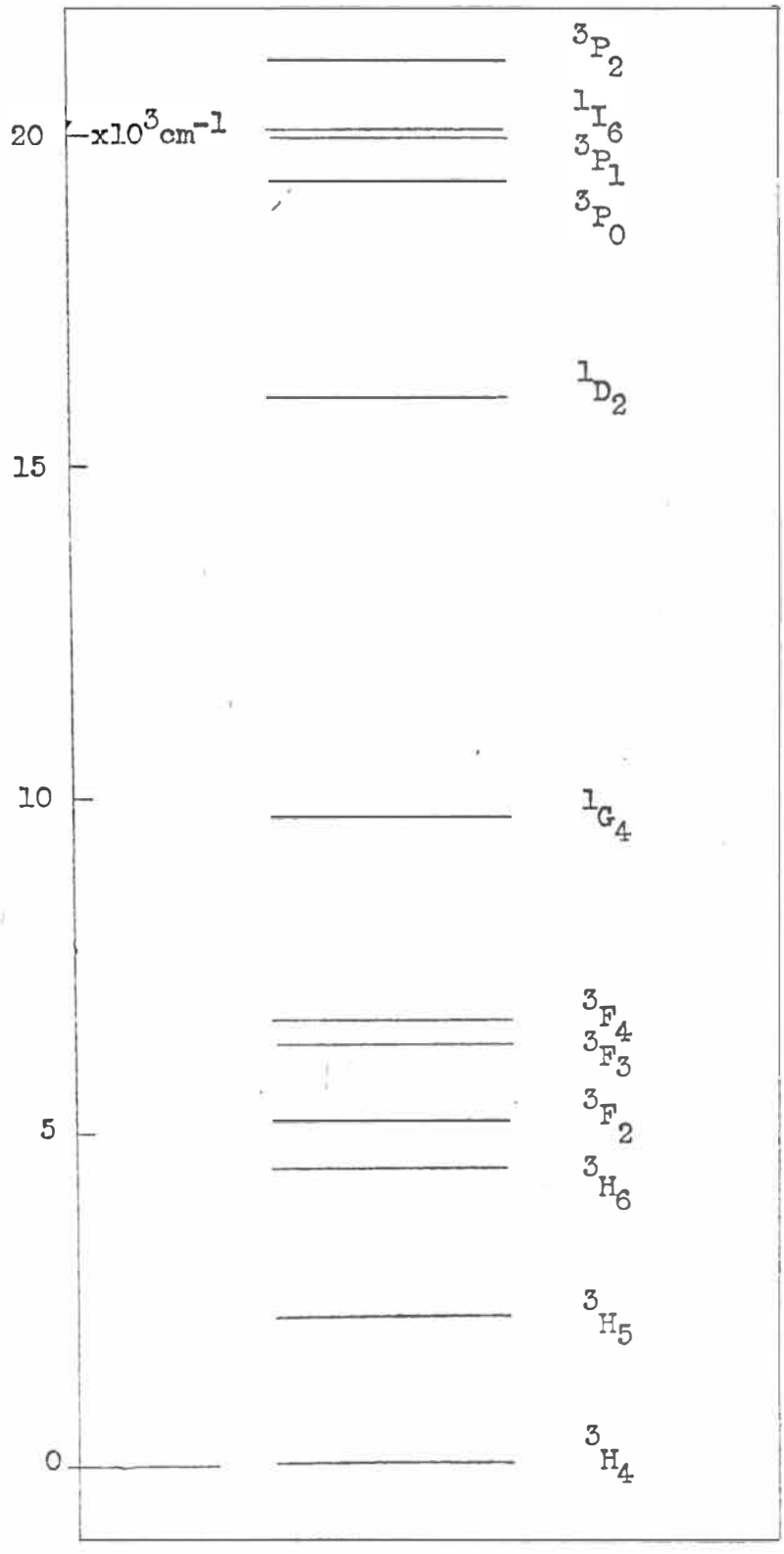

Fig (20). Approximate energy level diagram for Pr^{3+}.

The praseodymium ion has many excited 4f electronic levels, Fig. (20). Fluorescence transitions from these to the $^3H_4$ levels may in principle be used to locate these levels.

In the as grown crystals (0.05% Pr^{3+}) many sharp absorption lines are observed at liquid air temperatures and below in the 4300 Å region.

Baking the crystals for several hours at 800°C in high vacuum followed by rapid quenching to room temperature leaves three prominant lines which are included in figure (21). Their wavelengths are listed in table (13). These lines are assigned to the $^3H_4$ - $^3P_0$, $^3P_1$ transitions of praseodymium in interstitial fluorine ion tetragonal charge compensated sites.

Since these are f-f transitions the vibronic structure is extremely weak and is not at all evident in figure (21).

For the tetragonal fluorine charge compensated site fluorescence is observed at 4°K from the $^3P_0$ level only since phonon de-excitation successfully competes with radiative processes for the $^3P_1$ levels. The fluorescence transitions from $^3P_0$ to the ground state multiplet are shown in figure (22) and listed in table (14). Similar results are obtained for strontium fluoride host crystals with the characteristic small reductions in the crystal field splittings. The corresponding transitions are listed in table (14).

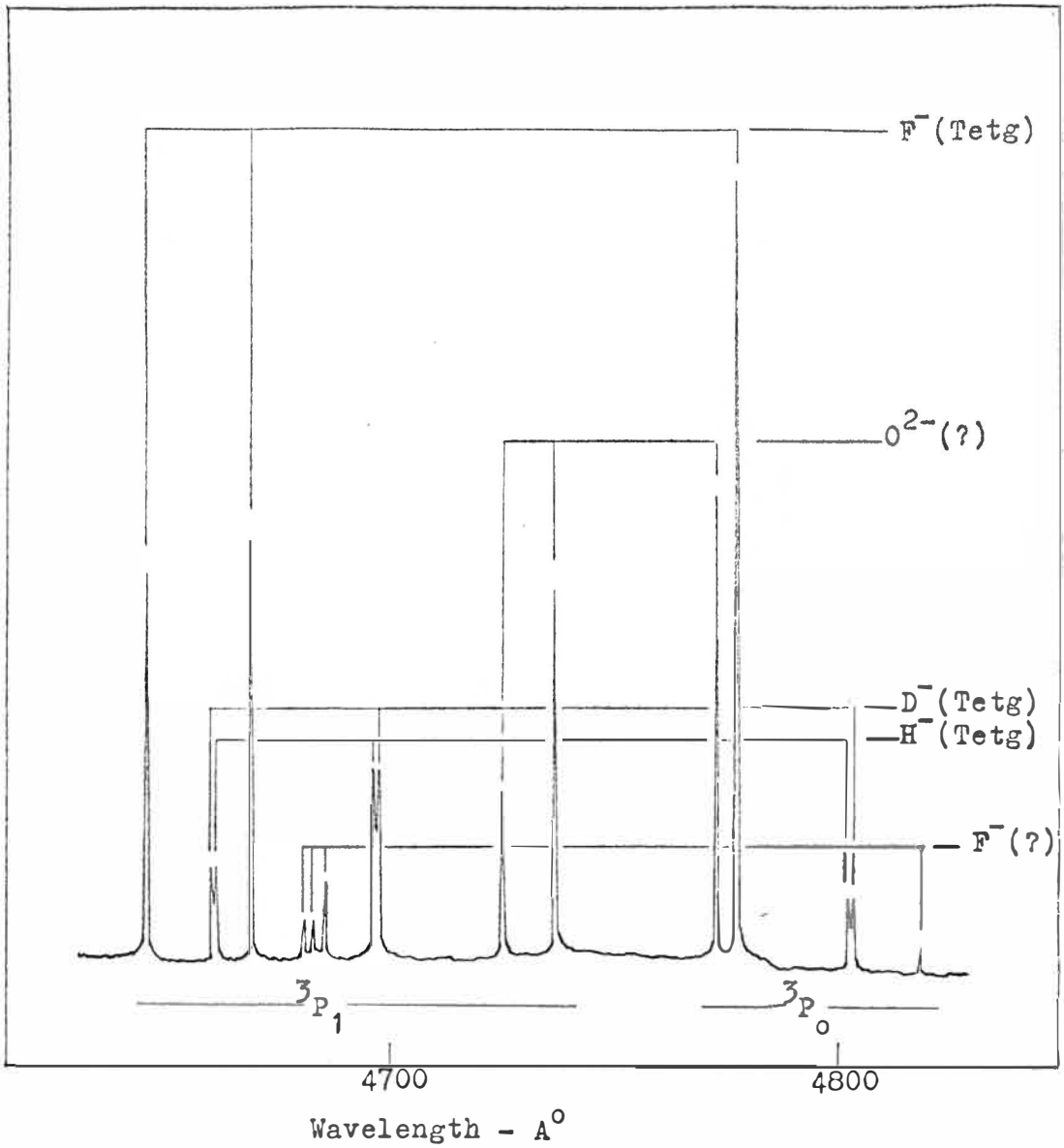

Fig (21).

Composite absorption spectrum of Pr^{3+} doped calcium fluoride at $8^{\circ}K$. Transitions from the ground state to the $^3P_0$ and $^3P_1$ excited levels are shown for five well characterised sites.

Crystal	Upper crystal field level of the electronic transition	Tetragonal symmetry fluoride ion charge compensated site A^o	Tetragonal symmetry hydride ion charge compensated site A^o	Tetragonal symmetry deuteride ion charge compensated site A^o
CaF_2	$\|^3P_0:\Gamma_1,\Gamma_1\rangle$	4771.1	4802.9	4803.4
	$\|^3P_1:\Gamma_4,\Gamma_5\rangle$	4680.3	4692.4	4693.3
	$\|^3P_1:\Gamma_4,\Gamma_2\rangle$	4634.7	4647.2	4646.6
SrF_2	$\|^3P_0:\Gamma_1,\Gamma_1\rangle$	4765.2	-	-
	$\|^3P_1:\Gamma_4,\Gamma_5\rangle$	4649.3	-	-
	$\|^3P_1:\Gamma_4,\Gamma_2\rangle$	4634.5	-	-

Table (13). Frequencies of the absorption lines due to electronic transitions from the ground state $|^3H_4:\Gamma_5,\Gamma_5\rangle$ crystal field level to crystal field levels of the $^3P_0$ and $^3P_1$ multiplets. Temperature: 8^oK.

Crystals either heated in oxygen at 900°C for several hours or grown without the addition of lead fluoride to the melt show new spectra indicative of the formation of a well characterised oxygen charge compensated centre. The upper $^3H_4$ level transforming as Γ_3 in cubic symmetry (see figure (24)) is split into two components. This is not, therefore, the trigonal site formed by the replacement of a single nearest neighbour F^- ion with an O^{2-} ion but must have still lower symmetry.

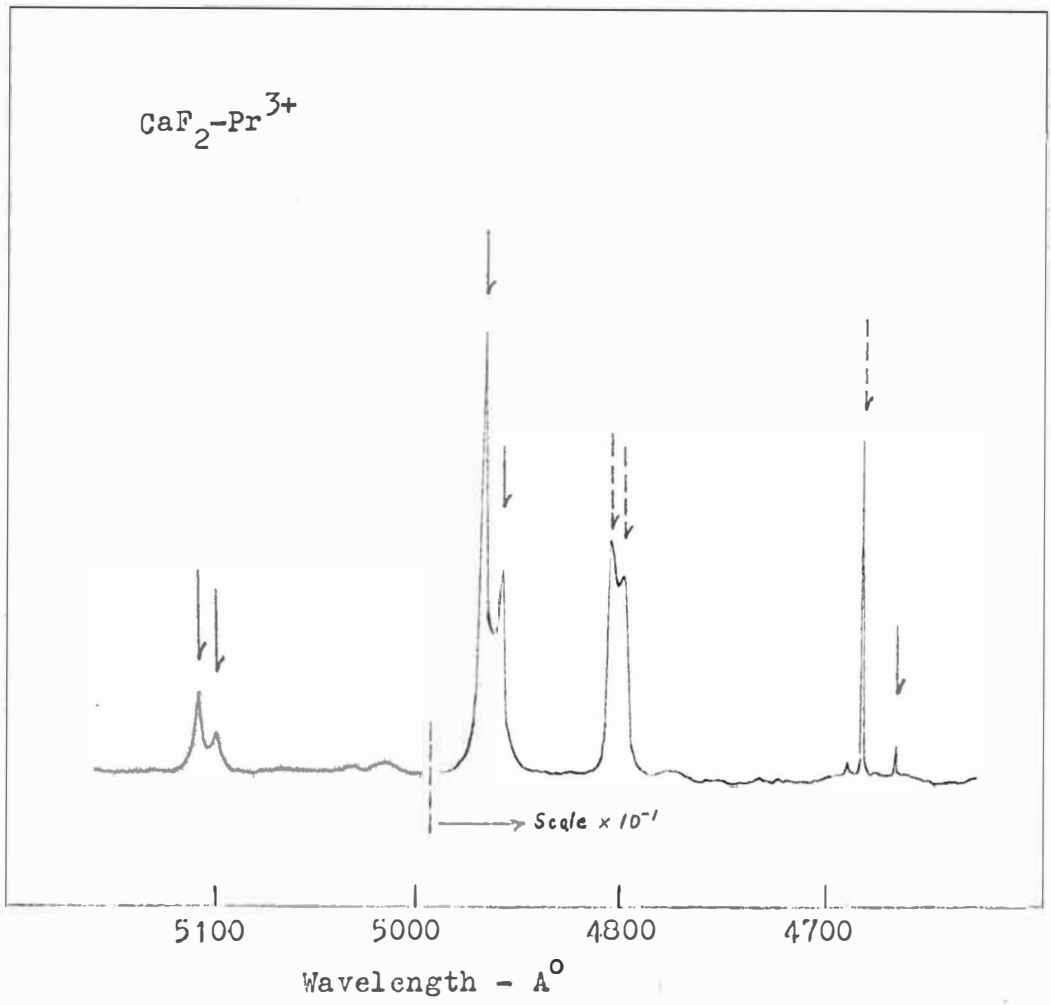

Fig (22).

Low temperature ($8^{o}K$) fluorescence spectrum of a Pr^{3+} doped calcium fluoride crystal containing both O^{2-} and F^{-} charge compensated sites. Transitions are seen from the excited $^{3}P_{o}$ level to several components of the $^{3}H_{4}$ groundstate multiplet. Lines associated with the tetragonal fluorine sites are identified with broken arrows and the oxygen sites with solid arrows.

Crystal	Terminating state of the fluorescence transitions from the one crystal field level of the $^3P_0$ multiplet	Tetragonal symmetry fluoride ion charge compensated site A^o	Oxygen ion charge compensated site A^o
CaF_2	$\|^3H_4:\Gamma_5,\Gamma_5\rangle$	4771.1	4759.1
	$\|^3H_4:\Gamma_4,\Gamma_2\rangle$	4896.1	4953.1
	$\|^3H_4:\Gamma_4,\Gamma_5\rangle$	4900.5	4961.9
	$\|^3H_4:\Gamma_3,\Gamma_1\rangle$	-	5096.5
	$\|^3H_4:\Gamma_3,\Gamma_3\rangle$	-	5105.7
SrF_2	$\|^3H_4:\Gamma_5,\Gamma_5\rangle$	4765.2	4758.4
	$\|^3H_4:\Gamma_4,\Gamma_2\rangle$	4872.4	4955.4
	$\|^3H_4:\Gamma_4,\Gamma_5\rangle$		4964.4
	$\|^3H_4:\Gamma_3,\Gamma_1\rangle$	-	5091.5
	$\|^3H_4:\Gamma_3,\Gamma_3\rangle$	-	5101.1

Table (13). Fluorescence spectral data for the tetragonal symmetry charge compensated site and for the oxygen ion charge compensated site in crystals of calcium and strontium fluorides containing praseodymium. Temperature: 8^oK

Praseodymium-Hydride Centres

Following hydrogenation the calcium fluoride crystals show new absorption lines, figure (21). The isotope shifts indicate at once that these are associated with hydrogenic sites and the observation of two very weak vibronics on the strongest line (table (15)) whose separations match the infrared local mode frequencies confirms the assignment of these lines to the tetragonal, interstitial hydride ion, charge compensated sites. The energy level diagram is given in figure (23). The ground state isotope shift has been obtained by assuming that the $^3P_0$ level which is not perturbed by the crystal field is coincident for H^- and D^-. It is immediately apparent that the $^3P_1$ levels which are split by the B_2 component of the tetragonal crystal field are more widely separated than for the interstitial fluorine site and the splitting for D^- is greater than for H^-. Unfortunately, as in similar cases (53) these hydrogenic sites do not fluoresce even at 4^oK since the next lowest energy level ^1D lies ~3000 cm^{-1} below and three and four phonon processes involving the local mode phonons successfully compete with radiative processes.

The remaining possibility for observing the excited $^3H_4$ energy levels directly is via infrared absorption transitions. These transitions are relatively weak and the lower lying ones cannot be observed because of the very

Electronic line A^o	Vibronic lines A^o	Separation cm^{-1}	Infrared energy cm^{-1}
4693.3	4539.8	720 ± 4	718
	4521.8	808 ± 4	810*

Table (15). Vibronic intervals observed in the Pr^{3+} - D^- tetragonal site absorption spectrum. The intervals match closely the energies of the infrared local mode lines.

*Estimate based on the hydride site value.

strong restrahlen absorption of the host crystals. The upper (cubic Γ_3) levels are expected to lie in the 900 cm^{-1} region and may be searched for in crystals as thick as 2 mm. The 0.05% crystals show no detectable lines in this region but in crystals with 0.2% Pr^{3+} two very weak lines are seen at 858 and 878 cm^{-1}. These are in the locations expected for the fluorine site lines (see below) and are tentatively identified as such.

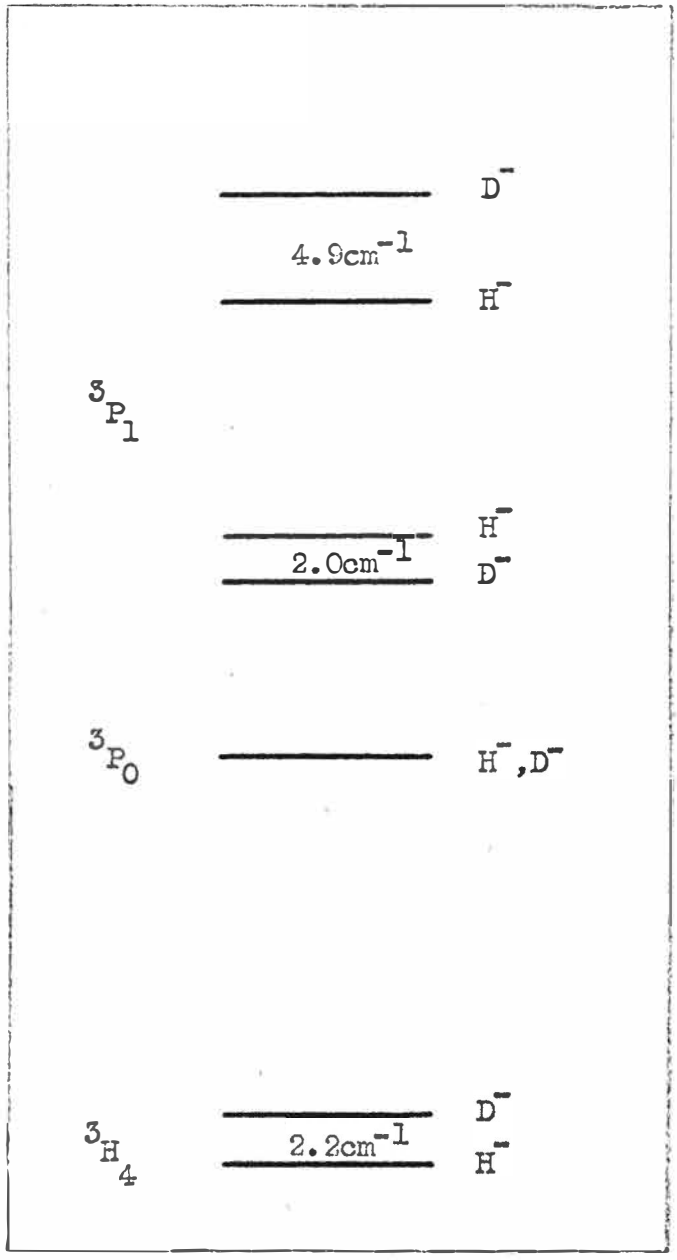

Fig (23).

Schematic energy level diagram for the tetragonal Pr^{3+}-H^-,D^- centres in CaF_2. (8^oK.)

The Praseodymium $^3H_4$ Ground State Multiplet

The splitting of this multiplet in a cubic crystal field has been calculated and is given in (38) from which figure (24) has been reproduced.

The splitting pattern is determined by the motion of fourth to sixth order crystal field terms. It is apparent from the spectra that in the calcium and strontium fluoride lattices the dominant splittings may be attributed to the cubic part of the crystal field and the non-cubic part is seen to raise the remaining degeneracies by relatively small amounts. Weber and Bierig using ESR data have estimated as 0.9 which places the spectra to the right of the cross-over of the Γ_1 and Γ_5 cubic levels in figure (24). For the oxygen sites above for which all the levels derived from the cubic Γ_3 and Γ_4 levels can be seen the ratio of their separations from the ground state also places the spectra just to the right of this cross-over. One would not expect this ratio to be very different for the fluorine compensated sites and the identification of the cubic Γ_3 levels in the infrared, while somewhat uncertain, maintains the above ratio.

It is found elsewhere that the cubic field parameters of F^- and H^- sites are very similar while the effects due to tetragonal distortion are increased by a factor of about two for the H^- sites(35). It is therefore not unreasonable

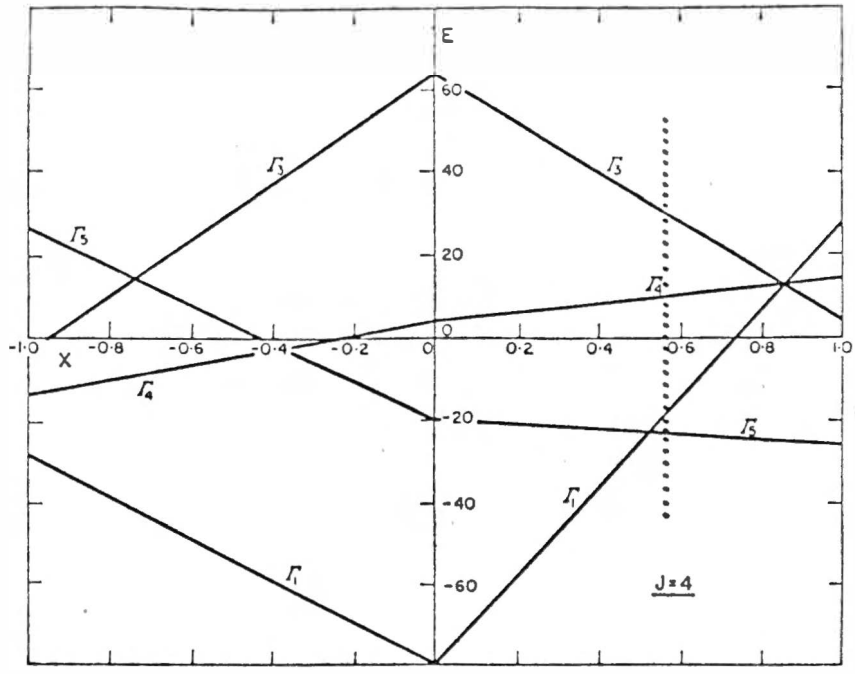

Fig (24).

Figure 9 of Lea Leask and Wolf (38) is reproduced above. It shows the cubic crystal field splitting of a J=4 level in terms of X which is defined so that $B_4/B_6 = 0$ for X=0 and $B_4/B_6 = \pm\infty$ for X=±1.

The vertical dashed line indicates the value of X from the optical spectra discussed in this section.

to assume that the $^3H_4$ energy level diagram will be approximated by adopting the fluorine site values for the dominant cubic splittings and by doubling the smaller tetragonal field splittings. While no claims may be made for the detailed accuracy of this extrapolation the energy levels so obtained reproduce the splitting pattern observed in the infrared for both host lattices (Chapter V).

The Electronic Isotope Shifts

The energy level diagram for both H^- and D^- sites is shown in figure (23). It is seen that the major contribution may be accounted for by a small increase in the tetragonal field splitting of the $^3P_1$ levels in changing from H^- to D^- as charge compensator.

Both the point charge and point dipole models employed with some success in accounting for many of the features of the spectra examined in this work must fail to account for this increase since they both predict shifts in the opposite direction.

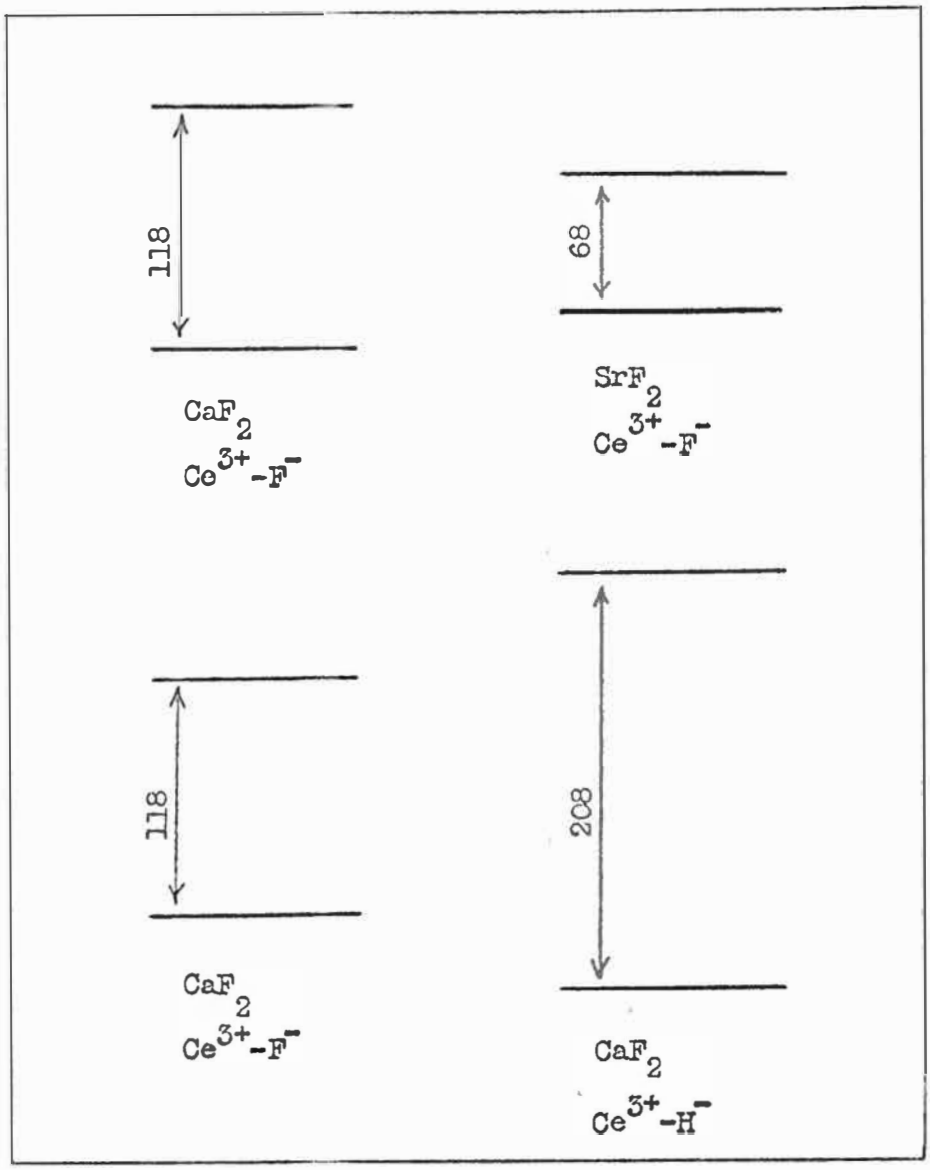

Fig (25).
The tetragonal field splitting of the $^3P_1$ praseodymium levels for two tetragonal sites in two host lattices. The separations are given in wavenumbers.

C H A P T E R I X

SUGGESTIONS FOR FUTURE WORK

The results of this work have improved the understanding of the tetragonal rare earth-hydride centres and made possible a positive reassignment of the hydride local mode components.

New observations of vibronic splittings have been made. Tritium doping has not been to date attempted elsewhere and tritiated crystals containing cerium have been supplied to Professor Baker for ENDOR studies and to Professor Royce for the extension of his ionic thermocurrent measurements.

The appearance of only the nondegenerate hydride vibronic in the cerium optical spectra and the relative intensity of the vibronics are accounted for on a simple model.

The well characterised isotope and vibronic shifts observed are an order of magnitude larger than similar shifts previously reported. There is a need for the development of a more sophisticated theory to account quantitatively for these shifts.

More data on the praseodymium optical spectra will allow a determination of crystal field parameters and a more satisfactory estimate of the low lying electronic energy levels. In particular, efforts are being made to locate

the weak $^1D_2$ levels.

In addition to the cerium tetragonal and U.V. sites a doublet appears in the CaF_2 absorption spectra. It was initially thought that this site may have involved the interaction of two close paramagnetic cerium ions. However, crystals double doped with Ce^{3+}; Nd^{3+} and Ce^{3+}; La^{3+} show no apparent change in the spectra. It is hoped that suitable treatments can be found to enhance this site to allow E.S.R. determination of the site symmetry. Optical Zeeman studies may in principle also be used provided large enough splittings can be achieved. Fields in excess of 60 Kg will probably be required.

The above observations indicate that although progress has been made the complete understanding of these spectra awaits further experimental and theoretical studies.

APPENDIX I

A Related Problem

In (12) Jones et al.have noted the quenching at room temperature of the Gd^{3+}-H^-:D^- tetragonal site fluorescence in CaF_2 which is in sharp contrast to the persistence of the fluorescence from other gadolinium sites. Similar intensity, temperature curves have been obtained in this laboratory by M. Presland for the H and D sites. This, together with the very large separation of the first excited levels from the ground state (30,000 cm^{-1}) rules out phonon de-excitation.

Jones et al. suggested that fast tunneling of the hydride ion may effectively remove the tetragonal site at elevated temperatures. However, absorption measurements made during this work indicate the persistence of the tetragonal site to elevated temperatures, see figure (A1). A careful search was therefore made for enhanced gadolinium fluorescence at room temperature from another site to which the excitation energy could be transferred. No such enhancement was found.

There remains the possibility that the excitation energy is transferred to another centre with a short lived electronic energy level close to the lowest excited Gd^{3+}-H^- level.

The tetragonal Ce^{3+}-F^- site studied here is such a centre. It is present in all the CaF_2-Gd^{3+} crystals studied in this laboratory in concentrations of at least 5×10^{-6}%.

(The cerium fluorescence is too short lived to be observed with the rotating mechanical chopper used to remove all the exciting radiation and thus to achieve sufficient sensitivity to observe the gadolinium fluorescence.)

Attempts are being made to obtain Gd^{3+}-H^- tetragonal centres in SrF_2 in sufficient concentrations to allow the observation of fluorescence in this lattice. Since the cerium energy levels lie considerably above the gadolinium levels in this lattice persistence of fluorescence to room temperature would indicate that the cerium was involved in the quenching. This information is awaited with interest.

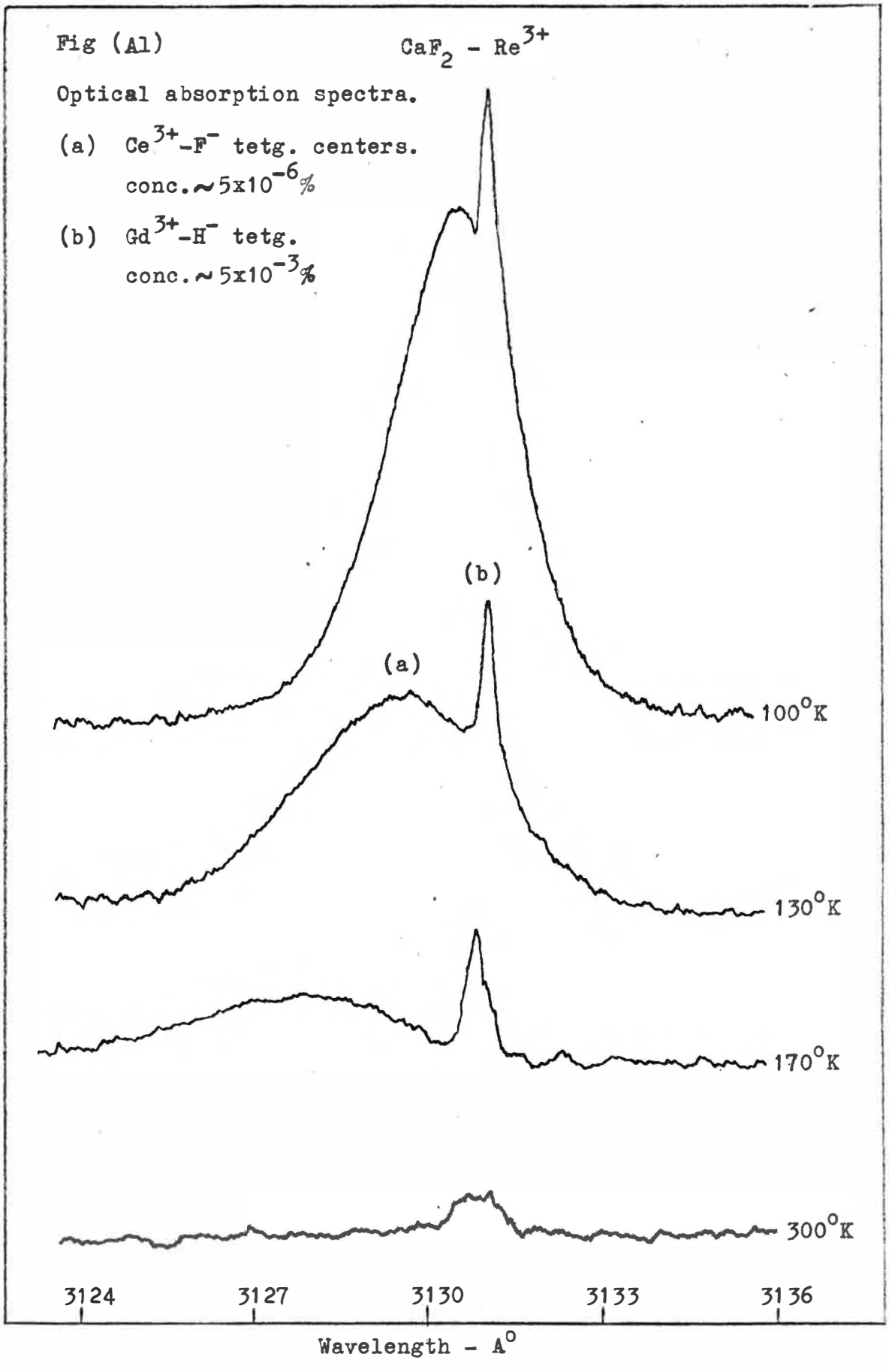
Fig (A1)
CaF_2 - Re^{3+}
Optical absorption spectra.
(a) Ce^{3+}-F^- tetg. centers.
conc. ~ $5x10^{-6}$%
(b) Gd^{3+}-H^- tetg.
conc. ~ $5x10^{-3}$%
(b)
(a)
100°K
130°K
170°K
300°K
3124
3127
3130
3133
3136
Wavelength - A°

REFERENCES

1. R.C. Newman, Advances in Physics, Vol. 18, No. 75 (1969).
2. Phonons in Perfect Lattices and in Lattices with Point Imperfections, Ed. R.W.H. Stevenson, Oliver and Boyd, London (1966).
3. Elementary Excitations in Solids, Plenum Press (1969).
4. R.J. Elliott, W. Hayes, G.D. Jones, H.F. McDonald, C.T. Sennett, Proc. R. Soc. A289 (1965).
5. G.H. Dieke, Spectra and Energy Levels of Rare Earth Ions in Crystals. Interscience, New York (1968). (Includes an estensive bibliography.)
6. B.G. Wybourne, Spectroscopic Properties of the Rare Earths. Interscience, New York (1965).
7. A.A. Kapalanskii, V.N. Medvedev and P.P. Feofilov, Opt. i Spektroskopiya 14, 664 (1963) [Opt. Spectry. (USSR) 14, 351 (1963)].
8. E. Loh, Phys. Rev. 147, 332 (1966).
9. J.M. Baker, E.R. Davies, J.P. Hurrell, Proc. Roy. Soc. A308, 403 (1968).
10. I.J. Ashburner, R.C. Newman and S.D. McLaughlan, Phys. Lett. A27, 212 (1968).
11. J.M. Baker, E.R. Davies and T.R. Reedy, Phys. Lett. A29, 118 (1969).

12. G.D. Jones, S. Peled, S. Rosenwaks and S. Yatsiv, Phys. Rev. 183, 353 (1969).

13. For a general discussion of Gadolinium in CaF_2 see J. Makovsky, J. Chem. Phys. 46, 390 (1967) and for the hydride sites see (12).

14. G.D. Jones and R.A. Satten, Phys. Rev. 147, 566 (1966).

15. G.F. Imbusch et al., Phys. Rev. 136, A481 (1964). See also J.A.D. Mathew, Proc. Phys. Soc. 2, 1, 1768 (1968).

16. A.F. Hughes, Proc. Phys. Soc. 88, 449 (1966).

17. A.A. Maradudin, Montvell and Weiss, Solid State Physics, Sup. 3 (1963).

18. Born and Huang, Dynamical Theory of Crystal Lattices. Oxford University Press (1954).

19. E.W. Montroll and R.B. Potts, Phys. Rev. 100, 525 (1955).

20. J.A. Krumhansl, J. App. Phys. 33, 307 (1962).

21. A.A. Maradudin et al., Rev. Mod. Phys. 30, 175 (1958).

22. Lord Rayleigh, Theory of Sound. Dover Reprint, New York (1940).

23. P. Mazur et al., J. Wash. Acad. Sci. 46, 2 (1956).

24. C. Kittel, Introduction to Solid State Physics. Wiley, New York (1966).

25. See (20).

26. P.G. Dawber and R.J. Elliot, Proc. Phys. Soc. 81, 453 (1963).

27. A.A. Maradudin, Solid St. Phys. 18, 273; 19, 1 (1966).

28. A.A. Maradudin et al., Rev. Mod. Phys. 30, 175 (1958).

29. S.S. Mitra, Solid State Phys. 13, (1962).

30. W. Cochran, Proc. R. Soc. 253, 260 (1959).

31. A.D.B. Woods, W. Cochran, B.N. Brockhouse, Phys. Rev. 119, 980 (1960).

32. W. Hayes, H.F. McDonald, and R.J. Elliott, Phys. Rev. Lett. 15, 961 (1965). (See also (4)).

33. W. Hayes, H.F. McDonald, Proc. Roy. Soc. A297, 503 (1967).

34. A.A. Maradudin and J. Peretti, Phys. Rev. 161, 852 (1967).

35. K. Zdansky and A. Edgar, Phys. Rev. B3, 2133 (1971).

36. H.A. Bethe, Ann. Physik. 3, 133 (1929).

37. H.A. Kramers, Z. Physik 53, 422 (1929).

38. K.R. Lea, M.J.M. Leask, W.P. Wolf, J. Phys. Chem. Solids 23, 1381 (1962).

39a. Private communication. Proctor (this laboratory).

39b. M.R. Brown et al., J. Chem. Phys. 50, 891 (1969).

40. A. Edgar, this laboratory (to be published).

41. D.N. Chambers and R.C. Newman, Phys. Status Solidi 35, 685 (1969).

42. G.F. Koster, J.O. Dimmock, R.G. Wheeler and H. Satz, Properties of the Thirty Two Point Groups, M.I.T. Press (1963).

43. R.G. Bessent and W. Hayes, Proc. Roy. Soc. (London) A285, 430 (1965).

44. W.E. Bron, Phys. Rev. 140, A, 2005 (1965).

45. R.G. Bessent, W. Hayes, Proc. Roy. Soc. A285, 430 (1965).

46. See for example R.E. Watson and A.J. Freeman, Phys. Rev. 156, 2, 251 (1967).

47. D. Sengupta, J.O. Artman, Phys. Rev. B1, 2986 (1970) and references 1-5 therein.

48. Yu.K. Voron'ko, A.A. Kaminskii and V.V. Osiko, Soviet Physics JETP 22, 2, 295 (1966).

49. D.N. Chambers, R.C. Newman, J.E. Whitehouse (to be published).

50. S. Fraga and G. Malli, Many Electron Systems: Properties and Interactions, Saunders, Philadelphia (1968). p. 84.

51. C.T. Sennett, Thesis Oxford University (1964).

52. U. El-Hanany, G. Rakavy, J.J. Wagschal and S. Yatsiv, Phys. Rev. 137, 5A, 1548 (1965).

53. M. Presland. This laboratory - optical work on Er^{3+}-H^- and Nd^{3+}-H^- centres in CaF_2 (unpublished).

54. N.V. Starostin, Opt. i Spektroskopiya 23, 807 (1967). [Opt. Spectry. (USSR) 23, 437 (1967)].

55. E. Loh, Phys. Rev. 154, 270 (1967).

56. W.J. Menthy (private communication); also J. Smalley, this laboratory (unpublished).

57. M.H. Weber and R.W. Bierig, Phys. Rev. 134, A1492 (1964).

58. This work Chapter VIII. The increase in splitting of the $^3P_1$, Pr^{3+} levels is clearly seen.

59. A. Edgar, this laboratory (unpublished), has found a similar increase in crystal field parameters in an ESR study of Gd^{3+}-F^- and H^- centres in SrF_2. See also (35).

60. J. Sierro, Phys. Rev. Lett. 4, 178 (1963).

61. Detrio et al., J. Chem. Phys. 53, 4372 (1970). c.f. (13).

62. W.E. Bron, Phys. Rev. 140, A2005 (1965).

63. M. Wagner, J. Chem. Phys. 41, 3939 (1964).

64. K. Rajnak, J. Chem. Phys. 37, 2440 (1962).

65. Jacobs et al. Phys. Rev. B3, 2888 (1971), included as an appendix to this thesis.

66. W. Kaiser, W.G. Spitzer, R.H. Kaiser and L.E. Howarth, Phys. Rev. 127, 1950 (1962).

67. S.J. Fray, F.A. Johnson and J.E. Quarrington, in Proceedings of the International Conference on Lattice Dynamics, Copenhagen, 1963 (Pergamon Press, Oxford, 1965), p.377.

68. E.J. Wood, this laboratory (unpublished).

69. Z.J. Kiss, Phys. Rev. 127, 3, 718 (1962).

70. D. Kiro, W. Low and A. Kafri, Phys. Rev. Lett. 22, 893 (1969).

71. E. Loh, Phys. Rev. 158, 2, 273 (1967).

APPENDIX II

Publication

Electron-Phonon Interaction Effects in the Spectra of Hydrogenated, Deuterated and Tritiated Crystals of Calcium and Strontium Fluorides Containing Cerium

by

I.T. Jacobs, G.D. Jones,
K. Zdansky and R.A. Satten